



Europäisches Patentamt
European Patent Office
Office européen des brevets



(11) **EP 1 037 940 B1**

(12) **EUROPEAN PATENT SPECIFICATION**

(45) Date of publication and mention of the grant of the patent:
08.09.2004 Bulletin 2004/37

(51) Int Cl.7: **C08J 9/00**, C08G 79/00,
C08G 79/10, C08G 79/12,
C01B 37/02, C04B 35/622

(21) Application number: **98967050.0**

(86) International application number:
PCT/US1998/026201

(22) Date of filing: **09.12.1998**

(87) International publication number:
WO 1999/037705 (29.07.1999 Gazette 1999/30)

(54) **BLOCK POLYMER PROCESSING FOR MESOSTRUCTURED INORGANIC OXIDE MATERIALS**

BLOCKCOPOLYMERVERARBEITUNG FÜR MESOSTRUKTURIERTE ANORGANISCHE OXIDMATERIALIEN

TRAITEMENT DE POLYMERES BLOCS DONNANT DES MATERIAUX MESOSTRUCTURES D'OXYDES INORGANIQUES

(84) Designated Contracting States:
**AT BE CH CY DE DK ES FI FR GB GR IE IT LI LU
MC NL PT SE**

- **FENG, Jianglin**
Charlottesville, VA 22903 (US)
- **YANG, Peidong**
Santa Barbara, CA 93117 (US)
- **PINE, David**
Santa Barbara, CA 93111 (US)
- **MARGOLESE, David**
Montecito, CA 93106 (US)
- **LUKENS, Wayne, Jr.**
Summerland, CA 93067 (US)
- **FREDRICKSON, Glenn, H.**
Santa Barbara, CA 93108 (US)
- **SCHMIDT-WINKEL, Patrick**
Goleta, CA 93117 (US)

(30) Priority: **09.12.1997 US 69143 P**
18.08.1998 US 97012 P

(43) Date of publication of application:
27.09.2000 Bulletin 2000/39

(73) Proprietor: **SBA Materials, Inc.**
Santa Barbara, California 93111 (US)

(74) Representative: **Hamilton, Alistair**
Castles,
17 Lansdowne Road
Croydon CR0 2BX (GB)

- (72) Inventors:
- **STUCKY, Galen, D.**
Goleta, CA 93117 (US)
 - **CHMELKA, Bradley, F.**
Goleta, CA 93117 (US)
 - **ZHAO, Dongyuan**
Isla Vista, CA 93117 (US)
 - **MELOSH, Nick**
Tucson, AZ 85750 (US)
 - **HUO, Qisheng**
Williamsville, NY 14221 (US)

(56) References cited:
US-A- 3 886 125 **US-A- 5 416 124**
US-A- 5 622 684

EP 1 037 940 B1

Note: Within nine months from the publication of the mention of the grant of the European patent, any person may give notice to the European Patent Office of opposition to the European patent granted. Notice of opposition shall be filed in a written reasoned statement. It shall not be deemed to have been filed until the opposition fee has been paid. (Art. 99(1) European Patent Convention).

Description

[0001] Large pore size molecular sieves are in high demand for reactions or separations involving large molecules and have been sought after for several decades. For example, Stringfield (U.S. Pat. No. 5,446,124) described polymeric adsorbent resins having both the both the high capacity associated with microporosity and the favorable kinetics associated with mesoporosity. which are useful for the chromatographic separation of organic compounds. Moreover, Chromecek (U.S. Pat. No. 3,886,125) disclosed solid macroporous polymer complexes that are suitable for use as carriers in various formulations of medical agents, antiperspirants, pesticides, flavorings, fragrances and the like.

[0002] Due to their low cost, ease of handling, and high resistance to photoinduced corrosion, many uses have been proposed for mesoporous metal oxide materials, such as SiO₂, particularly in the fields of catalysis, molecular separations, fuel cells, adsorbents, patterned-device development, optoelectronic devices, and chemical and biological sensors. One such application for these materials is the catalysis and separation of molecules that are too large to fit in the smaller 3-5 Å pores of crystalline molecular sieves, providing facile separation of biomolecules such as enzymes and/or proteins. Such technology would greatly speed processing of biological specimens, eliminating the need for time consuming ultracentrifugation procedures for separating proteins. Other applications include supported-enzyme biosensors with high selectivity and antigen expression capabilities. Another application, for mesoporous TiO₂, is photocatalytic water splitting, which is extremely important for environmentally friendly energy generation. There is also tremendous interest in using mesoporous ZrO₂, Si_{1-x}Al_xO_y, Si_{1-x}Ti_xO_y, as acidic catalysts. Mesoporous WO₃ can be used as the support for ruthenium, which currently holds the world record for photocatalytic conversion of CH₄ to CH₃OH and H₂. Mesoporous materials with semiconducting frameworks, such as SnO₂ and WO₃, can be also used in the construction of fuel cells.

[0003] Mesoporous materials in the form of monoliths and films have a broad variety of applications, particularly as thermally stable low dielectric coatings, non-linear optical media for optical computing and self-switching circuits, and as host matrices for electrically- active species (e.g. conducting and lasing polymers and light emitting diodes). Such materials are of vital interest to the semiconductor and communications industries for coating chips, as well as to develop optical computing technology which will require optically transparent, thermally stable films as waveguides and optical switches.

[0004] These applications, however, are significantly hindered by the fact that, until this invention, mesoscopically ordered metal oxides could only be produced with pore sizes in the range (15 - 100 Å), and with relatively poor thermal stability. Many applications of mesoporous metal oxides require both mesoscopic ordering and framework crystallinity. However, these applications have been significantly hindered by the fact that, until this invention, mesoscopically ordered metal oxides generally have relative thin and fragile channel walls.

[0005] Since mesoporous molecular sieves, such as the M41S family of materials, were discovered in 1992, surfactant-templated synthetic procedures have been extended to include a wide variety of compositions and conditions for exploiting the structure-directing functions of electrostatic and hydrogen-bonding interactions associated with amphiphilic molecules. For example, MCM-41 materials prepared by use of cationic cetyltrimethylammonium surfactants commonly have d(100) spacings of about 40 Å with uniform pore sizes of 20 - 30 Å. Cosolvent organic molecules, such as trimethylbenzene (TMB), have been used to expand the pore size of MCM-41 up to 100 Å, but unfortunately the resulting products possess less resolved XRD diffraction patterns. This is particularly the case concerning materials with pore sizes near the high-end of this range (ca. 100 Å) for which a single broad diffraction peak is often observed. Pinnavaia and coworkers, (See, e.g., US Patent No. 5,622,684) have used nonionic surfactants in neutral aqueous media (S0I0 synthesis at pH = 7) to synthesize worm-like disordered mesoporous silica with somewhat larger pore sizes of 20 - 58 Å (the nomenclature S⁰I⁰ or S⁺I⁻ are shorthand notations for describing mesophase synthesis conditions in which the nominal charges associated with the surfactant species S and inorganic species I are indicated). Extended thermal treatment during synthesis gives expanded pore sizes up to 50 Å; see D. Khushalani, A. Kuperman, G. A. Ozin, *Adv. Mater.* 7, 842 (1995).

[0006] The preparation of films and monolithic silicates using acidic sol-gel processing methods is an active research field, and has been studied for several decades. Many studies have focused on creating a variety of hybrid organic-silicate materials, such as Wojcik and Klein's polyvinyl acetate toughening of TEOS monoliths (Wojcik, Klein; *SPIE, Passive Materials for Optical Elements II*, 2018, 160-166 (1993)) or Lebeau et al's organ ic-inorgan ic optical coatings (B. Lebeau, Brasselet, Zyss, C. Sanchez; *Chem Mater.*, 9, 1012-1020 (1997)). The majority of these studies use the organic phase to provide toughness or optical properties to the homogeneous (non-mesostructured) monolithic composite, and not as a structure-directing agent to produce mesoscopically ordered materials. Attard and coworkers have reported the creation of monoliths with ~40 Å pore size, which were synthesized with low molecular weight nonionic surfactants, but did not comment on their thermal stability or transparency; see G. S. Attard; J. C. Glyde; C. G. G61tner, C. G. *Nature* 378, 366 (1995). Dabadie et al. have produced mesoporous films with hexagonal or lamellar structure and pore sizes up to 34 Å using cationic surfactant species as structure-directing species; see Dabadie, Ayral, Guizard, Cot, Lacan; *J. Mater Chem.*, 6, 1789-1794, (1996). However, large pore size (>50 Å) monoliths or films have not been

reported, and, prior to our invention, the use of block copolymers as structure-directing agents has not been previously explored. (after our invention, Templin et al. reported using amphiphilic block copolymers as the structure-directing agents, aluminosilicate mesostructures with large ordering lengths (>15 nm); see Templin, M., Franck, A., Chesne, A. D., Leist, H., Zhang, Y., Ulrich, R., Schädler, V., Wiesner, U. *Science* **278**, 1795 (December 5, 1997)). For an overview of advanced hybrid organic-silica composites, see Novak's review article, B. Novak; *Adv. Mater.*, **5**, 422-433 (1993).

[0007] While the use of low-molecular weight surfactant species have produced mesostructurally ordered inorganic-organic composites, the resulting materials have been in the form of powders, thin films, or opaque monoliths. Extension of prior art surfactant templating procedures to the formation of nonsilica mesoporous oxides has met with only limited success, although these mesoporous metal oxides hold more promise in applications that involve electron transport and transfer or magnetic interactions. The following mesoporous inorganic oxides have been synthesized with small mesopore sizes (< 4 nm) over the past few years:

MnO₂ (Tian, Z., Tong, W., Wang, J., Duan, N., Krishnan, V. V., Suib, S. L. *Science*.
Al₂O₃ (Bagshaw, S. A., Pinnavaia, T. J. *Angew. Chem. Int. Ed. Engl.* **35**, 1102 (1996)),
TiO₂ (Antonelli, D. M., Ying, J. Y. *Angew. Chem. Int. Ed. Engl.* **34**, 2014 (1995)),
Nb₂O₅ (Antonelli, D. M., Ying, J. Y. *Chem. Mater.* **8**, 874 (1996)),
Ta₂O₅ (Antonelli, D. M., Ying, J. Y. *Chem. Mater.* **8**, 874 (1996)),
ZrO₂ (Ciesla, U., Schacht, S., Stucky, G. D., Unger, K. K., Schüth, F. *Angew. Chem. Int. Ed. Engl.* **35**, 541 (1996)),
HfO₂ (Liu, P., Liu, J., Sayari, A. *Chem. Commun.* 557 (1997)), and reduced Pt (Attard, G. S., Barlett P. N., Coleman N. R. B., Elliott J. M., Owen, J. R., Wang, J. H. *Science*, **278**, 838 (1997)).

[0008] However these often have only thermally unstable mesostructures; see Ulagappan, N., Rao, C. N. R. *Chem Commun.* 1685 (1996), and Braun, P. V., Osenar, P., Stupp, S. I. *Nature* **380**, 325 (1996).

[0009] Stucky and co-workers first extended the surfactant templating strategy to the synthesis of non-silica-based mesostructures, mainly metal oxides. Both positively and negatively charged surfactants were used in the presence of water-soluble inorganic species. It was found that the charge density matching between the surfactant and the inorganic species is very important for the formation of the organic-inorganic mesophases. Unfortunately, most of these non-silica mesostructures are not thermally stable. Pinnavaia and co-workers, *supra*, used nonionic surfactants to synthesize mesoporous alumina in neutral aqueous media and suggested that the wormhole-disordered mesoporous materials are assembled by hydrogen-bonding interaction of inorganic source with the surfactants. Antonelli and Ying, *supra*, prepared stable mesoporous titanium oxide with phosphorus in a framework using a modified sol-gel method, in which an organometallic precursor was hydrolyzed in the presence of alkylphosphate surfactants. Mesoporous zirconium oxides were prepared using long-chain quaternary ammonium, primary amines, and amphoteric cocamidopropyl betaine as the structure-directing agents; see Kim, A., Bruinsma, P., Chen, Y., Wang, L., Liu, J. *Chem. Commun.* 161 (1997); Pacheco, G., Zhao, E., Garcia, A., Sklyaro, A., Fripiat, J. J. *Chem. Commun.* 491 (1997); and Pacheco G., Zhao, E., Garcia, A., Sklyarov, A., Fripiat, J. J. *J. Mater. Chem.* **8**, 219 (1998).

[0010] A scaffolding process was also developed by Knowles *et al.* for the preparation of mesoporous ZrO₂ (Knowles J. A., Hudson M. J. *J. Chem. Soc., Chem. Commun.* 2083 (1995)). Porous HfO₂ has been synthesized using cetyltrimethylammonium bromide as the structure-directing agent; see Liu, P., Liu, J., Sayari, A. *Chem. Commun.* 557 (1997). Suib et al, *supra*, prepared mixed-valent semiconducting mesoporous manganese oxide with hexagonal and cubic structures and showed that these materials are catalytically very active. A ligand-assisted templating approach has been successfully used by Ying and co-workers, *supra*, for the synthesis of Nb₂O₅ and Ta₂O₅. Covalent bond interaction between inorganic metal species and surfactant was utilized in this process to assemble the mesostructure. More recently, the surfactant templating strategy has been successfully extended to platinum by Attard, Barlett et al, *supra*.

[0011] For all these mesoporous non-silica oxides (except Pinnavaia's alumina work, in which copolymers were used to produce mesoporous alumina in neutral aqueous conditions), low-molecular-weight surfactants were used for the assembly of the mesostructures, and the resulting mesoporous materials generally had small mesopore sizes (<4 nm), and thin (1-3 nm) and fragile frameworks. The channel walls of these mesoporous metal oxides were exclusively amorphous. There have been claims, based solely on the X-ray diffraction data, of mesoporous ZrO₂ and MnO₂ with crystalline frameworks; see Bagshaw and Pinnavaia, *supra*, and Huang, Y., McCarthy, T. J., Sachtler, W. M. *Appl. Catal. A* **148**, 135 (1996). However, the reported X-ray diffraction patterns cannot exclude the possibility of phase separation between the mesoporous and crystalline materials, and therefore their evidence has been inconclusive. In addition, most of the syntheses were carried out in aqueous solution using metal alkoxides as inorganic precursors. The large proportion of water makes the hydrolysis and condensation of the reactive metal alkoxides and the subsequent mesostructure assembly extremely difficult to control.

[0012] For an overview of the non-silica mesoporous materials prior to this invention, see the Sayari and Liu review article, Sayari, A., Liu, P. *Microporous Mater.* **12**, 149 (1997).

[0013] There has also been a need for porous inorganic materials with structure function on different length scales,

for use in areas as diverse as large-molecule catalysis, biomolecule separation, the formation of semiconductor nanostructure, the development of medical implants and the morphogenesis of skeletal forms. The use of organic templates to control the structure of inorganic solid has proven very successful for designing porous materials with pore size ranging from angstroms to micrometers. For example, microporous aluminosilicate and aluminophosphate zeolite-type structures have been templated by organic moleculars such as amines. Larger mesoporous (20 - 300 Å) materials have been obtained by using long-chain surfactant as structure-directing-agents. Recent reports illustrate that techniques such as surfactant emulsion or latex sphere templating have been used to create TiO₂, ZrO₂, SiO₂ structures with pore sizes ranging from 100 nm to 1 μm. Recently, Nakanishi used a process that combined phase separation, solvent exchange with sol-gel chemistry to prepare macroscopic silica structures with random meso and macro-porous structure; see K. Nakanishi, *J. Porous Mater.* **4**, 67 (1997). Mann and coworkers used bacterial threads as the templates to synthesize ordered macrostructures in silica-surfactant mesophases; see Davis, S. L. Burkett, N. H. Mendelson, S. Mann, *Nature*, 385,420 (1997)

[0014] Researchers have commented on the assembly of inorganic composites directed by protein or organic surfactants, but little on the effect of inorganic salts on the self-assembly of macroscopic silica or calcium carbonate structures with diatom, coral morphologies; see Davis, S. L. Burkett, N. H. Mendelson, S. Mann, *Nature*, 385,420 (1997); A. M. Belcher, X. H. Wu, R. J. Christensen, P. K. Hansma, G. D. Stucky, *Nature*, 381,56 (1996); and X. Y. Shen, A. M. Belcher, P. K. Hansma, G. D. Stucky, et al., *Bio. Chem.*, 272,32472 (1997).

BRIEF SUMMARY OF THE INVENTION

[0015] The invention in its various embodiments is as set out in the accompanying claims.

[0016] The present invention overcomes the drawbacks of prior efforts to prepare mesoporous materials and mesoscopic structures, and provides heretofore unattainable materials having very desirable and widely useful properties. These materials are prepared by using amphiphilic block copolymer species to act as structure-directing agents for metal oxides in self-assembling systems. Aqueous metal cations partition within the hydrophilic regions of the self-assembled system and associate with the hydrophilic polymer blocks. Subsequent polymerization of the metalate precursor species under strongly acidic conditions (e. g., pH 1), produces a densely cross linked, mesoscopically ordered metal oxide network. Mesoscopic order is imparted by cooperatives self-assembly of the inorganic and amphiphilic species interacting across their hydrophilic-hydrophobic interface.

By slowly evaporating the aqueous solvent, the composite mesostructures can be formed into transparent, crack-free films, fibers or monoliths, having two-dimensional hexagonal (*p6mm*), cubic (*Im3m*), or lamellar mesostructures, depending on choice of the block copolymers. Heating to remove the organic template yields a mesoporous product that is thermally stable in boiling water. Calcination yields mesoporous structures with high BET surface areas. Unlike traditional sol-gel films and monoliths, the mesoscopically ordered silicates described in this invention can be produced with high degrees of order in the 100-200 Å length scale range, extremely large surface areas, low dielectric constants, large anisotropy, can incorporate very large host molecules, and yet still retain thermal stability and the transparency of fully densified silicates.

[0017] In accordance with a further embodiment of this invention, inorganic oxide membranes are synthesized with three-dimension (3-d) meso-macro structures using simultaneous multiphase assembly. Self-assembly of polymerized inorganic oxide species/amphiphilic block copolymers and the concurrent assembly of highly ordered mesoporous inorganic oxide frameworks are carried out at the interface of a third phase consisting of droplet of strong electrolyte inorganic salts/water solution. The result is a 2-d or 3-d macroporous/mesoporous membranes which, with silica, are coral-like, and can be as large as 4 cm x 4 cm with a thickness that can be adjusted between 10 μm to several millimeters. The macropore size (0.5 - 100 μm) can be controlled by varying the electrolyte strength of inorganic salts and evaporation rate of the solvents. Higher electrolyte strength of inorganic salts and faster evaporation result in a thicker inorganic oxide a framework and larger macropore size. The mesoscopic structure, either 2-d hexagonal (*p6mm*, pore size 40 - 90 Å) or 3-d cubic array, can be controlled by amphiphilic block copolymer templates. The resulting membranes are thermally stable and have large surface areas up to 1000 m²/g, and pore volume up to 1.1 cm³/g. Most importantly, these meso-macroporous coral-like planes provide excellent access to the mesopore surfaces for catalytic, sorption, catalysis, separation, and sensor arrays, applications.

BRIEF DESCRIPTION OF THE DRAWINGS

[0018]

Figure 1 shows a size comparison between two prior art porous inorganic materials, Faujasite and MCM-41, and SBA-15, prepared in accordance with this invention.

Figure 2 shows powder X-ray diffraction (XRD) patterns of as-synthesized and calcined mesoporous silica (SBA-15) prepared using the amphiphilic polyoxyalkylene block copolymer $\text{PEO}_{20}\text{PPO}_{70}\text{PEO}_{20}$.

Figure 3 shows scanning electron micrographs (SEM's) (a, b) of as-synthesized SBA-15 and transmission electron micrographs (TEM's) (c, d) with different orientations of calcined hexagonal mesoporous silica SBA-15 prepared using the block copolymer $\text{PEO}_{20}\text{PPO}_{70}\text{PEO}_{20}$.

Figure 4 shows nitrogen adsorption-desorption isotherm plots (top) and pore size distribution curves (bottom) measured using the adsorption branch of the isotherm for calcined mesoporous silica SBA-15 prepared using the block copolymer $\text{PEO}_{20}\text{PPO}_{70}\text{PEO}_{20}$ (a, b) without and (c, d) with TMB as an organic additive.

Figure 5 shows transmission electron micrographs with different pore sizes and silica wall thicknesses for calcined hexagonal mesoporous silica SBA-15 prepared using the block copolymer $\text{PEO}_{20}\text{PPO}_{70}\text{PEO}_{20}$. (a) pore size of 47 Å, silica wall thickness of 60 Å; (b) pore size of 89 Å, silica wall thickness of 30 Å; (c) pore size of 200 Å; (d) pore size of 260 Å.

Figure 6 shows powder X-ray diffraction (XRD) patterns of as-synthesized and calcined mesoporous silica SBA-15.

Figure 7 shows variation of the $d(100)$ spacing (solid) and pore size (open) for mesoporous hexagonal SBA-15 calcined at 500°C for 6 h in air (circles) and for mesoporous MCM-41 (squares) as functions of the TMB/amphiphile (copolymer or surfactant) ratio (g/g).

Figure 8 shows ^{29}Si MAS NMR spectra of as-synthesized silica-copolymer mesophase materials; (a) SBA-11 prepared by using Brij $\text{C}_{16}\text{EO}_{10}$ surfactant; (b) SBA-15 prepared using $\text{PEO}_{20}\text{PPO}_{70}\text{PEO}_{20}$ block copolymer.

Figure 9 shows thermogravimetric analysis (TGA) and differential thermal analysis (DTA) traces for the as-synthesized SBA-15 prepared by using the block copolymer $\text{PEO}_{20}\text{PPO}_{70}\text{PEO}_{20}$.

Figure 10 shows powder X-ray diffraction (XRD) patterns of (a), as-synthesized and, (b) calcined MCM-41 silica prepared using the cationic surfactant $\text{C}_{16}\text{H}_{33}\text{N}(\text{CH}_3)_3\text{Br}$; and (c), calcined MCM-41 after heating in boiling water for 6 h; Calcined SBA-15 (d, e) prepared by using the block copolymer $\text{PEO}_{20}\text{PPO}_{70}\text{PEO}_{20}$ after heating in boiling water for (d), 6 h; (e), 24 h.

Figure 11 shows photographs of transparent SBA-15 silica-copolymer monoliths incorporating (a) 27 wt% and (b) 34 wt% of the PEO-PPO-PEO structure-directing copolymer Pluronic F127.

Figure 12 shows a 200-keV TEM image of a 38 wt% SBA-15 silica-copolymer monolith prepared with Pluronic F127.

Figure 13 shows (a) a photograph of a transparent 50- μm -thick SBA-15 silicacopolymer film prepared with Pluronic P104. (b) an X-ray diffraction pattern of this film showing well resolved peaks that are indexable as (100), (110), (200), and (210) reflections associated with $p6mm$ hexagonal symmetry in which the one-dimensional axes of the aggregates lie horizontally in the plane of the film.

Figure 14 shows the predicted variation of optical dielectric constant and refractive index as a function of silica porosity.

Figure 15 shows low-angle and wide-angle X-ray diffraction (XRD) patterns of (a, c), as-made zirconium/ $\text{EO}_{20}\text{PO}_{70}\text{EO}_{20}$ composite mesostructure and (b, d) calcined mesoporous ZrO_2 . The XRD patterns were obtained with a Scintag PADX diffractometer using $\text{Cu K}\alpha$ radiation.

Figure 16 shows TEM micrographs of 2-dimensional hexagonal mesoporous ZrO_2 . (a) and (b) are recorded along the [110] and [001] zone axes, respectively. Inset in (b) is the selected-area electron diffraction pattern obtained on the image area. The images were recorded with a 200 kV JEOL transmission electron microscope. All samples were calcined at 400 °C for 5 hr to remove the block copolymer surfactant species.

Figure 17 shows TEM micrographs of 2-dimensional hexagonal mesoporous TiO_2 . (a) and (b) are recorded along the [110] and [001] zone axes, respectively. Inset in (a) is the selected-area electron diffraction pattern obtained on the image area.

Figure 18 shows TEM micrographs of 2-dimensional hexagonal mesoporous SnO₂. (a) and (b) are recorded along the [110] and [001] zone axes, respectively. Inset in (a) is selected-area electron diffraction pattern obtained on the image area.

5 Figure 19 shows TEM micrographs of 2-dimensional hexagonal mesoporous WO₃. (a) and (b) are recorded along the [110] and [001] zone axes, respectively.

Figure 20 shows TEM micrograph of 2-dimensional hexagonal mesoporous Nb₂O₅, recorded along the [001] zone axis. Inset is selected-area electron diffraction pattern obtained on the image area.

10 Figure 21 shows TEM micrograph of 2-dimensional hexagonal mesoporous Ta₂O₅ recorded along the [001] zone axis.

Figure 22 shows TEM micrographs of disordered hexagonal mesoporous Al₂O₃.

15 Figure 23 shows TEM micrograph of 2-dimensional hexagonal mesoporous HfO₂ recorded along the [110] zone axis.

20 Figure 24 shows TEM micrographs of 2-dimensional hexagonal mesoporous SiTiO₄ recorded along the [001] zone axis.

Figure 25 shows TEM micrographs of 2-dimensional hexagonal mesoporous SiAlO_{3.5}. (a) and (b) are recorded along the [110] and [001] zone axes, respectively.

25 Figure 26 shows TEM micrograph of 2-dimensional hexagonal mesoporous ZrTiO₄ recorded along the [001] zone axes.

Figure 27 shows (a) Bright field TEM image of a thin slice of the mesoporous TiO₂ sample. (b) Dark field image obtained on the same area of the same TiO₂ sample. The bright spots in the image correspond to TiO₂ nanocrystals.

30 Figure 28 shows (a) Bright field TEM image of a thin slice of the mesoporous ZrO₂ sample. (b) Dark field image obtained on the same area of the same ZrO₂ sample. The bright spots in the image correspond to ZrO₂ nanocrystals.

35 Figure 29 shows nitrogen adsorption-desorption isotherms and pore size distribution plots (inset) calculated using BJH model from the adsorption branch isotherm for calcined ZrO₂. The isotherms were measured using a Micromeritics ASAP 2000 system. The samples were outgassed overnight at 200 °C before the analyses.

40 Figure 30 shows nitrogen adsorption-desorption isotherms (a) and pore size distribution plots (b) calculated using BJH model from the adsorption branch isotherm for calcined TiO₂. Inset in (b) is the EDX spectrum obtained on the mesoporous samples.

45 Figure 31 shows nitrogen adsorption-desorption isotherms and pore size distribution plots (lower inset) calculated using BJH model from the adsorption branch isotherm for calcined Nb₂O₅. EDX spectrum obtained on the mesoporous samples is shown in the upper inset.

Figure 32 shows nitrogen adsorption-desorption isotherms and pore size distribution plots (lower inset) calculated using BJH model from the adsorption branch isotherm for calcined Ta₂O₅. EDX spectrum obtained on the mesoporous samples is shown in the upper inset.

50 Figure 33 shows nitrogen adsorption-desorption isotherms and pore size distribution plots (inset) calculated using BJH model from the adsorption branch isotherm for calcined Al₂O₃.

55 Figure 34 shows nitrogen adsorption-desorption isotherms and pore size distribution plots (inset) calculated using BJH model from the adsorption branch isotherm for calcined WO₃.

Figure 35 shows nitrogen adsorption-desorption isotherms (a) and pore size distribution plots (b) calculated using BJH model from the adsorption branch isotherm for calcined SiTiO₄.

Figure 36 shows nitrogen adsorption-desorption isotherms (a) and pore size distribution plots (b) calculated using BJH model from the adsorption branch isotherm for calcined ZrTiO₄.

Figure 37 shows low-angle and wide-angle X-ray diffraction (XRD) patterns of (a, c), as-made titanium/EO₂₀BO₇₅ composite cubic mesostructure and (b, d) calcined mesoporous TiO₂.

Figure 38 shows TEM micrograph of cubic mesoporous TiO₂.

Figure 39 shows TEM micrograph of cubic mesoporous ZrO₂.

Figure 40 shows SEM image of calcined mesoporous Al₂O₃ monolithic thick film. The image was recorded on JEOL 6300FX microscope.

Figure 41 shows scanning electron micrographs (SEM) of (a, b) as-synthesized meso-macro silica membranes prepared by using P123 block copolymer (EO₂₀PO₇₀EO₂₀) in NaCl solution after washing out NaCl with de-ionic water; (c), small macropore size silica membrane prepared by adding a little amount ethylene glycol in P123 block copolymer and NaCl solution; (d), silica membrane prepared with fast evaporation by using P123 block copolymer in NaCl solution. (e), silica membrane with grape vine morphology prepared with high concentration of NaCl; (f), inorganic salt NaCl crystals co-grown with the silica membrane.

Figure 42 shows scanning electron micrographs (SEM) of (a, b, c) as-synthesized meso-macro silica membranes prepared by using P123 block copolymer (EO₂₀PO₇₀EO₂₀) in (a), KCl; (b), NH₄Cl; (c), NaNO₃ solution after washing out inorganic salts with de-ionic water. (d), large macropore size silica membrane prepared by using P65 block copolymer (EO₂₆PO₃₉EO₂₆) in NaCl solution.

Figure 43 shows SEM images of as-synthesized silica membranes after washed with water prepared by (a), using F127 block copolymer (EO₁₀₆PO₇₀EO₁₀₆) in NaCl solution; (b, c, d), using P123 block copolymer in (b), MgSO₄ solution; (c), MgCl₂ solution; (d), Na₂SO₄ solution.

Figure 44 shows powder X-ray diffraction (XRD) patterns of as-synthesized and calcined mesomacro silica membranes prepared using the amphiphilic polyoxyalkylene block copolymer (a), P123, EO₂₀PO₇₀EO₂₀; (b), P103, EO₁₇PO₈₅EO₁₇; (c); P65, EO₂₆PO₃₉EO₂₆. The chemical composition of the reaction mixture was 1 g copolymer: 0.017 mol NaCl: 0.01 mol TEOS: 4 x 10⁻⁵ mol HCl: 0.72 mol H₂O: 0.33 mol EtOH.

Figure 45 shows transmission electron micrographs (TEM) (a, b) of calcined silica membrane prepared using the block copolymer P 123 in NaCl solution recorded in (a), (100); (b), (110) zone axes; (c, d) of calcined silica membrane prepared by adding a little amount of ethylene glycol. TEM were taken on a 2000 JEOL electron microscope operating at 200 kV.

Figure 46 shows thermogravimetric analysis (TGA) and differential thermal analysis (DTA) traces for the as-synthesized meso-macroporous silica membranes prepared by using the block copolymer P123 (EO₂₀PO₇₀EO₂₀) in NaCl solution, (top), after removal NaCl by washing with water; (bottom), without removal NaCl.

Figure 47 shows nitrogen adsorption-desorption isotherm plots (a) and pore size distribution curves (b) for meso-macro silica membranes prepared using block copolymer P123 in NaCl solution without removal inorganic salt NaCl.

Figure 48 shows nitrogen adsorption-desorption isotherm plots (top) and pore size distribution curves (bottom) for calcined meso-macro silica membranes prepared in NaCl solution using different block copolymers.

Figure 49 shows nitrogen adsorption-desorption isotherm plots (a) and pore size distribution curves (b) for calcined meso-macro silica membranes prepared using block copolymer F127 in NaCl solution.

Figure 50 shows nitrogen adsorption-desorption isotherm plots (a) and pore size distribution curves (b) for calcined meso-macro silica membranes prepared using non-ionic oligomeric surfactant Brij 76 (C₁₈H₃₇EO₁₀OH) in NaCl solution.

Figure 51 shows SEM images of (a)-(d), as-synthesized silica membranes prepared by using P123 block copolymer

in LiCl solution without washing recorded at different region, (a), top region; (b) middle region; (c), same (b) with large magnification; (d), bottom region of the membrane. (e)-(h) as-synthesized silica membranes prepared by using P123 block copolymer in NiSO₄ solution without washing recorded at different region, (a), top region; (b) same (a) with large magnification; (c) bottom region of the membrane; (d), disk-like NiSO₄ crystal.

Figure 52 shows the change of the compositions of the reaction mixture functioned with evaporation time. Change of the concentration in liquid phase of ethanol (open circle); water (solid circle); LiCl (open square); SiO₂ (solid square); Intensity ratio for (100) diffraction of silica-block copolymer mesophase (open triangle) and for (110) diffraction of LiCl crystal (solid triangle) at d spacing of 3.59 Å determined by XRD in solid phase.

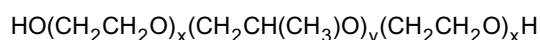
Figure 53 shows a schematic diagram of the simple procedure used to prepare coral-like meso-macro silica membranes.

Figure 54 shows progressively higher magnifications of a section of a meso-macro silica membrane made in accordance with this invention..

DETAILED DESCRIPTION OF THE INVENTION

[0019] This invention provides a simple and general procedure for the syntheses of ordered large-pore (up to 14 nm) mesoporous metal oxides, including TiO₂, ZrO₂, Nb₂O₅, Ta₂O₅, Al₂O₃, SiO₂, WO₃, SnO₂, HfO₂ and mixed oxides SiAlO_{3.5}, SiAlO_{5.5}, Al₂TiO₅, ZrTiO₄, SiTiO₄. Commercially available, low-cost, non-toxic, and biodegradable amphiphilic poly(alkylene oxide) block copolymers can be used as the structure-directing agents in non-aqueous solutions for organizing the network forming metal species. Preferably the block copolymer is a triblock copolymer in which a hydrophilic poly(alkylene oxide) such as poly(ethylene oxide (EO_x) is linearly covalent with the opposite ends of a hydrophobic poly(alkylene oxide) such as poly(propylene) oxide (PO_y) or a diblock polymer in which, for example, poly(ethylene oxide) is linearly covalent with poly(butylene oxide) (BO_y). This can variously be designated as follows:

poly(ethylene oxide)-poly(propylene oxide)-poly(polyethylene oxide)

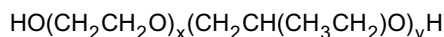


PEO-PPO-PEO



or

poly(ethylene oxide)-poly(butylene oxide)-poly(polyethylene oxide)



PEO-PBO-PEO



where x is 5 or greater and y is 30 or greater, with no theoretical upper limit to either value subject to practical considerations. Alternatively, for particular applications, one can use a reverse triblock copolymer or a star block amphiphilic poly(alkylene oxide) block copolymer, for example, a star di-block copolymer or a reversed star di-block copolymer. Inexpensive inorganic salts rather than alkoxides or organic metal complexes are used as precursors. Both two-dimensional hexagonal (*p6mm*) and cubic (*Im3m*) mesostructures can be obtained, as well as lamellar mesostructures, depending on the choice of the block copolymers. Calcination at 400 °C yields mesoporous structures with high BET

surface area (100 - 850 m²/g), porosity of 40 - 65%, large *d* spacings (60 - 200 Å), pore sizes of 30 -140 Å, and wall thickness of 30 - 90 Å.

[0020] These novel mesoporous metal oxides are believed to be formed through a mechanism that combines block copolymer self-assembly with chelating complexation of the inorganic metal species. A unique aspect of these thermally stable mesoporous oxides is their robust inorganic framework and thick channel walls, within which a high density of nanocrystallites can be nucleated during calcination without disrupting the mesoscopic ordering. In addition, variations of this simple sol-gel process yield mesoporous oxides with technologically important forms including thin films, monoliths and fibers. The nanocrystalline framework, periodic large-pore structures, and high versatility of the inexpensive synthetic methodology make these mesoporous materials an excellent choice for applications including catalysis, molecular separations, fuel cells, adsorbents, optoelectronic devices, and chemical and biological sensors. For example, due to its low cost, ease of handling, and high resistance to photoinduced corrosion, one application for mesoporous TiO₂ is photocatalytic water splitting, which is extremely important for environmentally friendly energy generation. There is also tremendous interest in using mesoporous ZrO₂, Si_{1-x}Al_xO_y, Si_{1-x}Ti_xO_y, as acidic catalysts. Mesoporous WO₃ can be used as the support for ruthenium, which currently holds the world record for photocatalytic conversion of CH₄ to CH₃OH and H₂. Mesoporous materials with semiconducting frameworks, such as SnO₂ and WO₃, can be also used in the construction of fuel cells.

[0021] Many applications of mesoporous metal oxides require both mesoscopic ordering and framework crystallinity. The mesoporous metal oxides of this invention are thermally stable and retain their mesoscopic ordering and structural integrity even after the nucleation of the high density of nanocrystallites within thick, robust channel walls. Development of such thermally stable, large-pore mesoporous metal oxide materials with nanocrystalline frameworks using lowcost, non-toxic, and biodegradable polyalkylene oxide block copolymers has enormous potential for a variety of immediate and future industrial applications.

[0022] In practicing this invention, one can use any amphiphilic block polymer having substantial hydrophilic and hydrophobic components and can use any inorganic material that can form crown-ether-type complexes with alkylene oxide segments through weak coordination bonds. The inorganic material can be any inorganic compound of a multi-valent metal species, such as metal oxides and sulphides, preferably the oxides. The metal species preferentially associates with the hydrophilic poly(ethylene oxide) (PEO) moieties. The resulting complexes then self-assemble according to the mesoscopic ordering directed principally by microphase separation of the block copolymer species. Subsequent crosslinking and polymerization of the inorganic species occurs to form the mesoscopically ordered inorganic/block-copolymer composites. The proposed assembly mechanism for these diverse mesoporous metal oxides uses PEO-metal complexation interactions, in conjunction with (for example) electrostatic, hydrogen bonding, and van der Waals forces to direct mesostructure formation.

[0023] As indicated above, one can carry out the assembly process in non-aqueous media using metal halides as the inorganic precursors, which effectively slows the hydrolysis/condensation rates of the metal species and hinders subsequent crystallization. Restrained hydrolysis and condensation of the inorganic species appears to be important for forming mesophases of most of the non-silica oxides, because of their strong tendency to precipitate and crystallize into bulk oxide phases directly in aqueous media.

[0024] The procedures of the present invention enable close control of the porosity of the final structure by varying the proportions of PEO and PPO or PBO and by adding an organic solvent to swell the PPO or PBO.

[0025] Because of their low cost, widespread use, and ease of preparation, we will first describe and exemplify the preparation of mesoporous silica, followed by the preparation of other metal oxides. We will then describe the multiphase assembly of meso-macro membranes, which we will exemplify with silica membranes.

Mesoporous silicas

[0026] In accordance with this invention, we have synthesized a family of high quality, hydrothermally stable and ultra large pore size mesoporous silicas by using amphiphilic block copolymers in acidic media. One member of the family, to which we have assigned the designation SBA-15, has a highly ordered, two-dimensional hexagonal (*p6mm*) honeycomb, hexagonal cage or cubic cage mesostructures. Calcination at 500°C yields porous structures with high BET surface areas of 690 - 1040 m²/g, and pore volumes up to 2.5 cm³/g, ultra large *d*(100) spacings of 74.5 - 450 Å, pore sizes from 46 - 500 Å and silica wall thicknesses of 31 - 64 Å. SBA-15 can be readily prepared over a wide range of specific pore sizes and pore wall thicknesses at low temperature (35 - 80°C) using a variety of commercially available, low-cost, non-toxic, and biodegradable amphiphilic block copolymers, including triblock polyoxyalkylenes, as described below. In general, all microphase-separating, domain-partitioning copolymer systems can be considered as candidates for the synthesis of such mesostructured materials, depending on solution composition, temperature, processing conditions, etc. The pore size and thickness of the silica wall is selectively controlled by varying the thermal treatment of SBA-15 in the reaction solution and by the addition of cosolvent organic molecules, such as 1,3,5-trimethylbenzene (TMB). The organic template can be easily removed by heating at 140°C for 3 h, yielding the mesoporous SBA-15

product, which is thermally stable in boiling water.

[0027] Transparent films, fibers, and monolithic materials with mesoscopic order can also be prepared by a similar process utilizing the same family of triblock polyoxyalkylene copolymers, yielding mesoporous structure in bulk. These materials are similarly synthesized in acidic media at low temperatures (20-80°C), and display a variety of well-ordered copolymer phases with mesostructures of about 100-500 Å. They can be processed (e.g., molded) into a variety of bulk shapes, which are also transparent. In addition, it is possible to use polymer processing strategies, such as shear alignment, spin casting, and fiber drawing to induce orientational order in these materials. After calcination at 350°C these monoliths and films retain their macroscopic shape and mesoscopic morphology. To our knowledge, these are the first reported thermally stable, transparent, monolithic, large pore-size materials with well-ordered mesostructure. Their dielectric constants can be varied to low values via the Lorentz-Lorenz relationship by tuning the pore volume fraction from 0.6 to as much as 0.86. The fluid sol processability, extraordinary periodic pore and cage structures, high pore volume fraction and inexpensive synthesis make them excellent low dielectric materials for inter-level dielectrics (LID) for ori-chip interconnects to provide high speed, low dynamic power dissipation and low cross-talk noise.

[0028] To produce the highly ordered, ultra large pore silica mesostructures we adopted an S⁺I-X⁻I⁺ synthesis processing strategy. This synthesis methodology is distinctly different from the S⁺I⁻ route (pH > 3) used to make the M41S family of mesoporous materials: the two methods employ conditions that are on opposite sides of the isoelectric point of aqueous silica (pH = 2). For example, mesoporous silica SBA-15 can be synthesized using block copolymers, which that have a polyoxyethylene-polyoxypropylene-polyoxyethylene (PEO-PPO-PEO) sequence centered on a (hydrophobic) polypropylene glycol nucleus terminated by two primary hydroxyl groups; see Table 1 The synthesis is carried out in acidic (e.g., HCl, HBr, H₂SO₄, HNO₃, H₃PO₄) media at 35 - 80°C using either tetraethylortho-silicate (TEOS), tetramethylorthosilicate (TMOS), or tetrapropoxysilane (TPOS) as the silica source.

[0029] Hexagonal SBA-15 has a wheat-like macroscopic morphology, a highly ordered (four to seven peaks in the X-ray diffraction pattern), two-dimensional hexagonal (*p6mm*) mesostructure, BET surface areas up to 1040 m²/g, pore volumes to 2.5 cm³/g, and thick silica walls (31 - 64 Å). The thick silica walls in particular are different from the thinner-walled MCM-41 mesostructures made with conventional low molecular weight cationic surfactants. The pore size and the thickness of the silica wall can be adjusted by varying the heating temperature (35 - 140°C) or heating time (11 - 72 h) of the SBA-15 in the reaction solution and by adding organic swelling agents such as 1,3,5-trimethylbenzene. The thick walls of the hexagonally ordered pores of these materials produce a novel combination of a high degree of both mesoscopic organization and hydrothermal stability. Based on the above properties, SBA-15 materials have potential applications in catalysis, separations, chemical sensors, and adsorbents.

[0030] Transparent films and monoliths have been synthesized with similar PEO-PPO-PEO copolymers as structure-directing agents in an acidic sol-gel reaction. These materials can be synthesized with various amounts of water, acid, silicate source, and polymer to yield different mesophase structures depending upon the polymer and processing conditions used. The materials consist of a collection of aggregates of an organic polymer component, such as the amphiphilic copolymer Pluronic F127, which for a hexagonal array that organizes a polymerized silica matrix in the interstices between the polymer aggregates. Such morphologies are formed by interactions among the block copolymer and the oligomeric silicate species, and solidified as the silica polymerizes to form a monolithic structure. The polymer is not strongly incorporated into the silica walls, as inferred from the remarkably low temperature (150°C) needed to remove the polymer, and supporting ¹H nuclear magnetic resonance (NMR) relaxation measurements. These structures possess characteristic length scales of 100-200 Å and have very large domain sizes (>1 μm), yet retain good transparency. Upon calcination the monoliths become opaque, though retain their bulk shape and possess mesoscopically ordered, hexagonally arranged pores (100-200 Å diameter), which impart high internal surface areas to the materials (ca. 1000 M²/g).

Synthesis of highly mesoscopically ordered ultra-large-pore, and hydrothermally stable mesoporous silica.

[0031] Referring to Figures 1a,b,c and d, there is shown, approximately to scale, two prior art inorganic oxide porous structures and the SBA-15 produced in accordance with this invention. As shown in Figures 1a and 1b Faujasite, a sub-nanoporous zeolite has a pore size of less than 1 nm. MCM-41, a mesoporous molecular sieve material, shown at Figure 1c, has a pore size of about 8nm. In contrast, as shown in Figure 1d, SBA-15, the ultra large pore mesoporous silica material produced by this invention, has a pore size of about 20nm, in this particular example.

[0032] Mesoporous silica SBA-15 was synthesized at 35 - 80°C using a hydrophilic-hydrophobic-hydrophilic PEO-PPO-PEO triblock copolymer as the structure-directing-agent. 4.0 g of Pluronic P123 (PEO₂₀PP0₇₀PEO₂₀) was dissolved in 30 g water and 120 g (2 M) HCl solution while stirring at 35°C. To the resulting homogeneous solution 8.50 g TEOS was added while stirring at 35°C for 22 h. The mixture was then aged at 100°C without stirring for 24 h. The solid product was filtered, washed, and air-dried at room temperature. Calcination was carried out in air by slowly increasing the temperature (from room temperature to 500°C over 8 h) and heating at 500°C for 6 h.

[0033] X-ray diffraction is an important means for characterizing the SBA-15 family of materials. Figures 2a and 2b

show small-angle XRD patterns for as-synthesized and calcined hexagonal mesoporous silica SBA-15 prepared by using the polyoxyalkylene triblock copolymer $\text{PEO}_{20}\text{PPO}_{70}\text{PEO}_{20}$ (Pluronic P123). The chemical composition of the reaction mixture was 4 g of the copolymer : 0.041 M TEOS : 0.24 M HCl : 6.67 M H_2O . The XRD patterns were acquired on a Scintag PADX diffractometer equipped with a liquid nitrogen cooled germanium solid-state detector using $\text{Cu K}\alpha$ radiation. The X-ray pattern of as-synthesized hexagonal SBA-15 (Figure 2a) shows four well-resolved peaks that are indexable as (100), (110), (200), and (210) reflections associated with $p6mm$ hexagonal symmetry. The as-synthesized SBA-15 possesses a high degree of hexagonal mesoscopic organization indicated by three additional weak peaks that are present in the 2θ range of $1 - 3.5^\circ$, corresponding to the (300), (220), and (310) scattering reflections, respectively. The intense (100) peak reflects a d -spacing of 104 Å, corresponding to a large unit cell parameter ($a = 120$ Å). After calcination in air at 500°C for 6 h, the XRD pattern (Figure 2b) shows that the $p6mm$ morphology has been preserved, although the peaks appear at slightly higher 2θ values with $d(100) = 95.7$ Å and a cell parameter (a_0) of 110 Å. Six XRD peaks are still observed, confirming that hexagonal SBA-15 is thermally stable. A similarly high degree of mesoscopic order is observed for hexagonal SBA-15 even after calcination to 850°C .

[0034] SEM images (Figures 3a, 3b) reveal that as-synthesized hexagonal SBA-15 has a wheat-like morphology with uniform particle sizes of about ~ 80 μm , and that these consist of many rope-like macrostructures. The SEM's were obtained on a JEOL 6300-F microscope. Calcined hexagonal SBA-15 at 500°C in air shows a similar particle morphology, reflecting the thermal stability of the macroscopic shape and structure. TEM images (Figure 3c, 3d) of calcined SBA-15 with different sample orientations show well ordered hexagonal arrays of mesopores (one-dimensional channels) and further confirm that SBA-15 has a two-dimensional $p6mm$ hexagonal structure. The TEM's were acquired using a 2000 JEOL electron microscope operating at 200 kV. For the TEM measurements, samples were prepared by dispersing the powder products as a slurry in acetone and subsequently deposited and dried on a holey carbon film on a Ni grid. From high-dark contrast in the TEM images, the distance between mesopores is estimated to be about 110 Å, in agreement with that determined from XRD data.

[0035] Nitrogen adsorption-desorption isotherm plots and the corresponding pore-size distribution curves are shown in Figure 4 for calcined hexagonal SBA-15 samples that were prepared using the copolymer $\text{PEO}_{20}\text{PPO}_{70}\text{PEO}_{20}$. The sample corresponding to the measurements shown in Figures 4a and 4b was prepared by reaction at 35°C for 20 h, heating at 100°C for 48 h, and subsequent calcination in air at 500°C , yielding a hexagonal SBA-15 product material with a mean pore size of 89 Å, a pore volume of 1.17 cm^3/g , and a BET surface area of 850 m^2/g . The sample corresponding to the measurements shown in Figures 4c and 4d was prepared under identical conditions but additionally used TMB as an organic swelling agent to increase the pore size of the subsequent product material. Using TMB yields hexagonal mesoporous SBA-15 silica with a mean pore size of 260 Å, a pore volume of 2.2 cm^3/g , and a BET surface area of 910 m^2/g . The isotherms were measured using a Micromeritics ASAP 2000 system. Data were analyzed by the BJH (Barrett-Joyner-Halenda) method using the Halsey equation for multilayer thickness. The pore size distribution curve was obtained from an analysis of the adsorption branch of the isotherm. The pore volumes were taken at $P/P_0 = 0.983$ signal point. Prior to the BET measurements, the samples were pretreated at 200°C overnight on a vacuum line. In both Figures 4a and 4c, three well-distinguished regions of the adsorption isotherm are evident: (1) monolayer-multilayer adsorption, (2) capillary condensation, and (3) multilayer adsorption on the outer particle surfaces. In contrast to N_2 adsorption results for MCM-41 mesoporous silica with pore sizes less than 40 Å, a clear type H, hysteresis loop in the adsorption-desorption isotherm is observed for hexagonal SBA-15 and the capillary condensation occurs at a higher relative pressure ($P/P_0 = 0.75$). The approximate pore size calculated using the BJH analysis is significantly smaller than the repeat distance determined by XRD, because the latter includes the thickness of the pore wall. Based on these results, the thickness of the pore wall is estimated to be ca. 31 Å (Table 1) for hexagonal SBA-15 prepared using the $\text{PEO}_{20}\text{PPO}_{70}\text{PEO}_{20}$ copolymer.

[0036] Heating as-synthesized SBA-15 in the reaction solution at different temperatures ($80 - 140^\circ\text{C}$) and for different lengths of time (11 72 h) resulted in a series of structures with different pore sizes ($47 - 89$ Å) and different silica wall thicknesses ($31 - 64$ Å) (as presented in Table 1). The pore sizes and the wall thicknesses determined for hexagonal SBA-15 from TEM images (such as shown in Figures 5a, 5b) are in agreement with those estimated from X-ray and N_2 adsorption measurements. The walls are substantially thicker than those typical for MCM-41 (commonly $10 - 15$ Å) prepared using alkylammonium ion surfactant species as the structure directing-agents. Higher temperatures or longer reaction times result in larger pore sizes and thinner silica walls, which may be caused by the high degree of protonation of the long hydrophilic PEO blocks of the copolymer under the acidic S^+X^- synthesis conditions. EOH moieties are expected to interact strongly with the silica species and to be closely associated with the inorganic wall. Increasing the reaction temperature results in increased hydrophobicity of the PEO block group, and therefore on average smaller numbers of the EOH groups that are associated with the silica wall (see below) and thus increased pore sizes.

[0037] The pore size of hexagonal mesoporous SBA-15 can be increased to ~ 300 Å by the addition of cosolvent organic molecules such as 1,3,5-trimethylbenzene (TMB). In a typical preparation, 4.0 g of Pluronic P123 was dissolved in 30 g water and 120 g (2 M) HCl solution with stirring at room temperature. After stirring to dissolve completely the polymer, 3.0 g TMB was added with stirring for 2 h at 35°C . 8.50 g TEOS was then added to the above homogeneous

solution with stirring at 35°C for 22 h. The mixture was then transferred to a Teflon autoclave and heated at 100 -140°C without stirring for 24 h. The solid product was subsequently filtered, washed, and air-dried at room temperature.

[0038] Figure 6 shows the typical XRD patterns of hexagonal SBA-15 prepared by adding an organic swelling agent. The chemical composition of the reaction mixture was 4 g of the copolymer : 3 g TMB : 0.041 M TEOS : 0.24 M HCl : 6.67 M H₂O. The X-ray pattern of as-synthesized product (Figure 6a) shows three well-resolved peaks with d spacings of 270, 154, and 133 Å at very low angle (2θ range of 0.2 -1°), which are indexable as (100), (110), and (200) reflections associated with p6mm hexagonal symmetry. The (210) reflection is too broad to be observed. The intense (100) peak reflects a d-spacing of 270 Å, corresponding to an unusually large unit cell parameter ($a = 310$ Å). After calcination in air at 500°C for 6 h, the XRD pattern (Figure 6b) shows improved resolution and an additional broad (210) reflection with d spacing of 100 Å. These results indicate that hexagonal SBA-15 is thermally stable, despite its unusually large lattice parameter. The N₂ adsorption-desorption results show that the calcined product has a BET surface area of 910 m²/g, a pore size of 260 Å, and a pore volume of 2.2 cm³/g. TEM images confirm that the calcined products have highly ordered, hexagonal symmetry with unusually large pore sizes (Figures 5c, 5d).

[0039] Figure 7 shows the change of the pore size and the d-spacing of the XRD $d(100)$ peak as a function of the TMB/copolymer mass ratio for calcined hexagonal SBA-15. The pore sizes of calcined SBA-15 were measured from the adsorption branch of the N₂ adsorption-desorption isotherm curve by the BJH (Barrette-Joyner-Halenda) method using the Halsey equation for multilayer thickness. The pore size data for the MCM-41 sample were taken from ref. 4. The chemical compositions of the reaction mixture were 4 g of the copolymer : x g TMB : 0.041 M TEOS : 0.24 M HCl : 6.67 M H₂O for SBA-15 and NaAlO₂ : 5.3 C₁₆TMACl : 2.27 TMAOH : 15.9 SiO₂ : x g TMB : 1450 H₂O for the MCM-41 (C₁₆TMACl = cetyltrimethylammonium chloride, TMAOH = tetramethyl- ammonium hydroxide). The ratios used in this study ranged from 0 to 3, with the $d(100)$ spacing and pore size increasing significantly, up to 320 Å and 300 Å, respectively, with increasing TMB/copolymer ratio. The increased pore size is accompanied by retention of the hexagonal mesostructure, with the X-ray diffraction patterns of each of these materials exhibiting 3 - 4 peaks.

[0040] To the best of our knowledge, hexagonal SBA-15 has the largest pore dimensions thus far demonstrated for mesoscopically ordered porous solids. As shown in Figure 7, the $d(100)$ spacing and pore size of calcined MCM-41 prepared by using cationic surfactant species can also be increased, but compared to SBA-15, the change is much less. In addition, although MCM-41 pore sizes of ca. 100 Å can be achieved by adding auxiliary organic species (e.g., TMB), the resulting materials have significantly reduced mesostructural order. The XRD diffraction patterns for such materials are substantially less resolved, and TEM micrographs reveal less ordering, indicating that the materials possess lower degrees of mesoscopic order. This is particularly the case near the high-end of this size range (~100 Å) for which a broad single peak is often observed. These materials also tend to suffer from poor thermal stability as well, unless additional treatment with wellTEOS (which reduces the pore size) is carried out. From our results, a family of highly ordered mesoporous SBA-15 silica can be synthesized with large uniform and controllable pore sizes (from 89 - 500 Å) by using PEO-PPO-PEO copolymer species as amphiphilic structure-directing agents, augmented by the use of organic swelling agents in the reaction mixture. The pore size for hexagonal SBA-15 determined by TEM images (Figures 5c, 5d) is in agreement with that established from separate N₂ adsorption measurements.

[0041] Magic-Angle Spinning ²⁹Si NMR spectra (Figure 8) of as-synthesized hexagonal SBA-15 show three broad peaks at 92, 99, and 109 ppm, corresponding to Q², Q³, and Q⁴ silica species, respectively. From the relative peak areas, the ratios of these species are established to be Q² : Q³ : Q⁴ = 0.07 : 0.78 : 1. These results indicate that hexagonal SBA-15 possesses a somewhat less condensed, but similarly locally disordered, silica framework compared to MCM-41.

[0042] TGA and DTA analyses (Figure 9) of hexagonal SBA-15 prepared using PEO₂₀PPO₇₀PEO₂₀ show total weight losses of 58 wt% apparently consisting of two apparent processes: one at 80 OC (measured using TGA) yields a 12 wt% loss, accompanied by an endothermic DTA peak due to desorption of water, followed by a second 46 wt% weight loss at 145°C with an exothermic DTA peak due to desorption of the organic copolymer. A Netzsch Thermoanalyzer STA 409 was used for thermal analysis of the solid products, simultaneously performing TGA and DTA with heating rates of 5 Kmin⁻¹ in air.

[0043] The desorption temperature of the large block copolymer (-150°C) is much lower than that of cationic surfactants (-360°C), so that the organic copolymer species can be completely removed and collected without decomposition by heating SBA-15 in an oven (air) at 140°C for 3 h. (The possibility to recover and reuse the relatively expensive triblock copolymer structure-directing species is an important economic consideration and benefit to these materials.) It should be noted that the pure block copolymer PEO₂₀PPO₇₀PEO₂₀ decomposes at 270 OC, which is substantially lower than that of cationic surfactants (-360°C) during calcination. For comparison, the TGA of the copolymer PEO₂₀PPO₇₀PEO₂₀ impregnated in SiO₂ gel shows that the copolymer can be desorbed at 190°C, which is -50°C higher than required for hexagonal SBA-15. Removal of the organic species from as-synthesized SBA-15 at these relatively low temperatures (e.g., 140°C) suggests the absence of strong electrostatic or covalent interactions between the copolymer species and the polymerized silica wall, together with facile mass transport through the pores. The possibility to recover and reuse the relatively expensive triblock copolymer structure-directing species is an important

economic consideration and advantage of these materials.

[0044] Hexagonal SBA-15 can be synthesized over a range of copolymer concentrations from 2 - 6 wt% and temperatures from 35 - 80° C. Concentrations of the block copolymer higher than 6 wt% yielded only silica gel or no precipitation of silica, while lower copolymer concentrations produced only dense amorphous silica. At room temperature, only amorphous silica powder or products with poor mesoscopic order can be obtained, and higher temperatures (> 80°C) yield silica gel. Like TEOS, tetramethylorthosilicate (TMOS) and tetrapropoxysilane (TPOS) can also be used as the silica sources for the preparation of hexagonal SBA-15.

[0045] SBA-15 can be formed in acid media (pH<1) using HCl, HBr, HI, HNO₃, H₂SO₄, or H₃PO₄. Concentrations of HCl (pH 2 - 6) above the isoelectric point of silica (pH 2) produce no precipitation or yield unordered silica gel. In neutral solution (pH 7), only disordered or amorphous silica is obtained. We also measured the precipitation time (*t*) of the silica as a function of the concentration of HCl and Cl⁻. The [Cl⁻] concentration was varied by adding extra NaCl, while keeping the H⁺ concentration constant. From these measurements, log (*t*) is observed to increase linearly with log *C* (where *C* is the concentration of HCl or Cl⁻). Slopes of 0.31 for [Cl⁻] and 0.62 for HCl indicate that Cl⁻ influences the synthesis of SBA-15 to a lesser extent than does H⁺. Based on these results, we propose that the structure-directed assembly of SBA-15 by the polyoxyalkylene block copolymer in acid media occurs by a S⁺X⁻I⁺ pathway. While both the EO and PO groups of the copolymer are positively charged in acidic media, the PO groups are expected to display more hydrophobicity upon heating to 35 - 80°C, thereby increasing the tendency for mesoscopic ordering to occur. The protonated polyoxyalkylene (S⁺), the anionic inorganic (X⁻) bonding, S⁺X⁻, and the positive silica species (I⁺) are cooperatively assembled by hydrogen bonding interaction forces. Assembly of the surfactant and inorganic species, followed by condensation of silica species, results in the formation of hexagonal SBA-15 mesophase silica. At high pH values (2 - 7), the absence of sufficiently strong electrostatic or hydrogen bonding interactions leads to the formation of amorphous or disordered silica.

[0046] One of the limitations of calcined MCM-41 materials prepared without additional treatment with TEOS is their poor hydrothermal stability. As shown in Figure 10, both as-synthesized and calcined (500°C for 6 h) MCM-41, prepared with C₁₆H₃₃N(CH₃)₃Br as previously described, show well resolved hexagonal XRD patterns (Figures 10a, 10b). However, after heating in boiling water for 6 h, the structure of calcined MCM-41 is destroyed and the material becomes amorphous, as evidenced by the absence of XRD scattering reflections in Figure 10c. By contrast, all of the calcined hexagonal SBA-15 samples prepared using the PEO-PPO-PEO block copolymers are stable after heating in boiling water for 24 h under otherwise identical conditions. For calcined hexagonal SBA-15 prepared by using the PEO₂₀PPO₇₀PEO₂₀ copolymer and after calcination in air at 500°C and subsequent heating in boiling water for 6 h, the (210) reflection becomes broader, the (300), (220), and (310) peaks become weaker, while the (100) peak is still observed with similar intensity (Figure 10d). After heating in boiling water for 24 h, the intensity of the (100) Bragg peak (Figure 10e) is still unchanged. Nitrogen BET adsorption isotherm measurements carried out after such hydrothermal treatment shows that the monodispersity of the pore size, surface area, and pore volume are retained. The results confirm that calcined hexagonal SBA-15 silica is significantly more hydrothermally stable than calcined hexagonal MCM-41 silica, most likely because SBA-15 has a thicker silica wall. This is an improved one-step alternative to two-step post-synthesis treatments that use tetraethylorthosilicate (TEOS) to stabilize mesoporous MCM-41 by reforming and structuring the inorganic wall with additional silica.

Preparation of mesoscopically ordered silica-copolymer monoliths and films.

[0047] A typical preparation of monolithic silica-copolymer mesostructures is outlined below. A series of samples was made with varying amounts of Pluronic F127 PEO₁₀₀PPO₆₅PEO₁₀₀ triblock copolymer, while holding other processing conditions constant. A calculated amount of a 20 wt% EtOH/Pluronic F127 solution (between 0.7 and 3.5 ml) is transferred into a 30 ml vial. 0.72 ml of an acidic solution of HCl (pH 1.5) is added to the polymer solution while stirring, followed by addition of 1.0 ml of tetraethylorthosilicate (TEOS). The solution is stirred until homogeneous, and allowed to gel uncovered under ambient conditions. After gelation (-2 days) the samples are covered for 2 weeks at room temperature. At the end of this period the gels have shrunk, yet done so uniformly to retain the shape of the container. Further research has shown that addition of a small amount of 3-glycidoxypropyltrimethoxysilane can prevent shrinkage. The cover is removed and the materials are dried at room temperature to eliminate excess solvent. The F127 series materials produced are transparent up to 38 wt% polymer, after which the polymer macro-phase separates creating a white opaque material. Figures 11a and 11b show optical photographs of two of the monoliths produced. These monoliths were produced using a 2:1 ratio of water to TEOS at pH 1.4 and room temperature, with aging for approximately 1 month. Note the high degree of transparency and only one crack in the 34 wt% sample. Subsequent research has allowed us to produce crack-free monoliths by varying the aging time and temperature. The monoliths pictured are approximately 3-mm thick; although thicker monoliths can be produced, the aging time for these samples increases significantly to eliminate cracking.

[0048] These monoliths were analyzed using XRD, TEM, and NIVIR to determine mesostructural morphology, as

well as the mechanism of the structure formation. The F127 polymer series above showed an aggregation point of roughly 25 wt% F127, below which the polymer was disordered and homogeneously dispersed within the matrix and above which aggregation of the polymers led to silica-copolymer mesophases. The copolymer weight percents required to produce specific phases vary depending upon the exact conditions and copolymer used, however this example may

5 be considered representative, though by no means all inclusive, of the results observed.
[0049] XRD patterns of powdered samples obtained from the monoliths show a single diffraction peak with increasing intensity for increasing polymer concentration with a maximum at 38 wt%. Below 27 wt% F127, no XRD intensity is observed. The $d(100)$ peak is centered at 112 Å for 27-34 wt% and increases to 120 Å for the 38 wt% sample. The change in the location of the peak is due to phase changes in the material, as observed by TEM and NMR. TEM reveals well ordered silica-copolymer mesophases in the samples with higher copolymer concentration, such as the lamellar phase in the 38 wt% sample shown in Figure 12. The image shows that the material has an extremely well ordered lamellar mesoscopic structure with a repeat distance of ~105 nm. The image region is 990 x 1200 nm. The large background stripes are artifacts produced by the microtome cutting process and are otherwise unrelated to the morphology of the material. Lower concentrations of copolymer produced hexagonal, gyroid, or micellar phases with spacings of about 110 Å. The domain sizes for these structures is quite large, well over 1 μm^2 for the lamellar phase, which makes it surprising that only one XRD peak is observed, although others have shown that single XRD patterns do not always imply poorly ordered materials (F. Schüth). Below 27 wt% no mesostructural ordering is observed.

10
[0050] NMR spectroscopy was utilized to provide information about copolymer-silicate interactions on the molecular level. ^1H $T_{1\rho}$ relaxation and two-dimensional ^{29}Si - ^1H and ^{13}C - ^1H heteronuclear correlation NMR experiments reveal that the polymer is rigidly incorporated in the silicate at 11 wt% and begins to microphase separate at 20 wt%. At 27 wt% the PEO and PPO are 80% separated from the silicate, and at 38 wt% the PPO is fully separated ($>10\text{Å}$) from the matrix. This indicates that a phase change has occurred in progressing from copolymer concentrations of 27 to 34 wt% in the samples, where some PPO- ^{29}Si correlation intensity is still observed. Some PEO was observed to be associated with the matrix at all concentrations, implying that the polymerizing silica and PEO blocks are compatible. This suggests that the material is produced by polymerization of silicate oligomers that selectively swell the PEO block of the composite mesostructure.

20
[0051] It is possible to use this chemistry and processing to produce thin SBA-15 silica-copolymer films by either spin-, drop-, or dip-casting. Such films can serve as robust permeable coatings for use in separation or chemical sensing applications or as host matrices for optically or electrically active guest molecules for use in optoelectronic devices. Figure 13 shows a photograph and X-ray diffraction pattern of an optically transparent hexagonal SBA-15-copolymer film formed by drop-casting the reaction solution (2 ml TEOS, 0.6 ml H_2O , 0.80 g Pluronic P104, 1 ml dimethylformamide) onto a glass slide and drying at room temperature. The film is 50- μm thick, crack-free and transparent. The X-ray diffraction pattern of this film shows well resolved peaks that are indexable as (100), (110), (200), and (210) reflections associated with $p6mm$ hexagonal symmetry in which the one-dimensional axes of the ca. 200 Å aggregates are highly ordered horizontally in the plane of the film.

30
[0052] High quality films can be produced generally as follows. A mixture of 5 ml tetraethylorthosilicate and 0.75-3.0 ml H_2O (pH=1.4) is stirred for approximately 30 min or until the silicate has hydrolyzed sufficiently to become miscible with water and thereby form a homogeneous solution. An appropriate amount (generally between 10-40 wt%) of block copolymer, such as Pluronic P104 polyethyleneoxide-polypropyleneoxide-polyethyleneoxide copolymer, is dissolved in the solution. An additive such as ethanol, dimethylformamide, or tetrahydrofuran can be added to vary the viscosity and coating properties. The mixture is allowed to age, then is dip-, drop-, or spin-coated onto a glass or Si wafer substrate. Thin films with variable thicknesses can also be produced using spin coating.

35
[0053] The XRD patterns confirm that these thin films have highly ordered hexagonal ($p6mm$), cubic ($1m3m$), or 3-d hexagonal ($p6_3/mmc$) mesostructures. They are highly ordered and can easily be shear aligned. BET measurements show that the thin films have narrow pore size distributions, pore sizes of 20-120 Å, pore volumes up to 1.7 cm^3/g and BET surface areas up to ~1500 m^2/g . SEM images of these thin films show a uniformly flat surface. The thickness of the films can be adjusted from 100 nm - 1 mm by varying the concentration of the solution, aging time and coating time.

40
[0054] The examples shown above use $\text{PEO}_{20}\text{PPO}_{70}\text{PEO}_{20}$ copolymer species as the structure-directing agents. Highly ordered, ultra large pore size SBA-15 materials can also be synthesized by using PEO-PPO-PEO block copolymers with different ratios of EO to PO and without adding supplemental organic swelling agents, such as TMB. Table 1 summarizes the physicochemical properties of mesoporous silica prepared by using triblock and reverse triblock copolymers. The $d(100)$ -spacings from X-ray diffraction measurements can be in the range of 74.5 - 118 Å, with pore sizes of 46 - 100 Å established by N_2 adsorption measurements. The EO/PO ratio and intramolecular distribution and sizes of the corresponding blocks affects the formation of SBA-15. A lower EO/PO ratio with a symmetric triblock PEO-PPO-PEO copolymer architecture favors the formation of $p6mm$ hexagonal SBA-15. For example, Pluronic L121, $\text{PEO}_5\text{PPO}_{70}\text{PEO}_5$, at low concentrations (0.5 - 1 wt%) forms hexagonal SBA-15, while use of higher concentrations of this copolymer (2 - 5 wt%) leads to an unstable lamellar mesostructured silica phase. Higher EO/PO ratios of the block copolymer, e.g. $\text{PEO}_{100}\text{PPO}_{39}\text{PEO}_{100}$ or $\text{PEO}_{80}\text{PPO}_{30}\text{PEO}_{80}$, yield cubic SBA-15 silica, including an $1m3m$ mor-

phology. These cubic mesophase materials yield large 54 - 80 Å mesoscopically ordered pores and high BET surface areas (up to 1000 m²/g). Hexagonal mesoporous silica SBA-15 can also be synthesized by using reverse PPO-PEO-PPO triblock copolymer configuration, for example, PPO₁₉PEO₃₃PPO₁₉.

[0055] In general, any microphase-separating, domain-partitioning copolymer architecture can be considered promising for the synthesis of such mesostructured materials, according to the specifications imposed by processing conditions and ultimately the product properties desired. Additionally, cubic (*Pm3m*) and hexagonal (*p6mm*) mesostructures can be formed by using Brij 56, C₁₆H₃₃(OCH₂CH₂)₁₀OH (C₁₈EO₁₀) surfactant species, with the pore sizes controllable from 25 - 40 Å and BET surface areas up to 1070 m²/g. Brij 76 (C₁₈EO₁₀) yields the three-dimensional hexagonal (*P6₃/mmc*) and two-dimensional hexagonal (*p6mm*) mesostructures with similar pore sizes and surface areas; see Table 2.

[0056] Films and monoliths can be produced with several variations of the solution conditions and/or sol-gel parameters, such as the ratio of water to TEOS, aging time, acidity, additives, temperature, and choices of copolymer or nonionic surfactants. Materials for specific applications can be formulated by appropriate modification of these parameters. Heat treatment after gelation can also produce harder materials that are less likely to crack.

[0057] We have found that silica-surfactant mesophases and MCM-41-type mesoporous materials can be aligned using liquid crystal processing strategies, including imposition of magnetic, shear, or electric fields. Similarly, polymer processing of the silica-copolymer composites is expected to be equally advantageous for producing aligned ultra large mesopore hydrothermally spH materials. For example, it should be possible to induce orientational ordering of the silica-copolymer composites and resultant mesoporous materials by applying shear to the sol-gel/copolymer system as it dries. Concerning variations on processing SBA-15-copolymer thin films (0.1-100 μm), use of shear alignment strategies, including spin-casting and dip-casting (i.e., drawing a vertical coverslip from a reservoir of the reaction solution), have been shown to induce larger degrees of orientational order than provided by drop-cast preparations. Moreover, guest molecules such as conducting or optically active organic species can be introduced to the reaction solution(s) and incorporated into the silica-copolymer monoliths, films or powders prior to or during processing. We have demonstrated the efficacy of this for the inclusion of conducting polymer moieties, such as poly(3,4-ethylenedioxythiophene) in SBA-15 silica-copolymer monoliths and spin-, drop-, and dip-cast films.

[0058] Methods currently available for the preparation of inorganic-organic mesophases or mesoscopically ordered porous materials typically involve one of five pathways that rely on Coulombic or hydrogen-bonding interactions, represented by the shorthand notations S⁺I⁻, S⁺X⁻I⁻, S⁻I⁺, S⁻X⁺I⁺, or S⁰I⁰. The most popular route used in syntheses of mesoporous materials has been the S⁺I⁻ approach in basic media, but the S⁻I⁺ and S⁻X⁺I⁺ syntheses generally yield unstable non-silica based mesoporous materials. Furthermore, the surfactants used as the structure-directing agents in these cases (e.g., alkylammonium, alkylamine) are expensive and/or environmentally noxious. The S⁰I⁰ synthesis route generally yields disordered or worm-like mesoporous solids due to the absence of strong electrostatic or hydrogen bonding interactions. The materials and synthesis method described here are less expensive, non-toxic, and considerably more versatile than the cases described above. They can be used to tune material properties, such as mesoscopic ordering, pore size, hydrothermal stability, monolith shape, orientational alignment, and compatibility with a wide range of guest molecules to a significantly greater extent than possible with the current state-of-the-art.

[0059] The ultra large mesopores in calcined SBA-15 materials provide new opportunities in chromatographic separations of large molecules, such as proteins, enzymes, or polymers. In addition, these materials have promise for new applications in environmental remediation, such as the clean up of polycyclic aromatics, porphyrins, other large organics, and heavy metals from process streams or soils. These properties can be enhanced and tailored by functionalizing molecular moieties along the inorganic walls to provide chemical as well as size selective specificity of adsorption interactions.

[0060] To the best of our knowledge there have been no reports of mesoscopically ordered silica monoliths or films with large characteristic structural length scales (>50 Å). The large dimensions of the inorganic-copolymer aggregates and large pore sizes of the composite or mesoporous materials detailed herein are superior to conventional mesoporous solids due to their thermal stability, transparency, monolithic form, and ability to incorporate large guest molecules. SBA-15 mesoporous silica also has distinct advantages over dense silica, particularly for applications requiring a lower dielectric constant material. SBA-15 has much lower density, long range mesoscopic order and possibilities for obtaining materials with high degrees of structural anisotropy, compared to dense silica. The improvements substantially exceed those provided by MCM-type materials, as discussed earlier. This has attractive implications for the development of low dielectric constant materials, particularly for reducing the capacitance of interconnects, which are among the most severely limiting factors in improving integrated and optical circuit performance. As shown in Figure 14, the quest for materials with dielectric constants significantly below 2 appears to be well within reach; calcined SBA-15 materials have been prepared with porosities of 0.6-0.86, which lead to calculated optical dielectric constants of 1.1-1.4. One can produce aligned morphologies or structures with unconnected spherical cavities to eliminate transverse channel connectivities, which are undesirable for dielectric materials applications.

[0061] Use of block copolymers with a hydrophobic core also produces the unique ability to stabilize hydrophobic

guest molecules that would not otherwise be compatible with the hydrophilic sol-gel reaction, such as some optically active dyes and polymers. Before now all optical moieties incorporated into sol-gel materials were either water soluble or had to be chemically grafted onto a compatible polymer. The inclusion of a hydrophobic region within our silicates, yet still smaller than optical wavelengths, allows an entirely new area of monoliths and coatings to be developed using hydrophobic dyes and optically active organics while retaining optical transparency. Furthermore, inclusion of guest conducting or optically active species, such as polymers and/or metal nanoparticles, in the pores can create quantum-effect materials. The controllability of the SBA-15 pore sizes, inorganic wall composition, organic composition, and guest species composition permit the properties (e.g., optoelectronic, mechanical, thermal, etc.) to be tuned over an enormous range. Indeed, sequential introduction of guest species, for example a conducting polymer coating on the interior of the inorganic wall, followed by a second polymer or metal/semiconductor species in the pore center, could lead to the first mesoscopically ordered arrays of nanosized coaxial quantum wires.

Generalized block copolymer syntheses of mesoporous metal oxides

[0062] Mesoporous metal oxides were synthesized at 30 - 70 °C using poly(alkylene oxide) block copolymers HO(CH₂CH₂O)_x(CH₂CH(CH₃)O)_y(CH₂CH₂O)_xH (EO_x-PO_y-EO_x) or HO(CH₂CH₂O)_x(CH₂CH(CH₃CH₂)O)_yH (EO_x-BO_y) block copolymers as the structure-directing agents. In a typical synthesis, 1 g of poly(alkylene oxide) block copolymer was dissolved in 10 g of ethanol (EtOH). To this solution, 0.01 mole of the inorganic chloride precursor was added with vigorous stirring. The resulting sol solution was gelled in an open petri dish at 40 - 60 °C in air. The aging time differs for different inorganic systems. Alternatively, the sol solution can be used to prepare thin films by dip coating. The as-made bulk samples or thin films were then calcined at 400 °C for 5 hours to remove the block copolymer surfactants. For the Al and Si_{1-x}Al_x systems, calcination was carried out at 600 °C for 4 hr. For WO₃, calcination at 300 °C is sufficient to yield ordered mesoporous oxides.

[0063] X-ray diffraction (XRD) is an important technique for characterizing these metal oxide mesostructures. Table 3 summarizes the synthetic conditions, including the inorganic precursors and aging temperatures and times for the mesostructured inorganic/copolymer composites (before calcination) using EO₂₀PO₇₀EO₂₀ as the structure-directing agent. A broad array of mesostructured composites have been successfully prepared, covering the first-, second- and third-row transition metals and some main group elements as well. The ordering lengths shown in Table 3 correspond to the largest d value observed from the low-angle XRD patterns; it ranges from 70 to 160 Å for the different systems. High-order low-angle diffractions are also observed for most of these systems. Quantitative elemental chemical analysis suggests that the frameworks of these mesostructured composites are made up of metal-oxygen-chlorine networks.

[0064] Upon calcination, mesoporous TiO₂, ZrO₂, Nb₂O₅, Ta₂O₅, Al₂O₃, WO₃, SiO₂, SnO₂, HfO₂, and mixed oxides Si_{1-x}Ti_xO_y, Zr_{1-x}Ti_xO_y, Al_{1-x}Ti_xO_y, Si_{1-x}Al_xO_y are obtained. X-ray diffraction, transmission and scanning electron microscopy imaging (TEM & SEM), and nitrogen adsorption/desorption are three crucial techniques for characterization of these materials. Table 4 summarizes the analysis results, including the ordering length, pore size, wall thickness, wall structure, porosity and Brunauer-Emmet-Teller (BET) surface area.

[0065] Figure 15 shows typical XRD patterns for mesostructured zirconium oxides prepared using EO₂₀PO₇₀EO₂₀ as the structure-directing agent before and after calcination. The as-made zirconium inorganic/polymer mesostructure (Figure 15a) shows three diffraction peaks with $d = 115, 65,$ and 59 \AA . After calcination, the diffraction peaks appear at higher 2θ angles with $d = 106, 60,$ and 53 \AA (Figure 15b). Both sets of diffraction peaks can be indexed as the (100), (110), and (200) reflections from 2-dimensional hexagonal mesostructures with lattice constants $a_0 = 132$ and 122 \AA , respectively. Similar XRD results are obtained in other mesoporous metal oxides. The ordering lengths of these mesoporous metal oxides (Table 4) are substantially larger than those of materials previously reported.

[0066] Thermogravimetric experiments indicate that the block copolymer is completely removed upon calcination at 400 °C. The appearance of low-angle diffraction peaks indicates that mesoscopic order is preserved in the calcined metal oxide materials. This is confirmed by TEM images obtained from mesoporous samples. As examples, Figures 16 - 26 show TEM images of mesoporous ZrO₂, TiO₂, SnO₂, WO₃, Nb₂O₅, Ta₂O₅, Al₂O₃, HfO₂, SiTiO₄, SiAlO_{3.5}, and ZrTiO₄ recorded along the [110] and [001] zone axes of the 2-dimensional hexagonal mesostructures. In each case, ordered large channels are clearly observed to be arranged in hexagonal arrays. The pore/channel walls are continuous and have thicknesses of 3.5 - 9 nm. They are substantially thicker than those typical of metal oxides prepared using alkylammonium ion surfactant species as the structure-directing agents. In addition, energy dispersive X-ray spectroscopy (EDX) measurements made on the calcined samples show the expected primary metal element signals with trace of Cl signal, which confirms that the inorganic walls consist predominantly of metal-oxygen networks.

[0067] Furthermore, selected area electron diffraction patterns (ED) recorded on mesoporous ZrO₂, TiO₂, SnO₂, and WO₃ show that the walls of these materials are made up of nanocrystalline oxides that show characteristic diffuse electron diffraction rings (Figures 16 - 18 and 20 insets). Wide-angle X-ray diffraction studies of calcined samples also clearly show broad peaks that can be indexed according to the corresponding oxide crystalline phase. Figure 15d shows a wide-angle diffraction pattern for the calcined ZrO₂ sample. The sizes of the nanocrystals in the calcined

materials are estimated to be - 2 nm using the Scherrer formula. In addition, bright-field and dark-field (BF/DF) TEM imaging were employed to study the distribution of these nanocrystals. Figures 27 and 28 show such images recorded on same area of one thin mesoporous TiO₂ and ZrO₂ sample. As can be seen in the dark field image (Figures 27b, 28b), the oxide nanocrystals (- 2 nm) are uniformly embedded in a continuous amorphous inorganic matrix to form semicrystalline wall structures. This is the first time that the combination of electron diffraction, X-ray diffraction, and bright field/dark field TEM imaging has been used to conclusively demonstrate that our mesoporous metal oxides have nanocrystalline framework.

[0068] Figures 29 - 36 show BET isotherms that are representative of mesoporous hexagonal ZrO₂, TiO₂, Nb₂O₅, Ta₂O₅, Al₂O₃, WO₃, SiTiO₄, and ZrTiO₄. Barrett-Joyner-Halenda (BJH) analyses show that the calcined hexagonal mesoporous metal oxides exhibit pore sizes of 35 - 140 Å, BET surface areas of 100 - 850 M²/g, and porosities of 40 - 60%. The pore sizes are again substantially larger than the previous reported values. For most of the isotherms obtained on these metal oxides, three well-distinguished regions of the adsorption isotherm are evident: (1) monolayer-multi layer adsorption, (2) capillary condensation, and (3) multilayer adsorption on the outer particle surfaces. In contrast to N₂ adsorption results obtained for mesoporous metal oxides prepared using low-molecular-weight surfactants with pore sizes less than 4 nm, large hysteresis loops that resemble typical H₁- and H₂- type isotherms are observed for these mesoporous metal oxides.

[0069] The foregoing examples used EO₂₀PO₇₀EO₂₀ copolymer species as the structure-directing agent Mesoporous metal oxides with other mesostructures can be synthesized by using EO_x-PO_y-EO_x or EO_x-BO_y block copolymers with different ratios of EO to PO or BO. For example, when EO₇₅BO₂₅ copolymer is used as the structure-directing agent, mesoporous TiO₂ with cubic mesostructure can be prepared. Figure 37 shows typical XRD patterns for mesostructured titanium oxides prepared using EO₇₅BO₂₅ as the structure-directing agent, before and after calcination. The as-made titanium inorganic/ polymer mesostructure (Figure 35a) shows six diffraction peaks with $d = 100, 70, 58, 44, 41, 25$ Å, which can be indexed as (110), (200), (211), (310), (222), (440) reflections of an Im3m mesophase. After calcination, the diffraction peaks appear at higher 2θ angles with $d = 76, 53, \text{ and } 43$ Å (Figure 35b). These diffraction peaks can be indexed as the (110), (200), and (211) reflections from Im3m mesostructures. The cubic mesostructure is confirmed by the TEM imaging (Figures 38 39).

[0070] Films and monoliths (Figure 40) can be produced by varying such synthetic conditions as the solvent, the ratio of inorganic/polymer, aging temperature, aging time, humidity, and choice of the block copolymer. Liquids that are common solvents for inorganic precursors and the block copolymers (e.g. methanol, ethanol, propanol, butanol) can be used during the synthesis. The temperature, the amount of water added, and the pH can adjusted to control formation of the mesostructures. Materials for specific applications can be formulated by appropriate modification of these parameters.

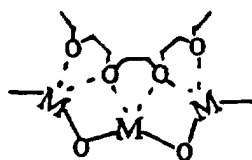
[0071] The advantages and improvements over existing practice can be summarized as follows:

- (1) Robust, thick channel walls (35 - 90 Å) which give enhanced thermal and chemical stabilities.
- (2) Very large pore sizes (3.5 - 14 nm)
- (3) Use of low-cost inorganic precursors
- (4) Versatile synthetic methodology using non-aqueous media that can be generally applied to vastly different compositions, among which mesoporous SnO₂, WO₃, and mixed oxides SiTiO₄, ZrTiO₄, Al₂TiO₅ are synthesized for the first time.
- (5) For the first time, conclusive demonstration of the nanocrystallinity of the framework in mesoporous ZrO₂, TiO₂, SnO₂, WO₃ using XRD, ED and BF/DF TEM imaging
- (6) Mesoporous metal oxides with various physical properties including semiconducting, low dielectric-constant, high dielectric-constant, and negative thermal expansion.

[0072] Crystallization of inorganic species during cooperative inorganic/organic self-assembly can lead to macroscopic phase separation of the inorganic and organic components. This is because crystallization energies often dominate the interaction energies that stabilize the inorganic-organic interface, thereby disrupting the establishment of mesostructural order. This is particular the case for non-lamellar phases. In the present invention, this situation is successfully circumvented by using conditions that initially produce a mesoscopically ordered material with an amorphous inorganic wall structure (Figures 15c and 35c) within which a high density of nanocrystals can subsequently be nucleated upon calcination. The thick wall and the noncrystallized inorganic matrix prevent this partially crystalline structure from collapsing by effectively sustaining the local strain caused by the nucleation of the nanocrystals. The coexistence of mesoscopic ordering and framework nanocrystallinity is extremely important for catalysis, sensor, and optoelectronic applications.

[0073] To the best of our knowledge, there has been no previous report of mesoporous metal oxide synthesis with such simplicity and versatility. The formation, with such unprecedented simplicity and generality, of large-pore mesoscopically ordered metal oxides suggests that the same general inorganic/ block polymer assembly mechanisms may

be operating. In fact, it is well documented that alkylene oxide segments can form crown-ether type complexes with many inorganic ions, through weak coordination bonds. The multivalent metal species (M) can associate preferentially with the hydrophilic PEO moieties, as indicated in Scheme 1, because of their different binding capabilities with poly (ethylene oxide) (PEO) and poly(propylene oxide) (PPO). The resulting complexes then self-assemble according to the mesoscopic ordering directed principally by the microphase separation of the block copolymer species, and subsequently cross-link and polymerize (Scheme 1) to form the mesoscopically ordered inorganic/polymer composites.



Scheme 1

The proposed assembly mechanism for these diverse mesoporous metal oxides uses PEO-metal chelating interactions in conjunction with electrostatics, van der Waals forces, etc., to direct mesostructure formation.

[0074] A unique feature of the current synthetic methodology is use of inorganic precursors in non-aqueous media. Because of the lower electronegativities of the transition metals compared to silicon, their alkoxides are much more reactive towards nucleophilic reactions such as hydrolysis and condensation. There has been some work on the non-hydrolytic sol-gel chemistry of inorganic oxides, a non-hydrolytic route involving carbon-oxygen bond cleavage instead of the metal-oxygen bond which has a general tendency to delay crystallization of the metal oxides, a very important for the first step of our inorganic-copolymer cooperative self-assembly process. In addition, the hydrolytic route to metal oxides often leads to difficulties in controlling stoichiometry and homogeneity. Homogeneity depends on the rate of homocondensation (i.e. formation of M-O-M and M'-O-M') versus the rate of heterocondensation, which can be hardly controlled in the hydrolytic process because of the different reactivities of the various precursors towards hydrolysis and condensation. However, in principle, the non-hydrolytic process should favor the formation of homogeneous binary oxides from different metal precursors because of the decreased difference in hydrolysis and condensation rates for different inorganic sources in non-aqueous media. This has been successfully demonstrated in the mesoporous mixed oxides syntheses using the methods of this invention.

[0075] This utilization of block copolymer self-assembly in conjunction with chelating complexation for inorganic/organic cooperative assembly in the non-aqueous media make it possible to synthesize mesoporous materials with vastly different compositions exemplified in Table 4.

Cooperative Multiphase Assembly of meso-macro silica membranes

[0076] Here we describe a novel procedure for the synthesis of artificial coral silica membranes with 3-d meso-macro structures. This process utilizes multiphase media while including microphase separation block copolymer/silica composite and macrophase separation between strong electrolytes and the composite in a single step. We find that strong electrolytes such as NaCl, LiCl, KCl, NH₄Cl, KNO₃, or even transition metal cationic salts such as NiSO₄, can be used to prepare meso-macro silica membranes that are formed at the interface of droplets of these inorganic salt solution. It is well known that in nature, macroscopic ordered silica structure such as diatom and coral are grown through a protein modified process in the ocean environments that are rich in inorganic salts such as NaCl. The process used in this study may be significant in understanding the formation of diatom and coral in nature which also can be considered as a 3-phase media process: the environment of the cell, the cell membrane and the aqueous media within the cell.

[0077] The silica membranes (size - 4 cm x 4 cm, thickness - 5 mm) with 3-d meso-macro silica network structures that we have prepared show oriented continuous rope, tyroid, and grape vine or dish pinwheel, and gyroid, morphologies depended on the electrolyte strength of the inorganic salts or amphiphilic block copolymer templates. The macropore size (0.5 - 100 μm) can be controlled by inorganic salts and evaporation rate of the solvent. The mesoscopic structures can be highly ordered 2-d honeycomb (pore size 40 - 90 Å) or 3-d cubic packing, and controlled by the amphiphilic block copolymer templates. These artificial coral meso-macro silica membranes are thermally stable and exhibit a large surface areas up to 1000 cm²/g and pore volumes up to 1.5 cm³/g.

[0078] The silica membranes were prepared by the use of two-step sol-gel chemistry. First oligomeric silica sol-gel was obtained by pre-hydrolyzing of tetraethoxysilane (TEOS) in ethanol solution by an acid-catalyzed process. Sec-

ond, the oligomeric silica sol-gel was added into a mixture solution of poly(ethylene oxide)-*block*-poly(propylene oxide)-*block*-poly(ethylene oxide) (PEO-PPO-PEO) triblock copolymer and inorganic salts in water and ethanol. The final composition of this mixture was range of 1 TEOS: (6.8 ~ 34) x 10⁻³ copolymer: 0.51 ~ 3.0 inorganic salt: 18 ~ 65 H₂O: 0.002 ~ 0.04 HCl: 11 ~ 50 EtOH. The silica membranes with 3-d meso-macro structures were obtained after drying at room temperature, washing with water to remove the inorganic salts, and calcination to completely remove the organic block copolymer,

[0079] In a typical synthesis, 2.08 g TEOS (Aldrich) were added to 5 g ethanol, 0.4 g water and 0.4 g (0.1 M) of HCl solution with stirring at room temperature for 0.5 h, then heated at 70°C without stirring for 1 h. After cooling to room temperature, 1 g EO₂₀PO₇₀EO₂₀ (Pluronic P123, Aldrich/BASF, average molecular weight 5800), 1 g NaCl, 10 g ethanol and 10 g water were added to this solution with stirring at room temperature for 1 h. The resultant solution was transferred into an open petri dish, allowed to evaporate at room temperature. After complete drying, the solid membrane was removed from the dish, 20 g water added and then heated in a sealed container at 100°C for 3 days to dissolved the inorganic salts. After cooling to room temperature, the solid silica membranes were washed with de-ionic water and dried at room temperature. The as-synthesized silica membranes were calcined at 500°C for 6 h in air to completely remove all organic block copolymers.

[0080] Figure 41 shows several representative scanning electron microscope (SEM) images, obtained on a JEOL 6300-F microscope, of the silica membranes and inorganic salt (NaCl) crystal co-grown with the membranes by sol-gel chemistry. The silica membranes prepared from NaCl solution show 3-d macroscopic network structures and a coral-like morphology (Figure 41a). The reticular 3-d network (thickness of ~ 1 μm) of the silica membrane is made up of continuous rope-like silica which exhibits highly mesoscopic ordering (see below). The silica membranes can be as large as - 4 cm x 4 cm depended on the size of the container that is used. The thickness of the silica membranes can be varied from 10 μm to 5 mm.

[0081] As shown in Figure 41b, the whole silica membrane shows similar local macroscopic structure that is not long-range ordering. The average macropore size of the silica membranes is about -2 μm (±0.4) (Figure 41a) and can be varied from -0.5 μm to -100 μm by changing the evaporation rate or the electrolyte strength of the inorganic salts. For example, when a small amount of ethylene glycol is added into the sol-gel solution to slow the evaporation rate, a small macropore size (-0.5 μm) is obtained as shown in Figure 41c. Of interest is finding that when the evaporation rate is low, the thickness of the silica network is decreased several hundreds nanometer as shown in Figure 41c. When the evaporation rate is high, the macropore size of the silica membranes can be as large as -10 μm, the framework thickness is increased (as shown in Figure 41d) and the macroscopic structure of the silica membranes is changed to a 2-d honey comb channel structure.

[0082] The electrolyte strength of the inorganic salts also can be used to control the macropore size. By using stronger electrolytes, for example, MgSO₄, the macropore size can be as much as -20 μm. In addition, the morphology of the silica membrane can be modified through changing the concentration of inorganic salts. Low concentrations of the inorganic salts result in an inhomogeneous silica membrane. While high concentrations, result in the grape vine morphology that makes up the silica membrane as shown in Figure 41e.

[0083] The morphologies of the inorganic salt crystals are also affected by the organic block copolymer. For example, without the amphiphilic block copolymer, cubic crystals of NaCl as large as -100 μm can be grown in the solution of water and ethanol, however, in the presence of the surfactant under our synthesis conditions, most NaCl crystals show an acicular (~1 μm in diameter) morphology (Figure 41f), with a length of as much as 1 cm. When NiSO₄ is used as the inorganic salts in our synthesis condition, a disk-like morphology of NiSO₄ crystal is observed at the bottom of the silica membranes. This suggests that the crystallization of the inorganic salts can also be directed by block copolymers.

[0084] Besides NaCl, other inorganic salts such as LiCl, KCl, NH₄Cl, Na₂SO₄, MgSO₄, NiSO₄, MgCl₂, chiral NaClO₃, and organic acids such as, malic acid, can be used to form the silica membranes. Figure 42 shows several representative scanning electron microscope (SEM) images of the meso-macroporous silica membranes prepared by using block copolymer P123 (a-c), or P65 (d) in different inorganic salt solutions. The morphology of the silica membranes is dependent on the electrolyte strength of the inorganic salts. For example, when LiCl, KCl, and NH₄Cl are used, with electrolyte strengths comparable to that for NaCl, a similar coral-like morphologies (Figures 42a, b, c) are observed, although the network morphology of the silica membranes is somewhat different. However, when the inorganic salts with stronger electrolyte strengths such as Na₂SO₄, MgSO₄, are used in the synthesis, the macroscopic structures consist silica networks made up of toroid, pinwheel, dish, and gyroid morphologies (Figure 43).

[0085] The macroscopic structure is also affected by the block copolymer. When higher average molecular weight block copolymers such as Pluronic F127 (EO₁₀₆PO₇₀EO₁₀₆) is used, cubic morphology is observed by SEM (Figure 43a). This morphology results from silica grown around cubic NaCl crystals, suggesting a macroscopic inorganic crystal templating process for the mesoporous silica growth. When block copolymers such as Pluronic P65 (EO₂₆PO₃₉EO₂₆) is used, the silica membrane with large macropore size is obtained (Figure 42d).

[0086] The mesoscopic ordering in these silica membranes formed by the cooperative self-assembly of inorganic silica species/amphiphilic block copolymer is mainly controlled by the block copolymer while can be characterized by

the low-angle X-ray diffraction patterns (Figure 44) and transmission electron microscope (TEM) (Figure 45). The XRD patterns of Figure 44 were acquired on a Scintag PADX diffractometer using Cu K α radiation. For the TEM of Figure 45 measurements, the sample was prepared by dispersing the powder products as a slurry in acetone and subsequently deposited and dried on a hole carbon film on a Cu grid. As shown in Figure 44a, the coral-like silica membranes synthesized by using P123 triblock copolymer after removal of NaCl by washing, shows a typical hexagonal ($p6mm$) XRD pattern for mesoporous materials with four diffraction peaks ($a = 118 \text{ \AA}$), which is similar to that of SBA-15 described above. After calcination at 500°C in air for 6 h, the four-peak XRD pattern is also observed and the intensity of the diffraction peaks is increased, suggesting that the $p6mm$ mesoscopic ordering is preserved and thermally stable, although the peaks appear at slightly larger 2θ values, with $a = 111 \text{ \AA}$. The cell parameters of mesoscopic ordering on the silica membranes can be varied by using different triblock copolymers. For example, $a = 101 \text{ \AA}$ for Plunroin P103 ($\text{EO}_{17}\text{PO}_{85}\text{EO}_{17}$) (Figure 44b) and $a = 73.5 \text{ \AA}$ for Plunronic P65 ($\text{EO}_{26}\text{PO}_{39}\text{EO}_{26}$) (Figure 44c), these materials have 2-d hexagonal ($p6mm$) mesoscopic highly ordered structures.

[0087] These results suggest that the presence of the inorganic salts such as NaCl does not greatly effect the cooperative self-assembly of block copolymer/silica to form highly ordered mesostructure. Figures 45a,b show TEM images of calcined silica membranes prepared by using P123 block copolymer in NaCl solution at different orientations, confirming that silica network of the membranes is made up of a 2-d $p6mm$ hexagonal mesostructure, with a well-ordered hexagonal array and one-dimensional channel structure. TEM images (Figure 45 c, d) of the silica membranes with small macropore size ($\sim 0.5 \mu\text{m}$ from SEM) prepared by adding a small amount of ethylene glycol show that the rope-like networks of the silica membranes is made up of loop-like mesoscopic silica with oriented 1-d channel arrays parallel to the long axis. These rope-like silicas form a 3-d network macroporous structure. It should be noted that when higher molecular weight block copolymer F127 is used as the mesoscopic structure-directing agents, a silica membrane with cubic mesostructure ($a = 217 \text{ \AA}$) can be obtained, based on XRD and TEM results.

[0088] SEM images of the silica membranes after calcination at 500°C in air show that the coral-like macrostructure is retained, demonstrating that the coral-like meso-macro silica membranes prepared with inorganic salts are thermally stable. Thermal gravimetric and differential thermal analyses (TGA and DTA) (Figure 46) in air of the silica membranes prepared by using P123 block copolymer in NaCl solution after removal of the inorganic salts, show total weight losses of only 24 weight % (Figure 46 top). A Netzsch Thermoanalyzer STA 409 was used for thermal analysis of the solid products, simultaneously performing TGA and DTA with heating rates of 5 Kmin^{-1} in air. At 100°C TGA registers a 18 weight % loss accompanied by an endothermic DTA peak caused from desorption of water, this is followed by a 6 weight % TGA loss at 190°C which coincides with an exothermic DTA peak associated with decomposition of the organic block copolymer. By comparison, the silica membranes obtained without removed the inorganic salts show total weight losses of 50 weight % (Figure 46 bottom). At 100°C TGA registers a 4 weight % loss from physical adsorption of water, followed by a 46 weight % TGA loss at 200°C from decomposition of the organic block copolymer.

[0089] The above observations confirm that the interaction between silica species and block copolymer species is weak, and after washing with water 84 weight % of the block copolymer in the silica membranes is removed. After washing by water and without calcination, these silica membranes already show similar nitrogen sorption behavior to that for calcined silica membranes, (Figure 47a, b) so that after washing, both macroporous ($\sim 2 \mu\text{m}$) and mesoporous (60 \AA) channels are already accessible. The isotherms of Figure 47 were measured using a Micromeritics ASAP 2000 system. Data were calculated by using the BdB (Broekhoff and de Boer) model. The pore size distribution curve was obtained from an analysis of the adsorption branch of the isotherm. The pore volume was taken at $P/P_0 = 0.985$ signal point. The BET sample was pre-treated at 200°C overnight on the vacuum line.

[0090] The representative nitrogen adsorption/desorption isotherms and the corresponding pore size distribution calculated by using Broekhoff and de Boer's model are shown in Figure 48. The isotherms of Figure 48. The isotherms were measured using a Micromeritics ASAP 2000 system. Data were calculated by using the BdB (Broekhoff and de Boer) model. The pore size distribution curve was obtained from an analysis of the adsorption branch of the isotherm. The pore volume was taken at $P/P_0 = 0.985$ signal point. The BET sample was pre-treated at 200°C overnight on the vacuum line. The coral-like silica membranes prepared using P123 block copolymers in a NaCl solution show a typical isotherm (type IV) of cylindrical channel mesoporous materials with H_1 -type hysteresis, and exhibit a narrow pore size distribution at the mean value of 84 \AA . This material has a Brunauer-Emmett-Teller (BET) surface area of $660 \text{ m}^2/\text{g}$, and a pore volume of $1.1 \text{ cm}^3/\text{g}$. The mesoscopic pore size of the silica membranes prepared in NaCl solution depended on the amphiphilic block copolymer, for example, the materials prepared by using P103 and P65 show similar isotherms and exhibit pore sizes of 77 and 48 \AA , BET surface areas of 720 and $930 \text{ m}^2/\text{g}$, and pore volumes of 1.12 and $0.99 \text{ cm}^3/\text{g}$ respectively (Figure 48). When large molecular weight F127 block copolymer is used as the templates, the silica membrane with cubic mesoscopic structure shows the isotherms with a large H_2 -type hysteresis (Figure 49a) much different with that for hexagonal mesoscopic array silica membranes and does not fits to cylinders model by using BdB model to calculate the pore size distribution. (Figure 49b) However, using spheres model, it shows quite narrow pore size distribution at a mean of 10.5 nm , and exhibit a BET surface area of $1003 \text{ m}^2/\text{g}$, pore volume of $0.8 \text{ cm}^3/\text{g}$ (Figure 49b). The silica membranes prepared by using nonionic oligomeric surfactant $\text{C}_{16}\text{H}_{33}\text{EO}_{10}$ also high BET surface area

of 710 m²/g and pore volume of 0.64 cm³/g, but slight smaller a mean pore size of 3.6 nm (Figures 50a,b).

[0091] In order to understand the formation of the coral-like meso-macro silica membranes, we have carefully investigated the macroscopic structures in different areas (Figure 51) of the as-made silica membranes prior to washing. As shown in Figures 51a-d, without washing out the inorganic salt (LiCl) the macroscopic coral-like structures of the membrane have been already formed in the middle region of the silica membrane. On the other hand, the image recorded in the top region of the silica membrane is quite different than that from the middle region and show disordered pillow windows that have similar average macro-window size compared that in the middle region. These results suggest that the silica membrane grown at the air interface is different than that water interface. Figure 51d shows the SEM image of the silica membrane prepared by LiCl recorded at the bottom region, suggesting that the mosaic-like inorganic salt LiCl crystals, which are confined by XRD and chemical analysis, are formed in the bottom of the silica membranes. The shape of the pillow-like LiCl crystals is somewhat similar to the fenestrated morphology observed at the top region of the silica membrane. SEM images of the silica membrane prepared by using NiSO₄ as the inorganic salt recorded on the top, middle, bottom regions of the membrane are shown in Figures 51e-h. Without washing out the inorganic salt (NiSO₄) (Figures 51e,f) SEM images reveal a disk-like window morphology at the top of the membrane, while inside this window, a coral-like morphology can be seen (Figure 46f). However, at the bottom of the membrane, grape vine-like silica macrostructures with disk-like inorganic salt-NiSO₄ crystals are observed (Figure 51g, h). The size of disk-like NiSO₄ crystals is the same as the window size of the silica membrane at the top. These results are consist with initial phase separation between the coral-like silica macrostructure and inorganic salts, followed by formation of the silica macrostructure above the inorganic salts.

[0092] In order to further confirm the formation of the materials, we investigate the change of composition as a function of the evaporation time (Figure 52). The chemical composition of the starting reaction mixture was 1 g P123 block copolymer: 0.01 mol TEOS: 1 g LiCl : 4 × 10⁻⁵ mol HCl: 0.55 mol H₂O: 0.33 mol EtOH. As shown in Figure 52, in the beginning, the concentration (weight %) of ethanol is decreased rapidly, and the concentration of water and SiO₂ and inorganic salt LiCl are increased since a large amount of ethanol is evaporated. After about 3 h, silica-block copolymer gel starts to form, in liquid phase, the concentration of silica is rapidly decreased and the concentration of LiCl is rapidly increased. When the silica mesostructure is formed as determined by XRD, almost all the ethanol has evaporated (in liquid phase, a concentration lower than 1%) and only a trace amount of silica is found in the liquid phase, suggesting that the silica/organic block copolymer composition has been already solidified at this time at the interface with salt water. When the concentration of salt LiCl is near saturation concentration (45%), the crystallization of the inorganic salt LiCl occurs. At this time, the formation of mesostructured silica has been almost completed. These results further indicate that the macroscopic silica structure is formed first at the interface of inorganic salt water, and sequentially, when the solution of the inorganic salt reaches saturation concentrations, crystal of inorganic salts are formed in the bottom of the membrane.

[0093] Based on above results, we postulate that macroscopic silica structure is formed around a droplet of inorganic salt solution as illustrated in Scheme A (Figure 53). Ethanol is first evaporated, then, water. As the inorganic salt solution becomes more concentrated, two domains are formed, one a water-rich domain, where most inorganic salt is located, another a water-poor domain, where silica and block copolymer compositions are located. The formation of two domains results in tri-phase separation, a droplet of inorganic salt solution phase separated by silica-block copolymer gel. The droplet of the solution serves as a template for the growth of silica-block copolymer composites. Once the macrostructure is rigidified, the inorganic salt solution approaches to the bottom of the container progressively. The cooperative self-assembly of silica/block copolymer occurs at the interface of the droplet, and results in coral-like mesomacroscopic silica structure. On the other hand, when the silica is formed at the interface of air and salt water, the droplet of the salt solution becomes flatters, resulting in the fenestrated membrane at the top.

[0094] Referring to Figure 54, progressively higher magnifications are shown of a section of a meso-macro silica membrane made in accordance with this invention. The membrane is shown in Figure 54a which has a macropore structure, as shown in Figure 54b. However the walls defining the macropores have a mesoporous structure.

[0095] In summary, artificial coral silica membranes with 3-d meso-macro structures have been synthesized by a novel process of an acidic catalyzed silica sol-gel chemistry in the present of inorganic salts. Inorganic salts play an important role on the formation of meso-macro silica membranes that are grown at the interface of a droplet of inorganic salt solution. The results are of general important for understanding multiphase processes such as the formation of diatoms coral silica structures in nature. The silica membranes (size - 4 cm x 4 cm, thickness - 5 mm) with 3-d meso-macro silica network structures show oriented continuous rope, toroid, and grape vine, or dish, pinwheel, gyroid, and cubic cage morphologies depending on the electrolyte strength of the inorganic salts or amphiphilic block copolymer templates. The macropore size (0.5 - 100 μm) can be controlled by inorganic salts and the evaporation rate of the solvent. The mesoscopic structures can be highly ordered 2-d honeycomb (pore size 40 - 90 Å) or 3-d cubic packing and are controlled by the amphiphilic block copolymer templates. The coral-like mesomacro silica membranes are thermally stable and exhibit large surface areas (to 1000 cm²/g) and pore volume (to 1.1 cm³/g). We anticipate that these new process ceramics material with structure and design on multiple length scales will have many applications

in the areas, including separation, sorption, medical implant, catalysis, and sensor array applications.

[0096] The example shown above in forming meso-macro silica membranes used Pluronic P123 block copolymer, $\text{EO}_{20}\text{PO}_{70}\text{EO}_{20}$ as the template to control mesoscopic ordering of the silica membranes. Besides P123, other surfactants can also be used in the synthesis. For example, one could use:

- (1) a diblock copolymer, poly(ethylene oxide)-*block*-poly(propylene oxide); poly(ethylene oxide)-*block*-poly(butylene oxide) (Dow Company); B50-6600, BL50-1500;
- (2), a triblock copolymer, poly(ethylene oxide)-*block*-poly(propylene oxide)-*block* poly(ethylene oxide); (BASF) poly(ethylene oxide)-*block*-poly(butylene oxide)-*block* poly(ethylene oxide) (Dow Company); such as Pluronic L64, L121, L122, P65, P85, P103, P104, P123, PF20, PF40, PF80, F68, F88, F98, F 108, F 127;
- (3) a reversed triblock copolymer Pluronic 25R8, 25R4, 25R2
- (4) a star di-block copolymer (BASF), Tetronic 901, 904, 908; and
- (5) a reversed star di-block copolymer Tetronic 90R1, 90R4, 90R8.

[0097] The inorganic salts can be electrolyte, such as KCl, NaCl, LiCl, NH_4Cl , MgCl, MgSO_4 , KNO_3 , NaClO_3 , Na_2SO_4 , NiSO_4 , CoCl_2 , water organic acid, such as DL tartaric acid, citric acid, malic acid. We claim that dissolvable alkali salts, alkaline earth salts, transition metal, sulfate, nitrate, halide, chlorate, per chlorate.

[0098] The preparation of meso-macro silica membrane are emulsion chemistry latex sphere template; phase separation and solvent exchanged; inorganic salts templating which was developed by ourselves here. This discovery should have great signification for understanding the formation of the diatom and coral in nature, The macromesoporous materials would have many applications in the areas of sorption, catalysis, separation, sensor arrays, optoelectronic devices. The materials and synthesis method described here are very versatile in that they can be used for many fields of application and for synthesis of any inorganic-surfactant composites, for example, aluminophosphate-based, TiO_2 , ZrO_2 , Al_2O_3 , Nb_2O_5 , Ta_2O_5 , Cr_2O_3 , Fe_2O_3 , ZrTiO_4 , Al_2SiO_5 , HfO_2 , meso-macroporous silica membranes. These materials would have many applications on sorption, catalysis, separation, sensor arrays, optoelectronic devices.

Table 1. Physicochemical Properties of Mesoporous Silica (SBA) prepared using Polyoxyalkylene Block Copolymers.

Block Copolymer	Formula	Mesophase	d(Å) ^a	BET surface area (m ² /g)	pore size ^b (Å)	pore volume(m ³ /g)	Wall ^c thickness (Å)
Pluronic L121	PEO ₃ PPO ₇₀ PEO ₅	lamellar	116				
Pluronic L121	PEO ₃ PPO ₇₀ PEO ₅	hexagonal	118(117)	633	100	1.04	35
Pluronic F127	PEO ₁₀₈ PPO ₇₀ PEO ₁₀₈	cubic	124(118)	742	54	0.454	
Pluronic F88	PEO ₁₀₀ PPO ₃₉ PEO ₁₀₀	cubic	118(101)	696	35	0.363	
Pluronic F68	PEO ₆₀ PPO ₃₀ PEO ₆₀	cubic	91.6(88.9)				
Pluronic P123	PEO ₂₀ PPO ₇₀ PEO ₂₀	hexagonal	104(95.7)	692	47	0.557	64
Pluronic P123	PEO ₂₀ PPO ₇₀ PEO ₂₀	hexagonal	105(97.5) ^d	780	60	0.795	53
Pluronic P123	PEO ₂₀ PPO ₇₀ PEO ₂₀	hexagonal	103(99.5) ^e	820	77	1.03	38
Pluronic P123	PEO ₂₀ PPO ₇₀ PEO ₂₀	hexagonal	108(105) ^f	920	85	1.23	36
Pluronic P123	PEO ₂₀ PPO ₇₀ PEO ₂₀	hexagonal	105(104) ^g	850	89	1.17	31
Pluronic P103	PEO ₁₇ PPO ₆₉ PEO ₁₇	hexagonal	97.5(80.6)	768	46	0.698	47
Pluronic P65	PEO ₂₀ PPO ₃₀ PEO ₂₀	hexagonal	77.6(77.6)	1003	51	1.26	39
Pluronic P85	PEO ₂₈ PPO ₃₉ PEO ₂₈	hexagonal	92.6(88.2)	962	60	1.08	42
Pluronic L64	PEO ₁₃ PPO ₇₀ PEO ₁₃	hexagonal	80.6(80.5)	950	59	1.19	34
Pluronic 25R4	PEO ₁₉ PPO ₃₃ PEO ₁₉	hexagonal	74.5(71.1)	1040	48	1.15	34
Tetronic 908		cubic	101(93.6)	1054	30	0.692	
Tetronic 901		cubic	73.9(70.1)				
Tetronic 90R4		cubic	7.39(68.5)	1020	45	0.910	--

a, d(100) spacing or d value of characteristic reflection of the as-synthesized products and the value inside brackets is the d value after calcination at 500 °C for 6 h; b, calculated from adsorption branch; c, calculated by $a_0 = 2 \times d(100)/\sqrt{3}$.

* reaction at 35 °C for 20 h, then heating: (d) at 80 °C for 24 h; (e) at 80 °C for 48 h; (f) at 90 °C for 24 h; (g) at 100 °C for 24 h.

Table 2. Physicochemical Properties of Mesoporous Silica (SBA) Prepared Using Nonionic Alkyl Polyethylene Oxide Surfactants.

Surfactant	Reaction Temperature	Mesophase	d(Å) ^a	BET surface area (m ² /g)	pore size ^b (Å)	pore volume (m ³ /g)
C ₁₀ EO ₂	RT	lamellar	64.3			
C ₁₂ EO ₄	RT	cubic	45.3(44.7)	665	22	0.375
C ₁₂ EO ₄	RT	lamellar (La)	45.7	570		
C ₁₂ EO ₄	60°C	lamellar	42.4	606	24	0.392
C ₁₆ EO ₁₀	RT	cubic	56.6(47.6)	1070	25	0.678
C ₁₆ EO ₁₀	100°C	hexagonal	64.1(62.8)	910	35	1.02
C ₁₆ EO ₂₀	RT	cubic	73.7(49.6)	602	22	0.291
C ₁₈ EO ₁₀	RT	P6 ₃ /mmc	63.5(51.0)	1150	31	0.826
C ₁₈ EO ₁₀	100°C	hexagonal	77.4(77.0)	912	40	0.923
C ₁₈ H ₃₅ EO ₁₀	RT	P6 ₃ /mmc	49.1(47.7)	1004	27	0.587
C ₁₂ EO ₂₃	RT	cubic	64.8(43.3)	503	16	0.241

Table 2 (continued)

Surfactant	Reaction Temperature	Mesophase	d(Å) ^a	BET surface area (m ² /g)	pore size ^b (Å)	pore volume (m ³ /g)
Tween 20	RT	cubic	55.1(46.8)	795	19	0.370
Tween 40	RT	cubic	52.4(49.6)	704	20	0.363
Tween 60	RT	cubic	62.4(54.4)	720	24	0.516
Tween 60	RT	lamellar	28.7			
Tween 80	RT	cubic	62.2(53.9)	712	25	0.431
Span 40	RT	lamellar	55.5			
Triton X100	RT	cubic	41.8(35.5)	776	17	0.353
Triton X114	RT	cubic	42.2(36.7)	989	16	0.453
Teritor TMN 6	RT	cubic	44.3(39.9)	1160	23	0.568
Teritor TMN 10	RT	cubic	42.3(36.5)	804	20	0.379

a, d(100) spacing or d value of characteristic reflection of the as-synthesized products and the number inside brackets is the d value after calcination at 500 °C for 6 h.

b, calculated from adsorption branch.

Table 3

System	Inorganic Precursor	Aging Temperature, °C	Aging time (day)	d (Å)
Zr	ZrCl ₄	40	1	125
Ti	TiCl ₄	40	7	123
Al	AlCl ₃	40	2	130
Si	SiCl ₄	40	2	171
Sn	SnCl ₄	40	2	124
Nb	NbCl ₅	40	2	106
Ta	TaCl ₅	40	2	110
W	WC1 ₆	60	15	126
Hf	HfCl ₄	40	1	124
Ge	GeCl ₄	40	15	146
V	VC1 ₄	60	7	111
Zn	ZnCl ₂	60	30	120
Cd	CdCl ₂	40	7	111
In	InCl ₃	60	30	124
Sb	SbCl ₅	60	30	93
Mo	MoCl ₅	60	7	100
Re	ReCl ₅	60	7	121
Ru	RuCl ₃	40	3	95
Ni	NiCl ₂	40	2	100
Fe	FeCl ₃	40	7	116
Cr	CrCl ₃	40	4	117
Mn	MnCl ₂	40	7	124
Cu	CuCl ₂	40	7	98
SiAl	AlCl ₃ /SiCl ₄	40	2	120
Si ₂ Al	AlCl ₃ /SiCl ₄	40	2	120
ZrTi	ZrCl ₄ /TiCl ₄	40	2	110
Al ₂ Ti	AlCl ₃ /TiCl ₄	40	7	112
SiTi	SiCl ₄ /TiCl ₄	40	3	103
ZrW ₂	ZrCl ₄ /WC1 ₆	40	3	140
SnIn	SnCl ₄ /InCl ₃	40	30	83

Table 4

Oxide	d_{100} (Å)	Wall Structure	Wall Thickness (Å)	Nanocrystal Size (Å)	Pore Size (Å)	BET Surface Area (m^2/g)	Porosity	Physical Properties
ZrO ₂	106	Tetra. ZrO ₂	65	15	58	150	0.43	dielectric
TiO ₂	101	Anatase	51	24	65	205	0.46	semicond.
Nb ₂ O ₅	75	Nb ₂ O ₅	40	<10	45	196	0.50	dielectric
Ta ₂ O ₅	68	Ta ₂ O ₅	40	<10	35	165	0.50	dielectric
WO ₃	95	WO ₃	50	30	50	125	0.48	semicond.
SnO ₂	106	Cassiterite	50	30	68	180	0.52	semicond.
HfO ₂	105	amorphous	50	--	70	105	0.52	dielectric
Al ₂ O ₃	186	amorphous	35	--	140	300	0.61	dielectric
SiO ₂	198	amorphous	86	--	120	810	0.63	dielectric
SiAlO _{3.5}	95	amorphous	38	--	60	310	0.59	dielectric
Si ₂ AlO _{5.5}	124	amorphous	40	--	100	330	0.55	dielectric
Al ₂ TiO ₅	105	amorphous	40	--	80	270	0.59	dielectric
ZrTiO ₄	103	amorphous	35	--	80	130	0.46	dielectric
SiTiO ₄	95	amorphous	45	--	80	495	0.63	dielectric
ZrW ₂ O ₈	100	amorphous	45	--	50	170	0.51	NTE

Claims

1. A method of forming a mesoscopically structured material, comprising:
 - 5 combining an amphiphilic block copolymer with a metalate precursor species under acidic conditions whereby the block copolymer and metalate precursor species are self-assembled and the metalate precursor species are polymerized to form a mesoscopically structured inorganic-organic composite.
- 10 2. The method of claim 1, wherein the amphiphilic block copolymer functions as a structure-directing agent with an aqueous soluble metalate precursor species, where the metalate precursor species partitions within hydrophilic regions of a self-assembling block copolymer system.
- 15 3. The method of claim 1, wherein the amphiphilic block polymer is an amphiphilic poly(alkylene oxide) block copolymer having hydrophilic and hydrophobic components that function as structure-directing moieties with the metalate precursor species,
4. The method of claim 3, wherein the metalate precursor species form complexes through coordination bonds with alkylene oxide segments of the block copolymer.
- 20 5. The method of claim 4, wherein the complexes self-assemble according to mesoscopic ordering directed principally by microphase separation of the block copolymer.
- 25 6. The method of claim 1 in which said block copolymer and metalate precursor species are in an aqueous or polar solvent and including the step of evaporating said solvent to form a transparent mesoscopically structured inorganic-organic composite.
7. The method of claim 1 wherein said metalate precursor species, upon calcination, forms an oxide selected from TiO_2 , ZrO_2 , Nb_2O_5 , Ta_2O_5 , Al_2O_3 , SiO_2 , WO_3 , SnO_2 , HfO_2 , $\text{SiAlO}_{3.5}$, $\text{SiAlO}_{5.5}$, Al_2TiO_5 , ZrTiO_4 , and SiTiO_4 .
- 30 8. The method of claim 1 wherein said metalate precursor species, upon calcination, forms SiO_2 .
9. A method of forming a mesoscopically structured material, comprising the steps of
 - 35 combining in a polar solvent an amphiphilic block copolymer that functions as a structure-directing agent with an inorganic compound of a multivalent metal species whereby the block copolymer and inorganic compounds are self-assembled; and
 - polymerizing the inorganic compounds under non-aqueous conditions to form a mesoscopically structured inorganic-organic composite.
 - 40
10. The method of claim 9, including the step, after polymerizing the mesoscopically structured inorganic-organic composite, of evaporating said solvent to form a transparent mesostructured material with a uniform characteristic ordering length scale.
- 45 11. The method of claim 1 or 9 including the step of removing said polymer from the mesoscopically structured inorganic-organic composite to form a thermally stable mesoporous material.
12. The method of claim 1 or 9 including the step-of calcining or solvent extracting said mesoscopically structured inorganic-organic composite to remove the organic species and thereby form a mesoporous multivalent metal oxide material with a high surface area.
- 50 13. The method of claim 11 including the step of adding an organic cosolvent to said amphiphilic block polymer to increase the pore size and wall thickness of said mesoporous material.
- 55 14. The method of claim 13 in which mesopore sizes are controlled by the block copolymer and cosolvent swelling agents.
15. The method of claim 11 including the step of thermally treating said combination of amphiphilic block polymer and

inorganic compound to increase the pore size, wall thickness, and thermal stability of the mesoporous material.

16. A method of forming a three-dimensional meso-macro structured material, comprising the steps of:

5 placing an amphiphilic block copolymer in an aqueous solution of inorganic salt;

10 combining the aqueous solution containing the block copolymer with an inorganic compound of a multivalent metal species to form a multiphase medium that enables microphase separation of inorganic compounds and the block copolymer, thereby forming an inorganic-block copolymer composite wherein the block copolymer functions as a structure-directing agent and also enables macrophase separation of the inorganic-block copolymer composite and the aqueous solution of inorganic salt; and

polymerizing the inorganic compounds to form a meso-macro structured inorganic-organic composite.

15 17. The method of claim 16 in which said inorganic compound is added to said block polymer solution in the form of a sol gel.

20 18. The method of claim 16 in which said block copolymer and inorganic compounds are combined in an aqueous or polar solvent and including the step of evaporating said solvent from said meso-macro structured composite to form a transparent mesostructured material with a uniform characteristic ordering length scale.

19. The method of claim 16 including the step of removing the block copolymer from said meso-macro structured inorganic-organic composite to form said meso-macro structured material.

25 20. The method of claim 16 including the step of calcining or solvent extracting the meso-macro structured composite to form a multivalent metal oxide material with macroporosity and a mesoporous surface area.

30 21. The method of claim 16 including the step of adding an organic cosolvent to said amphiphilic block polymer to increase the pore size and wall thickness of said mesoscopically structured inorganic material.

22. The method of claim 16 including the step of thermally treating said combination of amphiphilic block polymer and inorganic compound to increase the pore size and wall thickness, and thermal stability.

35 23. The method of claim 16 in which macropore sizes are controlled by varying the electrolyte strength of the inorganic salt.

24. The method of claim 16 in which mesopore sizes are controlled by the block copolymer and cosolvent swelling agents.

40 25. The method of claim 1, 9 or 16 in which said block copolymer is a triblock polymer.

26. The method of claim 25 in which said triblock copolymer is a poly(ethylene oxide)-poly(alkylene oxide)- poly(ethylene oxide) polymer where the alkylene oxide moiety has at least three carbon atoms.

45 27. The method of claim 25 in which said triblock copolymer is a poly(ethylene oxide)-poly(propylene oxide)- poly(ethylene oxide) polymer.

50 28. The method of claim 25 in which said triblock copolymer is a poly(ethylene oxide)-poly(butylene oxide)- poly(ethylene oxide) polymer.

29. The method of claim 1, 9 or 16 in which said block copolymer is a diblock polymer.

30. The method of claim 1, 9 or 16 in which said block copolymer is a reversed triblock polymer.

55 31. The method of claim 1, 9 or 16 in which said block copolymer is a star di-block polymer.

32. The method of claim 1, 9 or 16 in which said block polymer is a reversed star di-block polymer.

EP 1 037 940 B1

33. The method of claim 9 or 16 wherein said inorganic compound, upon calcination, forms an oxide selected from TiO_2 , ZrO_2 , Nb_2O_5 , Ta_2O_5 , Al_2O_3 , SiO_2 , WO_3 , SnO_2 , HfO_2 , $\text{SiAlO}_{3.5}$, $\text{SiAlO}_{5.5}$, Al_2TiO_5 , ZrTiO_4 , and SiTiO_4 .
- 5 34. The method of claim 9 or 16 wherein said inorganic compound, upon calcination, forms SiO_2 .
35. A mesostructured material made according to claim 1 or 9, wherein the mesostructured material is a mesoscopically structured composite of an amphiphilic block copolymer and a compound of a multivalent metal species.
- 10 36. The mesostructured material of claim 35 in which said block copolymer is a triblock polymer.
37. The mesostructured material of claim 35 in which said triblock copolymer is a poly(ethylene oxide)-poly(alkylene oxide)- poly(ethylene oxide) polymer where the alkylene oxide moiety has at least three carbon atoms.
- 15 38. The mesostructured material of claim 35 in which said triblock copolymer is a poly(ethylene oxide)-poly(propylene oxide)- poly(ethylene oxide) polymer.
39. The mesostructured material of claim 35 in which said triblock copolymer is a poly(ethylene oxide)-poly(butylene oxide)- poly(ethylene oxide) polymer.
- 20 40. The mesostructured material of claim 35 in which said block copolymer is a diblock polymer.
41. The mesostructured material of claim 35 in which said block copolymer is a reversed triblock polymer.
42. The mesostructured material of claim 35 in which said block copolymer is a star di-block polymer.
- 25 43. The mesostructured material of claims 35 in which said block polymer is a reversed star di-block polymer.
44. A transparent mesostructured material made according to claim 6 or 10.
- 30 45. The transparent mesostructured material of claim 44 in which said transparent material is crack-free.
46. The transparent mesostructured material of claim 44 in which said transparent material is in the form of a meso-oscopically ordered, mesoporous, crack-free thin film.
- 35 47. A mesostructured material made according to claim 12, wherein the mesostructured material is a thermally stable mesoscopically ordered porous material comprised of a multivalent metal compound and having a narrow distribution of pore sizes in the mesoscopic size regime.
- 40 48. The mesostructured material of claim 35, 44 or 47 comprising a two dimensional hexagonal mesostructure.
49. The mesostructured material of claim 35, 44 or 47 comprising a cubic mesostructure.
- 50 50. The mesostructured material of claim 35, 44 or 47 comprising a lamellar mesostructure.
- 45 51. The mesostructured material of claim 35, 44 or 47 in the form of fibers.
52. The mesostructured material of claim 35, 44 or 47 in the form of thin films.
53. The mesostructured material of claim 35, 44 or 47 in the form of monoliths.
- 50 54. The mesostructured material of claim 47 having a porosity of at least 40%.
- 55 55. The mesostructured material of claim 47 having a dielectric constant of 2-2.5.
56. A meso-macrostructured material made according to claim 25, wherein the meso-macrostructured material is a macroporous multivalent metal oxide material having an ordered mesoporous surface area.
57. The meso-macrostructured material of claim 56 wherein said multivalent metal oxide is selected from the group

EP 1 037 940 B1

consisting of TiO_2 , ZrO_2 , Nb_2O_5 , Ta_2O_5 , Al_2O_3 , SiO_2 , WO_3 , SnO_2 , HfO_2 , $\text{SiAlO}_{3.5}$, $\text{SiAlO}_{5.5}$, Al_2TiO_5 , ZrTiO_4 , and SiTiO_4 .

- 5
58. The meso-macrostructured material of claim 56 wherein said multivalent metal compound is SiO_2 .
59. The meso-macrostructured material of claim 56 comprising a two dimensional hexagonal mesostructure.
60. The meso-macro structured material of claim 56 comprising a cubic mesostructure.
- 10
61. The meso-macrostructured material of claim 57 comprising a lamellar mesostructure.
62. The mesostructured material of claim 56 in the form of fibers.
63. The mesostructured material of claim 56 in the form of thin films.
- 15
64. The mesostructured material of claim 56 in the form of monoliths.
65. The mesostructured material of claim 56 having a porosity of at least 40%.
- 20
66. A method of separating biomolecules from a biological specimen or synthesis mixture, comprising passing said biological specimen or mixture through the mesostructured material of claim 47.
67. The method of claim 66 in which said biomolecules comprise enzymes and/or proteins.
- 25
68. A method of separating biomolecules from a biological specimen or synthesis mixture, comprising passing said biological specimen or mixture through meso-macrostructured material of claim 56.
69. The method of claim 68 in which said biomolecules comprise enzymes and/or proteins.
- 30
70. A method of separating organics from a solution, comprising passing said solution through the mesostructured material of claim 47.
71. A method of separating organics from a solution, comprising passing said solution through the meso-macrostructured material of claim 56.
- 35
72. A method of separating inorganics from a solution, comprising passing said solution through the mesostructured material of claim 47.
73. A method of separating inorganics from a solution, comprising passing said solution through the meso-macrostructured material of claim 56.
- 40
74. A method of imparting adsorption and catalytic reaction selectivities to the meso-macrostructured material of claim 56, comprising functionalizing separately the different mesoscopic and macroscopic pore surfaces of said material of to provide said selectivities.
- 45

Patentansprüche

- 50
1. Ein Verfahren zur Bildung eines mesoskopisch strukturierten Materials, umfassend:
- Kombinieren eines amphiphilen Blockcopolymers mit einer Metallatprecursorspezies unter sauren Bedingungen, wobei das Blockcopolymer und die Metallatprecursorspezies selbst-organisiert sind und die Metallatprecursorspezies polymerisiert werden, um ein mesoskopisch strukturiertes anorganisch-organisches Verbundsystem zu bilden.
- 55
2. Das Verfahren gemäß Anspruch 1, wobei das amphiphile Blockcopolymer als ein struktur-dirigierendes Mittel mit einer wasserlöslichen Metallatprecursorspezies fungiert, wobei die Metallatprecursorspezies innerhalb hydrophiler Bereiche eines selbst-organisierenden Blockcopolymersystems partitioniert.

EP 1 037 940 B1

3. Das Verfahren gemäß Anspruch 1, wobei das amphiphile Blockpolymer ein amphiphiles Poly(alkylenoxid)-Blockcopolymer ist, das hydrophile und hydrophobe Komponenten besitzt, die mit der Metallatprecursorspezies als struktur-dirigierende Teile fungieren.
- 5 4. Das Verfahren gemäß Anspruch 3, wobei die Metallatprecursorspezies Komplexe mittels Koordinationsbindungen mit Alkylenoxidsegmenten des Blockcopolymers bilden.
5. Das Verfahren gemäß Anspruch 4, wobei sich die Komplexe gemäß der mesoskopischen Orientierung, die hauptsächlich von einer Mikrophasentrennung des Blockcopolymers dirigiert wird, selbst-orientieren.
- 10 6. Das Verfahren gemäß Anspruch 1, wobei sich das Blockcopolymer und die Metallatprecursorspezies in einem wässrigen oder polaren Lösungsmittel befinden und der Verdampfungsschritt des Lösungsmittels beinhaltet ist, um ein durchsichtiges mesoskopisch strukturiertes anorganisch-organisches Verbundsystem zu bilden.
- 15 7. Das Verfahren gemäß Anspruch 1, wobei die Metallatprecursorspezies nach Kalzinierung eines der folgenden Oxide bildet: TiO_2 , ZrO_2 , Nb_2O_5 , Ta_2O_5 , Al_2O_3 , SiO_2 , WO_3 , SnO_2 , HfO_2 , $\text{SiAlO}_{3,5}$, $\text{SiAlO}_{5,5}$, Al_2TiO_5 , ZrTiO_4 und SiTiO_4 .
- 20 8. Das Verfahren gemäß Anspruch 1, wobei die Metallatprecursorspezies nach Kalzinierung SiO_2 bildet.
9. Ein Verfahren der Bildung eines mesoskopisch strukturierten Materials, umfassend die folgenden Schritte:
 - 25 Kombinieren eines amphiphilen Blockcopolymers, das als ein struktur-dirigierendes Mittel fungiert, mit einer anorganischen Verbindung einer multivalenten Metallspezies in einem polaren Lösungsmittel, wobei das Blockcopolymer und die anorganischen Verbindungen selbst-organisiert sind; und
 - 30 Polymerisieren der anorganischen Verbindungen unter wasserfreien Bedingungen, um ein mesoskopisch strukturiertes anorganisch-organisches Verbundsystem zu bilden.
- 30 10. Das Verfahren gemäß Anspruch 9, umfassend nach Polymerisierung des mesoskopisch strukturierten anorganisch-organischen Verbundsystems den Schritt des Verdampfens des Lösungsmittels, um ein durchsichtiges mesostrukturiertes Material mit einer einheitlichen charakteristischen Orientierungslängenskala zu bilden.
- 35 11. Das Verfahren gemäß Anspruch 1 oder 9, umfassend den Schritt des Entfernens des Polymers aus dem mesoskopisch strukturierten anorganisch-organischen Verbundsystem, um ein thermisch stabiles mesoporöses Material zu bilden.
- 40 12. Das Verfahren gemäß Anspruch 1 oder 9, umfassend den Kalzinierungs- oder Lösungsmittlextraktionsschritt des mesoskopisch strukturierten anorganisch-organischen Verbundsystems, um die organische Spezies zu entfernen und dadurch ein mesoporöses multivalentes Metalloxidmaterial mit einem großen Oberflächenbereich zu bilden.
- 45 13. Das Verfahren gemäß Anspruch 11, umfassend den Additionsschritt eines organischen Kosolvens zum amphiphilen Blockpolymer, um die Porengröße und Wanddicke des mesoporösen Materials zu erhöhen.
- 50 14. Das Verfahren gemäß Anspruch 13, wobei die Mesoporengrößen mittels dem Blockcopolymer und Kosolvensquellenmitteln gesteuert werden.
15. Das Verfahren gemäß Anspruch 11, umfassend den thermischen Behandlungsschritt der Kombination des amphiphilen Blockpolymers und der anorganischen Verbindung, um die Porengröße, Wanddicke und thermische Stabilität des mesoporösen Materials zu erhöhen.
- 55 16. Ein Verfahren zur Bildung eines drei-dimensionalen mesomakro-strukturierten Materials, umfassend die folgenden Schritte:
 - Platzieren eines amphiphilen Blockcopolymers in eine wässrige Lösung eines anorganischen Salzes;
 - Kombinieren der das Blockcopolymer beinhaltenden wässrigen Lösung mit einer anorganischen Verbindung einer multivalenten Metallspezies, um ein mehrphasiges Medium zu bilden, das eine Mikrophasentrennung

der anorganischen Verbindungen ermöglicht, und das Blockcopolymer dabei ein anorganisches Blockcopolymer-Verbundsystem bildet, wobei das Blockcopolymer als ein struktur-dirigierendes Mittel fungiert und ebenfalls eine Makrophasentrennung des anorganischen Blockcopolymer-Verbundsystems und der wässrigen Lösung des anorganischen Salzes ermöglicht; und

5

Polymerisieren der anorganischen Verbindungen, um ein mesomakro-strukturiertes anorganisch-organisches Verbundsystem zu bilden.

- 10 17. Das Verfahren gemäß Anspruch 16, wobei die anorganische Verbindung in der Form eines Sol-Gels zur Blockpolymerlösung zugegeben wird.
- 15 18. Das Verfahren gemäß Anspruch 16, wobei das Blockcopolymer und die anorganischen Verbindungen in einem wässrigen oder polaren Lösungsmittel kombiniert werden und umfassend den Verdampfungsschritt des Lösungsmittels aus dem mesomakro-strukturierten Verbundsystem, um ein durchsichtiges mesostrukturiertes Material mit einer einheitlichen charakteristischen Orientierungslängenskala zu bilden.
- 20 19. Das Verfahren gemäß Anspruch 16, umfassend den Entfernungsschritt des Blockcopolymer aus dem mesomakro-strukturierten anorganisch-organischen Verbundsystem, um das mesomakro-strukturierte Material zu bilden.
- 25 20. Das Verfahren gemäß Anspruch 16, umfassend den Kalzinierungs- oder Lösungsmittlextraktionsschritt des mesomakro-strukturierten Verbundsystems, um ein multivalentes Metalloxidmaterial mit einer Makroporosität und einem mesoporösen Oberflächenbereich zu bilden.
- 30 21. Das Verfahren gemäß Anspruch 16, umfassend den Additionsschritt eines organischen Kosolvens zum amphiphilen Blockpolymer, um die Porengröße und Wanddicke des mesoskopisch strukturierten anorganischen Materials zu erhöhen.
- 35 22. Das Verfahren gemäß Anspruch 16, umfassend den thermischen Behandlungsschritt der Kombination des amphiphilen Blockpolymers und der anorganischen Verbindung, um die Porengröße, Wanddicke und thermische Stabilität zu erhöhen.
- 40 23. Das Verfahren gemäß Anspruch 16, wobei die Makroporengrößen mittels Variation der Stärke des Elektrolyten des anorganischen Salzes gesteuert werden.
- 45 24. Das Verfahren gemäß Anspruch 16, wobei die Mesoporengrößen mittels dem Blockcopolymer und den Kosolvensquellungsmitteln gesteuert werden.
- 50 25. Das Verfahren gemäß Anspruch 1, 9 oder 16, wobei das Blockcopolymer ein Tri-Blockpolymer ist.
- 55 26. Das Verfahren gemäß Anspruch 25, wobei das Tri-Blockcopolymer ein Poly(ethylenoxid)-poly(alkylenoxid)-poly(ethylenoxid)polymer ist, wobei der Alkylenoxid-Rest wenigstens drei Kohlenstoffatome besitzt.
27. Das Verfahren gemäß Anspruch 25, wobei das Tri-Blockcopolymer ein Poly(ethylenoxid)-poly(propylenoxid)-poly(ethylenoxid)polymer ist.
28. Das Verfahren gemäß Anspruch 25, wobei das Tri-Blockcopolymer ein Poly(ethylenoxid)-poly(butylenoxid)-poly(ethylenoxid)polymer ist.
29. Das Verfahren gemäß Anspruch 1, 9 oder 16, wobei das Blockcopolymer ein Di-Blockpolymer ist.
30. Das Verfahren gemäß Anspruch 1, 9 oder 16, wobei das Blockcopolymer ein umgedrehtes Tri-Blockpolymer ist.
31. Das Verfahren gemäß Anspruch 1, 9 oder 16, wobei das Blockcopolymer ein Stern-diblockpolymer ist.
32. Das Verfahren gemäß Anspruch 1, 9 oder 16, wobei das Blockcopolymer ein umgedrehtes Stern-diblockpolymer ist.
33. Das Verfahren gemäß Anspruch 9 oder 16, wobei die anorganische Verbindung nach Kalzinierung eines der fol-

EP 1 037 940 B1

genden Oxide bildet: TiO_2 , ZrO_2 , Nb_2O_5 , Ta_2O_5 , Al_2O_3 , SiO_2 , WO_3 , SnO_2 , HfO_2 , $\text{SiAlO}_{3,5}$, $\text{SiAlO}_{5,5}$, Al_2TiO_5 , ZrTiO_4 und SiTiO_4 .

- 5
34. Das Verfahren gemäß Anspruch 9 oder 16, wobei die anorganische Verbindung nach Kalzinierung SiO_2 bildet.
35. Ein gemäß Anspruch 1 oder 9 hergestelltes mesostrukturiertes Material, wobei das mesostrukturierte Material ein mesoskopisch strukturiertes Verbundsystem eines amphiphilen Blockcopolymers und einer Verbindung einer multivalenten Metallspezies ist.
- 10
36. Das mesostrukturierte Material gemäß Anspruch 35, wobei das Blockcopolymer ein Tri-Blockcopolymer ist.
37. Das mesostrukturierte Material gemäß Anspruch 35, wobei das Tri-Blockcopolymer ein Poly(ethylenoxid)-poly(alkylenoxid)-poly(ethylenoxid)polymer ist, wo der Alkylenoxid-Rest wenigstens drei Kohlenstoffatome besitzt.
- 15
38. Das mesostrukturierte Material gemäß Anspruch 35, wobei das Tri-Blockcopolymer ein Poly(ethylenoxid)-poly(propylenoxid)-poly(ethylenoxid)-polymer ist.
39. Das mesostrukturierte Material gemäß Anspruch 35, wobei das Tri-Blockcopolymer ein Poly(ethylenoxid)-poly(butylenoxid)-poly(ethylenoxid)polymer ist.
- 20
40. Das mesostrukturierte Material gemäß Anspruch 35, wobei das Blockcopolymer ein Di-Blockpolymer ist.
41. Das mesostrukturierte Material gemäß Anspruch 35, wobei das Blockcopolymer ein umgedrehtes Tri-Blockpolymer ist.
- 25
42. Das mesostrukturierte Material gemäß Anspruch 35, wobei das Blockcopolymer ein Stern-diblockpolymer ist.
43. Das mesostrukturierte Material gemäß Anspruch 35, wobei das Blockpolymer ein ungedrehtes Stern-diblockpolymer ist.
- 30
44. Ein gemäß Anspruch 6 oder 10 hergestelltes durchsichtiges mesostrukturiertes Material.
45. Das durchsichtige mesostrukturierte Material gemäß Anspruch 44, wobei das durchsichtige Material rissfrei ist.
- 35
46. Das durchsichtige mesostrukturierte Material gemäß Anspruch 44, wobei das durchsichtige Material in der Form eines mesoskopisch orientierten, mesoporösen und rissfreien Films vorliegt.
47. Ein gemäß Anspruch 12 hergestelltes mesostrukturiertes Material, wobei das mesostrukturierte Material ein thermisch stabiles mesoskopisch orientiertes poröses Material ist, das aus einer multivalenten Metallverbindung besteht und eine enge Porengrößenverteilung im mesoskopischen Größenregime besitzt.
- 40
48. Das mesostrukturierte Material gemäß Anspruch 35, 44 oder 47, das eine zweidimensionale hexagonale Mesostruktur umfasst.
- 45
49. Das mesostrukturierte Material gemäß Anspruch 35, 44 oder 47, das eine kubische Mesostruktur umfasst.
50. Das mesostrukturierte Material gemäß Anspruch 35, 44 oder 47, das eine lamellare Mesostruktur umfasst.
51. Das mesostrukturierte Material gemäß Anspruch 35, 44 oder 47 in der Form von Fasern.
- 50
52. Das mesostrukturierte Material gemäß Anspruch 35, 44 oder 47 in der Form von dünnen Filmen.
53. Das mesostrukturierte Material gemäß Anspruch 35, 44 oder 47 in der Form von Monolithen.
- 55
54. Das mesostrukturierte Material gemäß Anspruch 47, das eine Porosität von wenigstens 40% besitzt.
55. Das mesostrukturierte Material gemäß Anspruch 47, das eine Dielektrizitätskonstante von 2 - 2,5 besitzt.

EP 1 037 940 B1

56. Ein gemäß Anspruch 25 hergestelltes mesomakro-strukturiertes Material, wobei das mesomakro-strukturierte Material ein makroporöses multivalentes Metalloxidmaterial ist, das einen orientierten mesoporösen Oberflächenbereich besitzt.
- 5 57. Das mesomakro-strukturierte Material gemäß Anspruch 56, wobei das multivalente Metalloxid aus der folgenden Gruppe ausgewählt wird: TiO_2 , ZrO_2 , Nb_2O_5 , Ta_2O_5 , Al_2O_3 , SiO_2 , WO_3 , SnO_2 , HfO_2 , $\text{SiAlO}_{3,5}$, $\text{SiAlO}_{5,5}$, Al_2TiO_5 , ZrTiO_4 und SiTiO_4 .
- 10 58. Das mesomakro-strukturierte Material gemäß Anspruch 56, wobei die multivalente Metallverbindung SiO_2 ist.
59. Das mesomakro-strukturierte Material gemäß Anspruch 56, das eine zweidimensionale hexagonale Mesostruktur umfasst.
- 15 60. Das mesomakro-strukturierte Material gemäß Anspruch 56, das eine kubische Mesostruktur umfasst.
61. Das mesomakro-strukturierte Material gemäß Anspruch 56, das eine lamellare Mesostruktur umfasst.
62. Das mesostrukturierte Material gemäß Anspruch 56 in der Form von Fasern.
- 20 63. Das mesostrukturierte Material gemäß Anspruch 56 in der Form von dünnen Filmen.
64. Das mesostrukturierte Material gemäß Anspruch 56 in der Form von Monolithen.
- 25 65. Das mesostrukturierte Material gemäß Anspruch 56, das wenigstens eine Porosität von 40% besitzt.
66. Ein Verfahren zur Trennung von Biomolekülen aus einer biologischen Probe oder Synthesemischung, welches das Durchlaufen der biologischen Probe oder Mischung durch das mesostrukturierte Material gemäß Anspruch 47 umfasst.
- 30 67. Das Verfahren gemäß Anspruch 66, wobei die Biomoleküle Enzyme und/oder Proteine umfassen.
68. Ein Verfahren zur Trennung von Biomolekülen aus einer biologischen Probe oder Synthesemischung, welches das Durchlaufen der biologischen Probe oder Mischung durch das mesomakro-strukturierte Material gemäß Anspruch 56 umfasst.
- 35 69. Das Verfahren gemäß Anspruch 68, wobei die Biomoleküle Enzyme und/oder Proteine umfassen.
70. Ein Verfahren zur Trennung organischer Verbindungen aus einer Lösung, welches das Durchlaufen der Lösung durch das mesostrukturierte Material gemäß Anspruch 47 umfasst.
- 40 71. Ein Verfahren zur Trennung organischer Verbindungen aus einer Lösung, welches das Durchlaufen der Lösung durch das mesomakro-strukturierte Material gemäß Anspruch 56 umfasst.
- 45 72. Ein Verfahren zur Trennung anorganischer Verbindungen aus einer Lösung, welches das Durchlaufen der Lösung durch das mesostrukturierte Material gemäß Anspruch 47 umfasst.
73. Ein Verfahren zur Trennung anorganischer Verbindungen aus einer Lösung, welches das Durchlaufen der Lösung durch das mesomakro-strukturierte Material gemäß Anspruch 56 umfasst.
- 50 74. Ein Verfahren zur Vermittlung von Adsorptions- und katalytischen Reaktionsselektivitäten an das mesomakro-strukturierte Material gemäß Anspruch 56, welches die getrennte Funktionalisierung der verschiedenen mesoskopischen und makroskopischen Porenoberflächen des Materials umfasst, um die Selektivitäten bereitzustellen.

55 Revendications

1. Procédé de formation d'un matériau à structure mésoscopique comprenant :

la combinaison d'un copolymère séquencé amphiphile avec une espèce précurseur métalate dans des conditions acides telles que le copolymère séquencé et l'espèce précurseur métalate sont auto-assemblés et que les espèces précurseur métalate sont polymérisées pour former un composite inorganique-organique à structure mésoscopique ; et

- 5
2. Procédé selon la revendication 1, dans lequel le copolymère séquencé amphiphile fonctionne comme un agent directeur de structure avec une espèce précurseur métalate soluble aqueuse, où l'espèce précurseur métalate se segmente à l'intérieur de régions hydrophiles d'un système de copolymère séquencé qui s'auto-assemble.
- 10
3. Procédé selon la revendication 1, dans lequel le polymère séquencé amphiphile est un copolymère séquencé poly (alkylène oxyde) amphiphile ayant des composantes hydrophiles et hydrophobes qui fonctionnent comme groupes fonctionnels directeurs de structure avec les espèces précurseur métalate.
- 15
4. Procédé selon la revendication 3, dans lequel les espèces précurseur métalate forment des complexes par l'intermédiaire de liaisons de coordination avec des segments d'oxyde d'alkylène du copolymère séquencé.
5. Procédé selon la revendication 4, dans lequel les complexes s'auto-assemblent selon une organisation mésoscopique dirigée principalement par séparation en microphases du copolymère séquencé.
- 20
6. Procédé selon la revendication 1, dans lequel lesdits copolymère séquencé et espèce précurseur métalate sont dans un solvant polaire ou aqueux et comprenant l'étape consistant à faire évaporer ledit solvant pour former un composite inorganique-organique à structure mésoscopique transparent.
- 25
7. Procédé selon la revendication 1, dans lequel ladite espèce précurseur métalate, lors de la calcination, forme un oxyde sélectionné à partir de TiO_2 , ZrO_2 , Nb_2O_5 , Ta_2O_5 , Al_2O_3 , SiO_2 , WO_3 , SnO_2 , HfO_2 , $\text{SiAlO}_{3,5}$, $\text{SiAlO}_{5,5}$, Al_2TiO_5 , ZrTiO_4 et SiTiO_4 .
- 30
8. Procédé selon la revendication 1, dans lequel ladite espèce précurseur métalate, lors de la calcination, forme du SiO_2 .
- 35
9. Procédé de formation d'un matériau à structure mésoscopique, comprenant les étapes consistant à :
- combiner dans un solvant polaire un copolymère séquencé amphiphile qui fonctionne comme un agent de direction de structure avec un composé inorganique d'une espèce métallique polyvalente de sorte que le copolymère séquencé et les composés inorganiques sont auto-assemblés ; et
- polymériser les composés inorganiques dans des conditions non aqueuses pour former un composite inorganique-organique à structure mésoscopique.
- 40
10. Procédé selon la revendication 9, comprenant l'étape, après polymérisation du composite inorganique-organique à structure mésoscopique, consistant à faire évaporer ledit solvant pour former un matériau mésostructuré transparent avec une échelle de longueur d'organisation caractéristique uniforme.
- 45
11. Procédé selon la revendication 1 ou 9, comprenant l'étape consistant à retirer ledit polymère du composite inorganique-organique à structure mésoscopique pour former un matériau mésoporeux thermiquement stable.
- 50
12. Procédé selon la revendication 1 ou 9, comprenant l'étape consistant à calciner ou à extraire par solvant ledit composite inorganique-organique à structure mésoscopique pour retirer l'espèce organique et former ainsi un matériau d'oxyde métallique polyvalent mésoporeux avec une surface élevée.
- 55
13. Procédé selon la revendication 11, comprenant l'étape consistant à ajouter un cosolvant organique audit polymère séquencé amphiphile pour augmenter la dimension des pores et l'épaisseur des parois dudit matériau mésoporeux.
14. Procédé selon la revendication 13, dans lequel les dimensions de mésopores sont contrôlées par le copolymère séquencé et des agents gonflants de cosolvant.
15. Procédé selon la revendication 11, comprenant l'étape consistant à traiter thermiquement ladite combinaison de polymère séquencé amphiphile et de composé inorganique pour augmenter la dimension des pores et l'épaisseur

des parois, ainsi que la stabilité thermique du matériau mésoporeux.

16. Procédé de formation d'un matériau méso-macro structuré à trois dimensions, comprenant les étapes consistant à :

5 placer un copolymère séquencé amphiphile dans une solution aqueuse de sel inorganique ;

10 combiner la solution aqueuse contenant le copolymère séquencé avec un composé inorganique d'une espèce métallique polyvalente pour former un milieu à plusieurs phases qui permet une séparation en microphases de composés inorganiques et du copolymère séquencé, formant ainsi un composite inorganique - copolymère séquencé dans lequel le copolymère séquencé fonctionne comme un agent directeur de structure et permet également une séparation en macrophases du composite inorganique - copolymère séquencé et de la solution aqueuse de sel inorganique ; et

15 polymériser les composés inorganiques pour former un composite inorganique-organique méso-macro structuré.

17. Procédé selon la revendication 16, dans lequel ledit composé inorganique est ajouté à ladite solution de polymère séquencé sous la forme d'un gel sol.

20 18. Procédé selon la revendication 16, dans lequel ledit copolymère séquencé et les composés inorganiques sont combinés dans un solvant polaire ou aqueux et comprenant l'étape consistant à faire évaporer ledit solvant dudit composite méso-macro structuré pour former un matériau mésostructuré transparent avec une échelle de longueur d'organisation caractéristique uniforme.

25 19. Procédé selon la revendication 16, comprenant l'étape consistant à retirer le copolymère séquencé dudit composite inorganique-organique méso-macro structuré pour former ledit matériau méso-macro structuré.

30 20. Procédé selon la revendication 16, comprenant l'étape consistant à calciner ou à extraire par solvant le composite méso-macro structuré pour former un matériau d'oxyde métallique polyvalent avec une macroporosité et une surface mésoporeuse.

35 21. Procédé selon la revendication 16, comprenant l'étape consistant à ajouter un cosolvant organique audit polymère séquencé amphiphile pour augmenter la dimension des pores et l'épaisseur des parois dudit matériau inorganique à structure mésoscopique.

22. Procédé selon la revendication 16, comprenant l'étape consistant à traiter thermiquement ladite combinaison de polymère séquencé amphiphile et de composé inorganique pour augmenter la dimension des pores et l'épaisseur des parois, ainsi que la stabilité thermique.

40 23. Procédé selon la revendication 16, dans lequel les dimensions des macropores sont contrôlées en faisant varier la puissance de l'électrolyte du sel inorganique.

45 24. Procédé selon la revendication 16, dans lequel les dimensions des mésopores sont contrôlées par le copolymère séquencé et des agents gonflants du cosolvant.

25. Procédé selon la revendication 1, 9 ou 16, dans lequel ledit copolymère séquencé est un polymère tribloc.

50 26. Procédé selon la revendication 25, dans lequel ledit copolymère tribloc est un polymère poly(éthylène oxyde)-poly(alkylène oxyde)-poly(éthylène oxyde) où le groupe fonctionnel oxyde d'alkylène a au moins trois atomes de carbone.

27. Procédé selon la revendication 25, dans lequel ledit copolymère tribloc est un polymère poly(éthylène oxyde)-poly(propylène oxyde)-poly(éthylène oxyde).

55 28. Procédé selon la revendication 25, dans lequel ledit copolymère tribloc est un polymère poly(éthylène oxyde)-poly(butylène oxyde)-poly(éthylène oxyde).

29. Procédé selon la revendication 1, 9 ou 16, dans lequel ledit copolymère séquencé est un polymère dibloc.

30. Procédé selon la revendication 1, 9 ou 16, dans lequel ledit copolymère séquencé est un polymère tribloc inversé.
31. Procédé selon la revendication 1, 9 ou 16, dans lequel ledit copolymère séquencé est un polymère dibloc en étoile.
- 5 32. Procédé selon la revendication 1, 9 ou 16, dans lequel ledit polymère séquencé est un polymère dibloc en étoile inversé.
33. Procédé selon la revendication 9 ou 16, dans lequel ledit composé inorganique, lors de la calcination, forme un oxyde sélectionné à partir de TiO_2 , ZrO_2 , Nb_2O_6 , Ta_2O_5 , Al_2O_3 , SiO_2 , WO_3 , SnO_2 , HfO_2 , $\text{SiAlO}_{3,5}$, $\text{SiAlO}_{5,5}$, Al_2TiO_5 , ZrTiO_4 et SiTiO_4 .
- 10 34. Procédé selon la revendication 9 ou 16, dans lequel ledit composé inorganique, lors de la calcination, forme du SiO_2 .
- 15 35. Matériau mésostructuré réalisé selon la revendication 1 ou 9, dans lequel le matériau mésostructuré est un composite à structure mésoscopique d'un copolymère séquencé amphiphile et d'un composé d'une espèce métallique polyvalent.
36. Matériau mésostructuré selon la revendication 35, dans lequel ledit copolymère séquencé est un polymère tribloc.
- 20 37. Matériau mésostructuré selon la revendication 35, dans lequel ledit copolymère tribloc est un polymère poly(éthylène oxyde)-poly(alkylène oxyde)-poly(éthylène oxyde) où le groupe fonctionnel oxyde d'alkylène a au moins trois atomes de carbone.
- 25 38. Matériau mésostructuré selon la revendication 35, dans lequel ledit copolymère tribloc est un polymère poly(éthylène oxyde)-poly(propylène oxyde)-poly(éthylène oxyde).
39. Matériau mésostructuré selon la revendication 35, dans lequel ledit copolymère tribloc est un polymère poly(éthylène oxyde)-poly(butylène oxyde)-poly(éthylène oxyde).
- 30 40. Matériau mésostructuré selon la revendication 35, dans lequel ledit copolymère séquencé est un polymère dibloc.
41. Matériau mésostructuré selon la revendication 35, dans lequel ledit copolymère séquencé est un polymère tribloc inversé.
- 35 42. Matériau mésostructuré selon la revendication 35, dans lequel ledit copolymère séquencé est un polymère dibloc en étoile.
43. Matériau mésostructuré selon la revendication 35, dans lequel ledit polymère séquencé est un polymère dibloc en étoile inversé.
- 40 44. Matériau mésostructuré transparent réalisé selon la revendication 6 ou 10.
- 45 45. Matériau mésostructuré transparent selon la revendication 44, dans lequel ledit matériau transparent est dépourvu de craquelures.
46. Matériau mésostructuré transparent selon la revendication 44, dans lequel ledit matériau transparent est sous la forme d'un film mince sans craquelures, mésoporeux, organisé mésoscopiquement.
- 50 47. Matériau mésostructuré réalisé selon la revendication 12, dans lequel le matériau mésostructuré est un matériau poreux organisé de manière mésoscopique thermiquement stable composé d'un composé métallique polyvalent et présentant une répartition étroite des dimensions de pores dans le régime des dimensions mésoscopiques.
- 55 48. Matériau mésostructuré selon la revendication 35, 44 ou 47, comprenant une mésostructure hexagonale à deux dimensions.
49. Matériau mésostructuré selon la revendication 35, 44 ou 47, comprenant une mésostructure cubique.

EP 1 037 940 B1

50. Matériau mésostructuré selon la revendication 35, 44 ou 47, comprenant une mésostructure lamellaire.
51. Matériau mésostructuré selon la revendication 35, 44 ou 47 sous forme de fibres.
- 5 52. Matériau mésostructuré selon la revendication 35, 44 ou 47 sous forme de films minces.
53. Matériau mésostructuré selon la revendication 35, 44 ou 47 sous forme de monolithes.
- 10 54. Matériau mésostructuré selon la revendication 47 ayant une porosité d'au moins 40%.
55. Matériau mésostructuré selon la revendication 47, ayant une constante diélectrique de 2 à 2,5.
- 15 56. Matériau méso-macro structuré réalisé selon la revendication 25, dans lequel le matériau méso-macro structuré est un matériau d'oxyde métallique polyvalent macroporeux ayant une surface mésoporeuse organisée.
57. Matériau méso-macro structuré selon la revendication 56, dans lequel ledit oxyde métallique polyvalent est sélectionné parmi le groupe composé de TiO_2 , ZrO_2 , Nb_2O_5 , Ta_2O_5 , Al_2O_3 , SiO_2 , WO_3 , SnO_2 , HfO_2 , $\text{SiAlO}_{3,5}$, $\text{SiAlO}_{5,5}$, Al_2TiO_5 , ZrTiO_4 et SiTiO_4 .
- 20 58. Matériau méso-macro structuré selon la revendication 56, dans lequel ledit composé métallique polyvalent est du SiO_2 .
59. Matériau méso-macro sttucturé selon la revendication 56, comprenant une mésostructure hexagonale à deux dimensions.
- 25 60. Matériau méso-macro structuré selon la revendication 56, comprenant une mésostructure cubique.
61. Matériau méso-macro structuré selon la revendication 57, comprenant une mésostructure lamellaire.
- 30 62. Matériau mésostructuré selon la revendication 56 sous forme de fibres.
63. Matériau mésostructuré selon la revendication 56 sous forme de films minces.
64. Matériau mésostructuré selon la revendication 56 sous forme de monolithes.
- 35 65. Matériau mésostructuré selon la revendication 56 ayant une porosité d'au moins 40%.
66. Procédé de séparation de biomolécules d'un spécimen biologique ou d'un mélange de synthèse, comprenant le fait de faire passer ledit spécimen biologique ou mélange à travers le matériau mésostructuré de la revendication 47.
- 40 67. Procédé selon la revendication 66, dans lequel lesdites biomolécules comprennent des enzymes et/ou des protéines.
- 45 68. Procédé de séparation de biomolécules d'un spécimen biologique ou d'un mélange de synthèse, comprenant le fait de faire passer ledit spécimen biologique ou mélange à travers le matériau méso-macro structuré de la revendication 56.
- 50 69. Procédé selon la revendication 68, dans lequel lesdites biomolécules comprennent des enzymes et/ou des protéines.
70. Procédé de séparation de matières organiques d'une solution, comprenant le fait de faire passer ladite solution à travers le matériau mésostructuré de la revendication 47.
- 55 71. Procédé de séparation de matières organiques d'une solution, comprenant le fait de faire passer ladite solution à travers le matériau méso-macro structuré de la revendication 56.
72. Procédé de séparation de matières inorganiques d'une solution, comprenant le fait de faire passer ladite solution

à travers le matériau mésostructuré de la revendication 47.

73. Procédé de séparation de matières inorganiques d'une solution, comprenant le fait de faire passer ladite solution à travers le matériau méso-macro structuré de la revendication 56.

5
74. Procédé permettant de transmettre des sélectivités de réactions catalytiques et d'adsorption au matériau méso-macro structuré de la revendication 56, comprenant la fonctionnalisation séparée des différentes surfaces de pores mésoscopiques et macroscopiques dudit matériau pour fournir lesdites sélectivités.

10

15

20

25

30

35

40

45

50

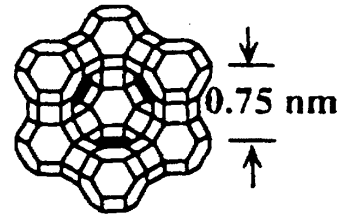
55

sub-Nanoporous Zeolites : < 1nm

Faujasite



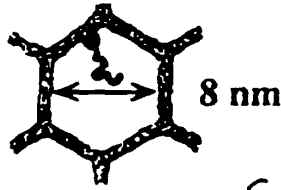
a



b

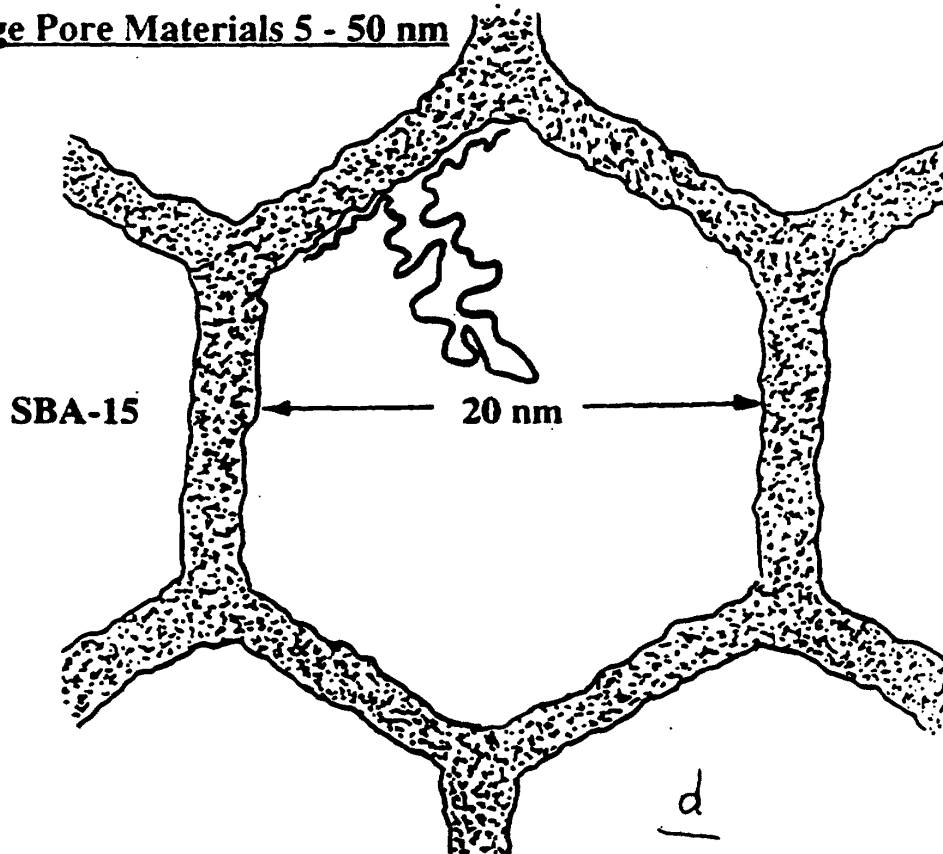
Mesoporous Molecular Sieves: 2- 10 nm

MCM-41



c

Ultra Large Pore Materials 5 - 50 nm



d

Fig. 1

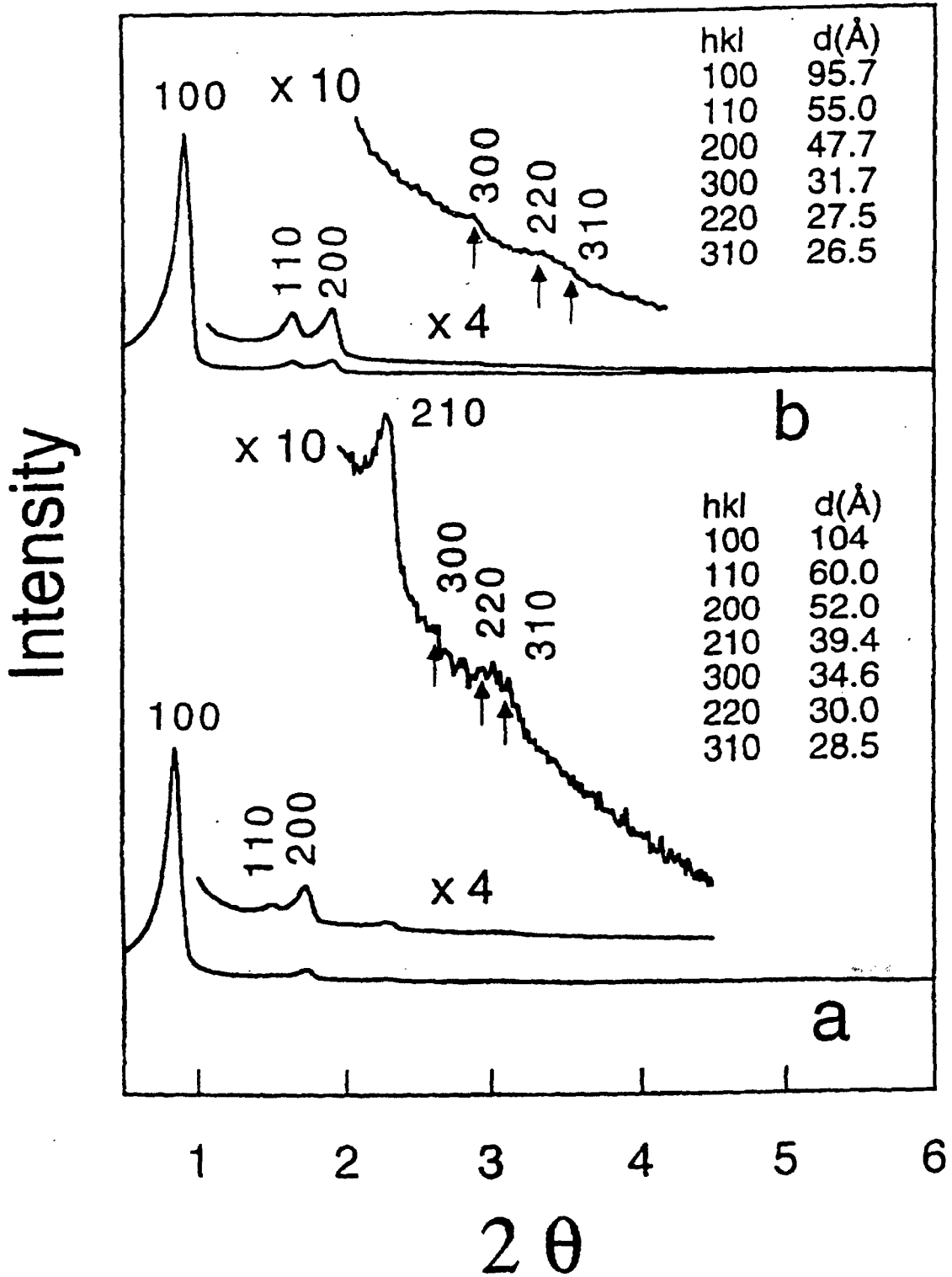


Fig. 2

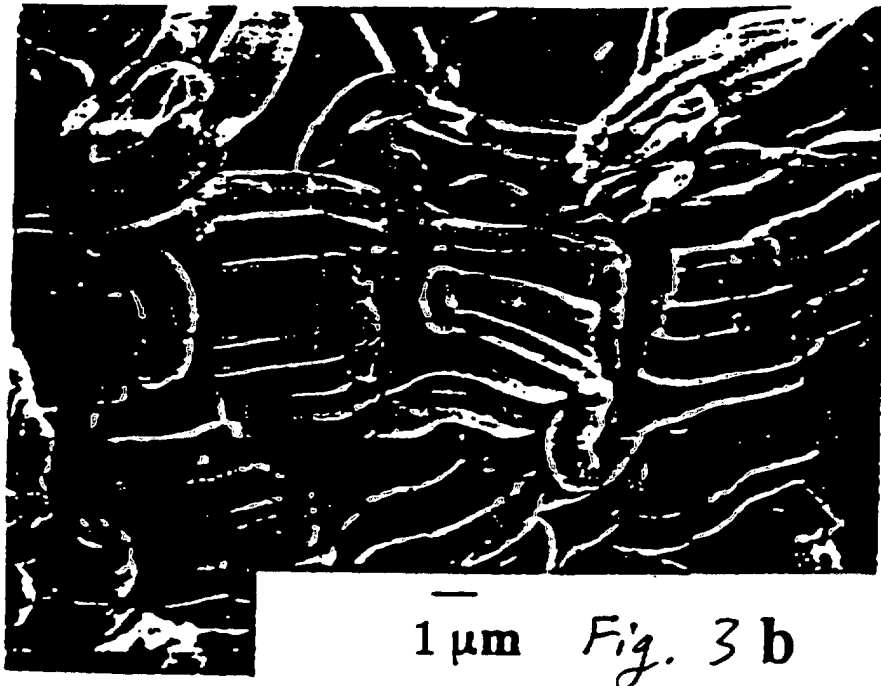
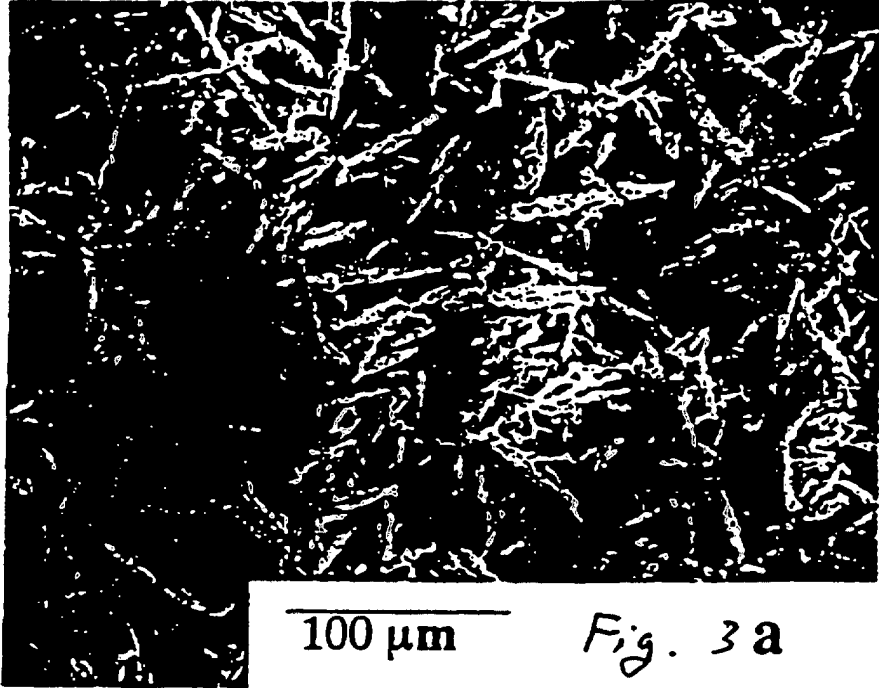


Fig. 3a

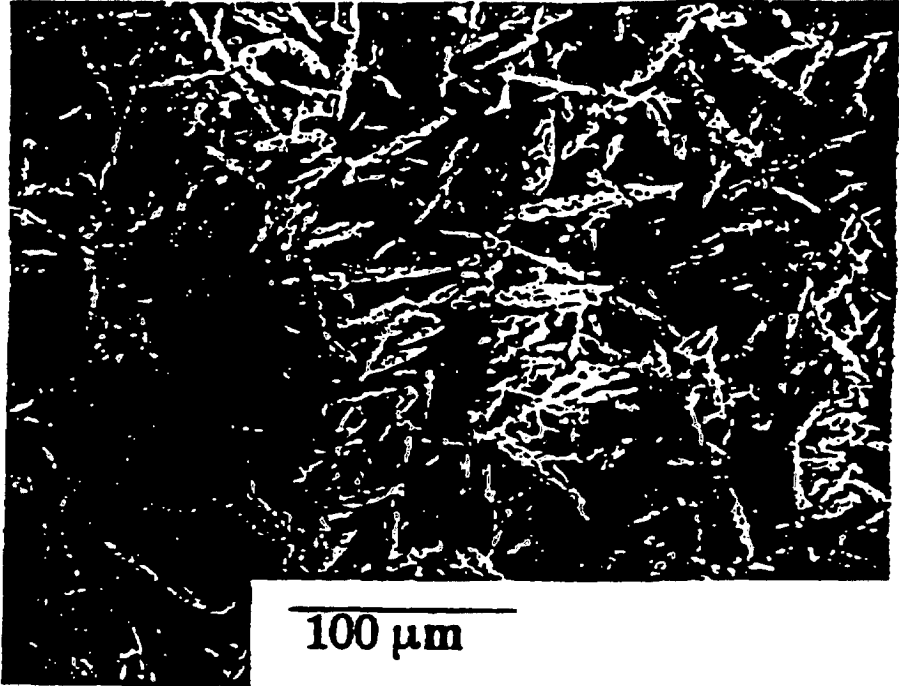


Fig. 3b

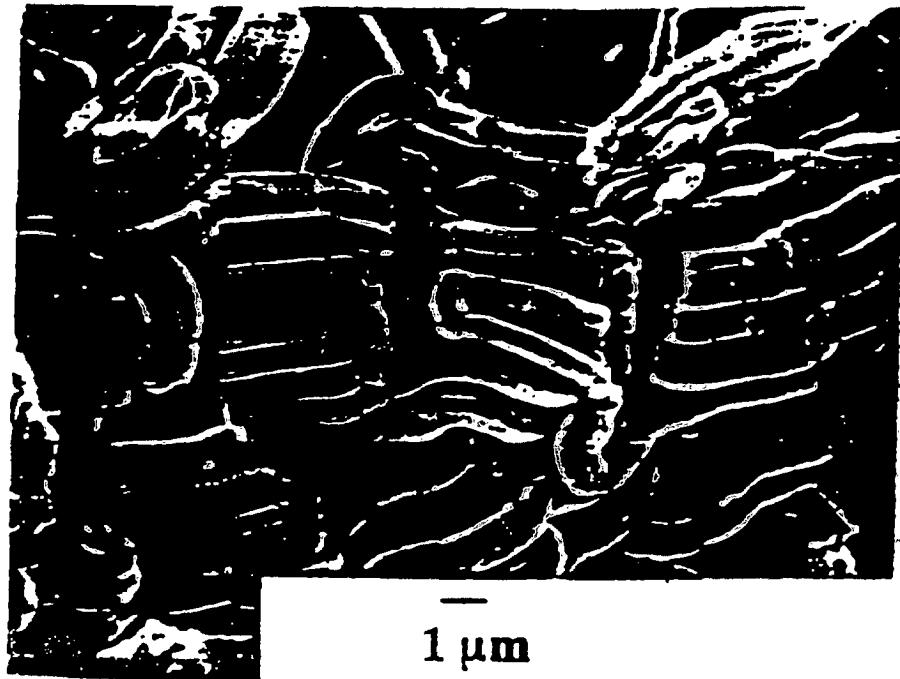


Fig. 3c

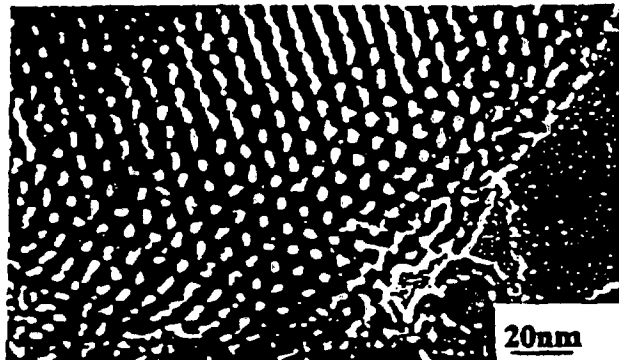
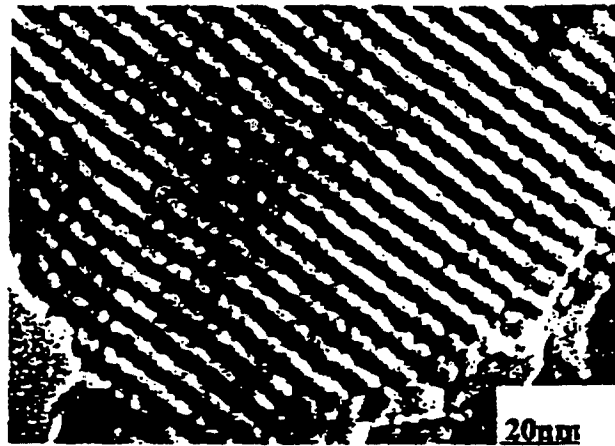


Fig. 3d



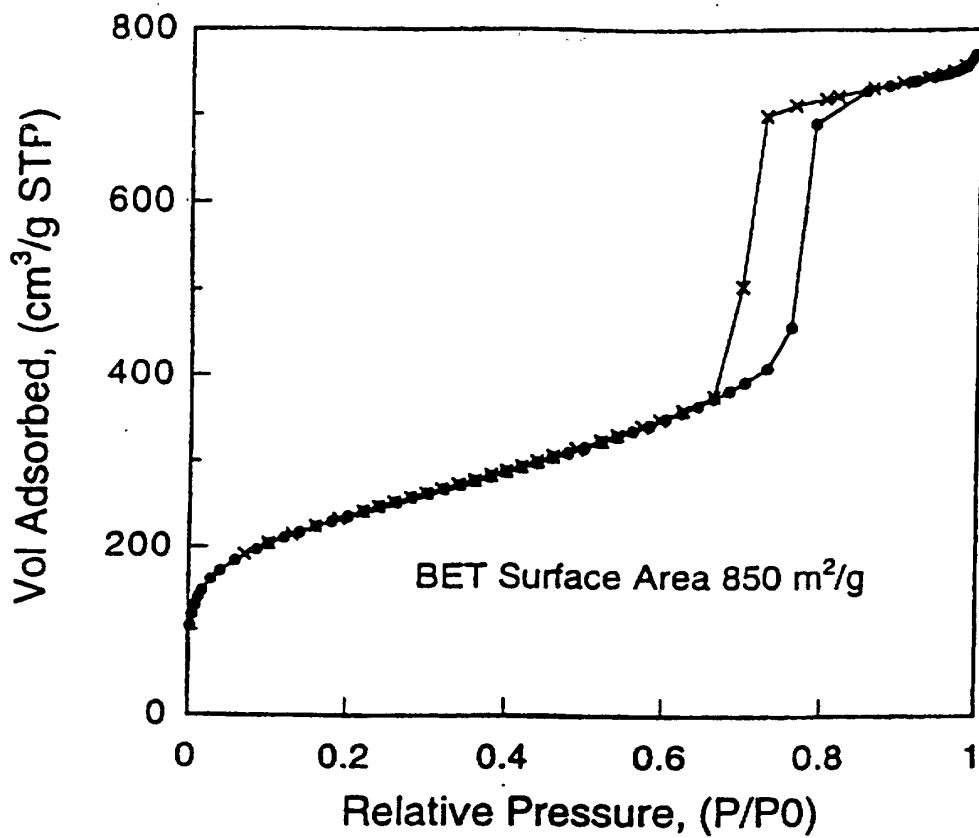


Fig. 4a

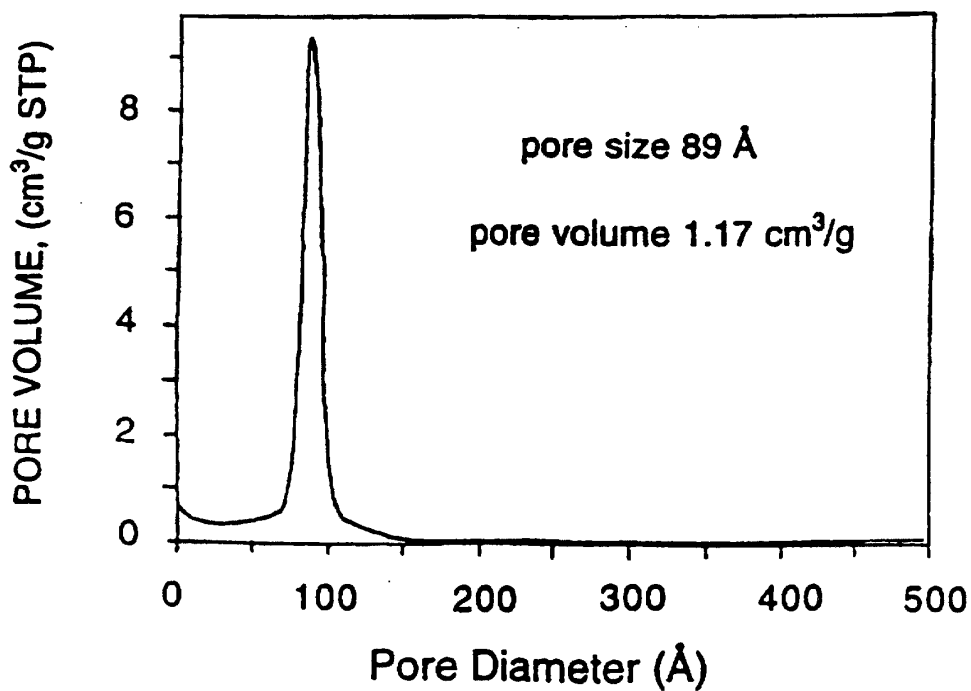


Fig. 4b

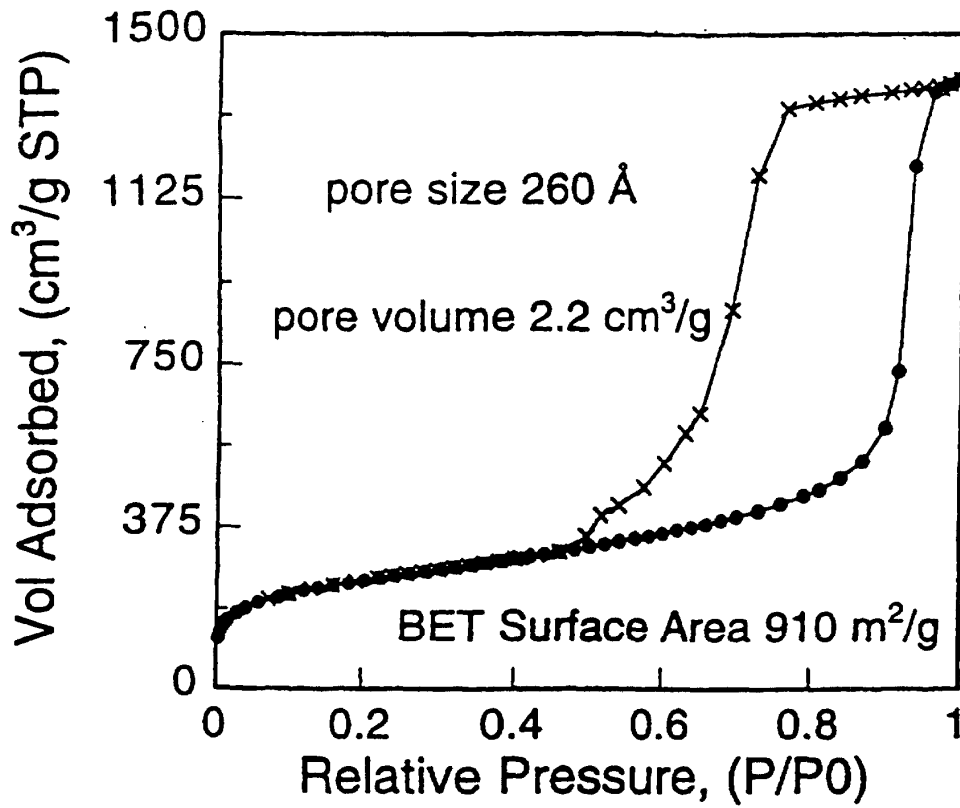


Fig. 4c

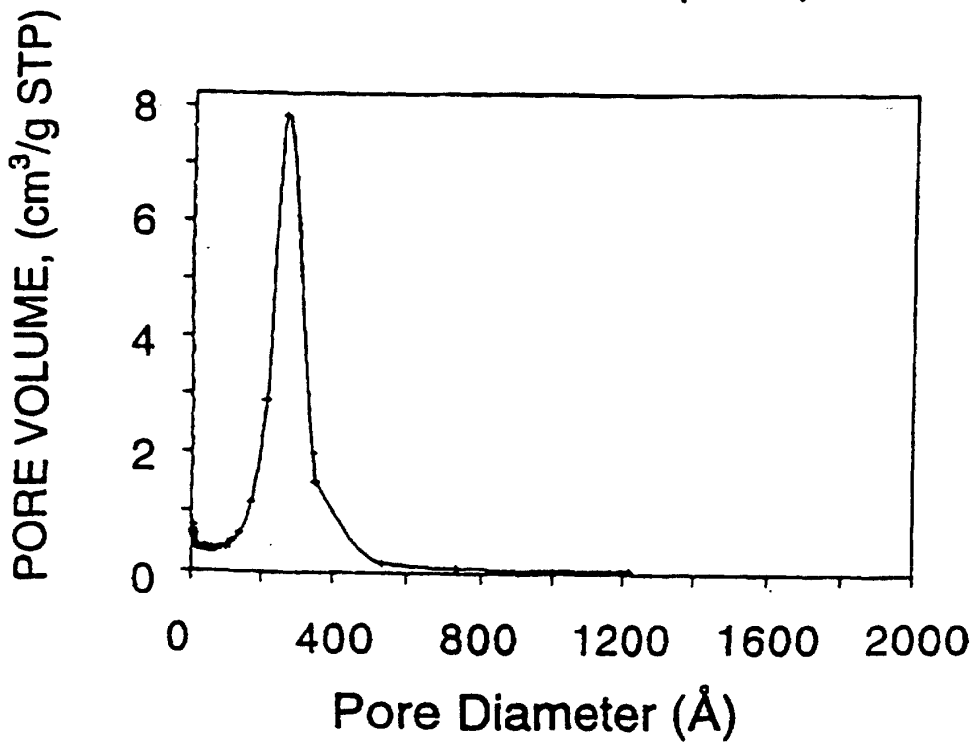


Fig. 4d

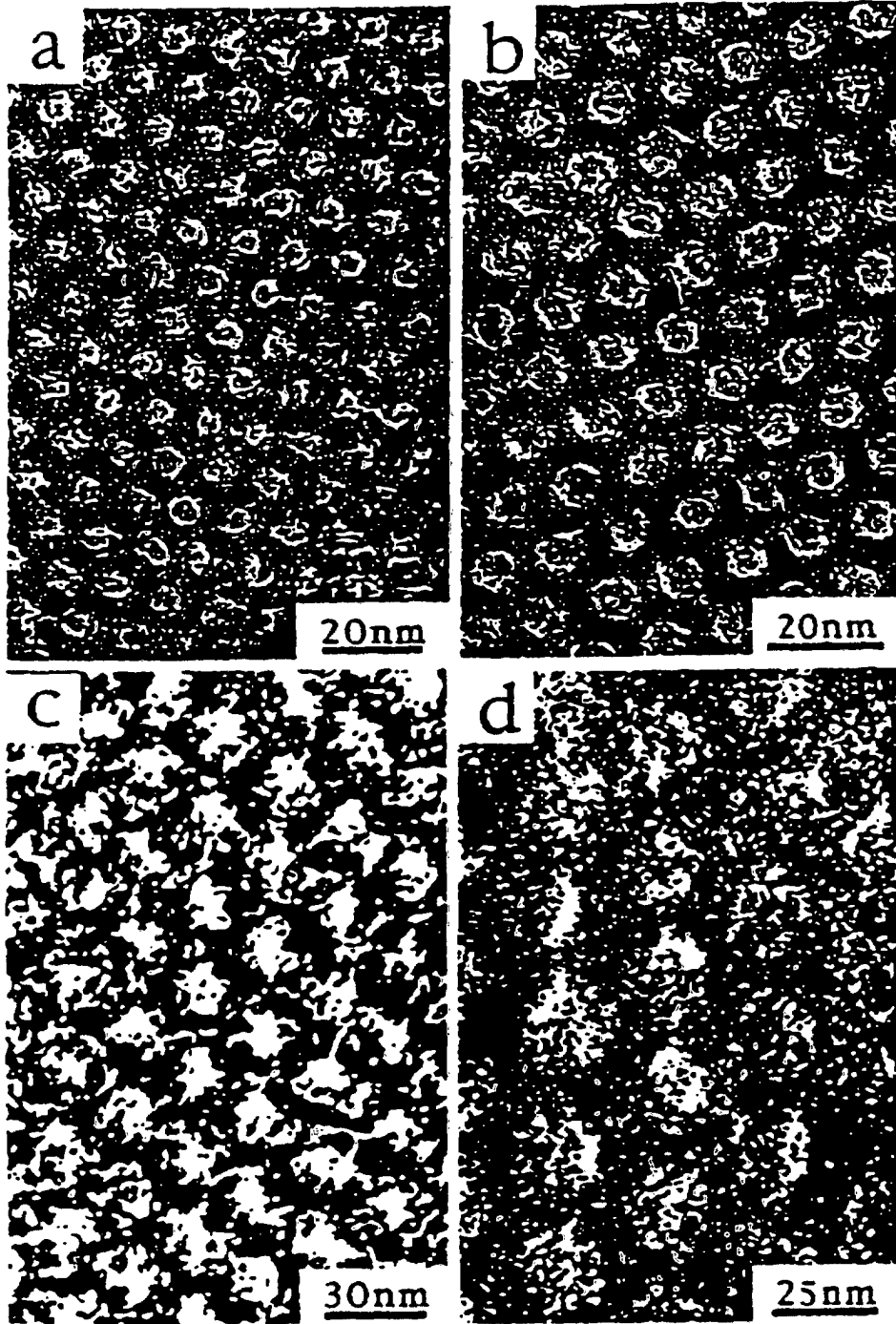


Fig. 5

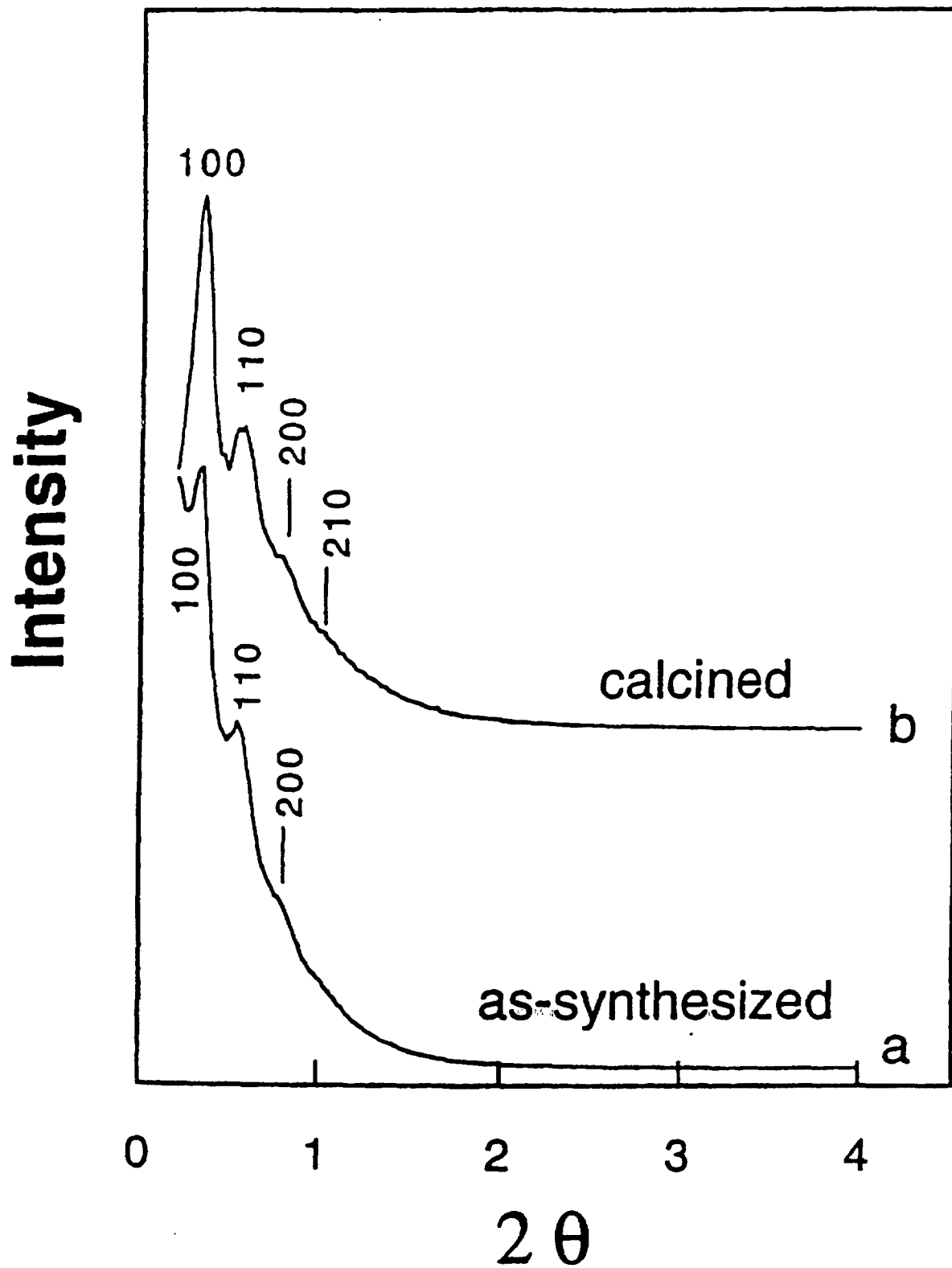


Fig. 6

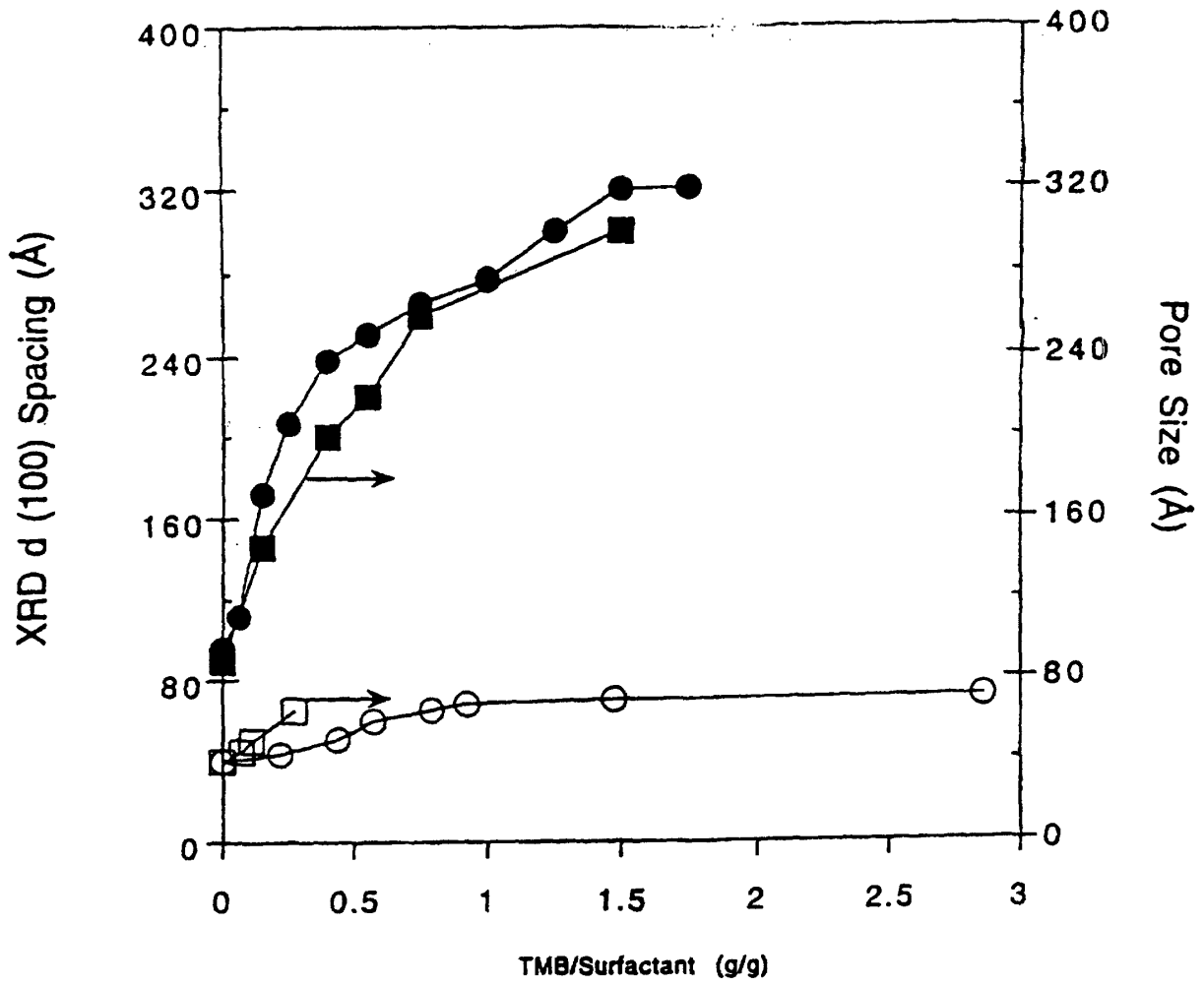


Fig. 7

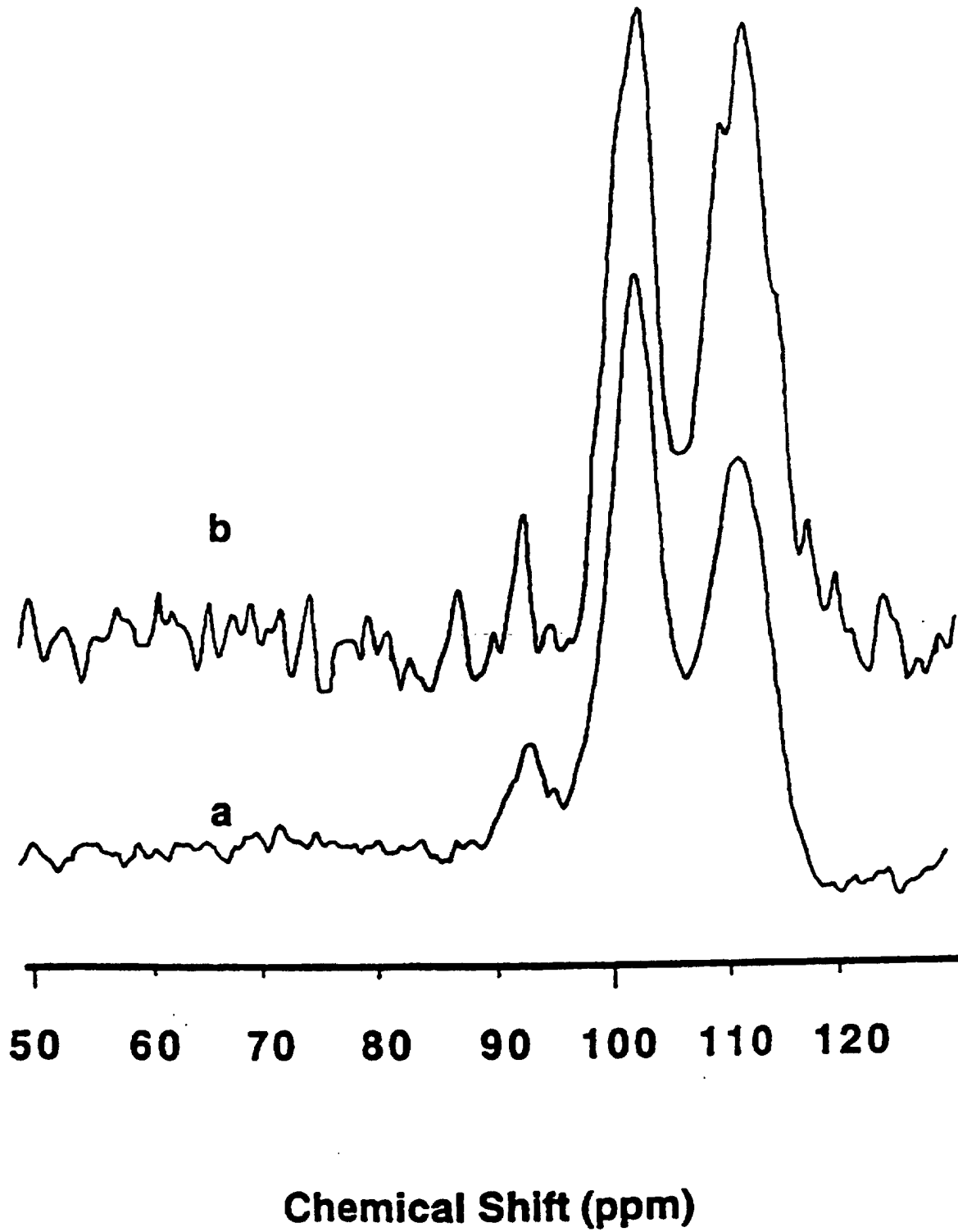


Fig. 8

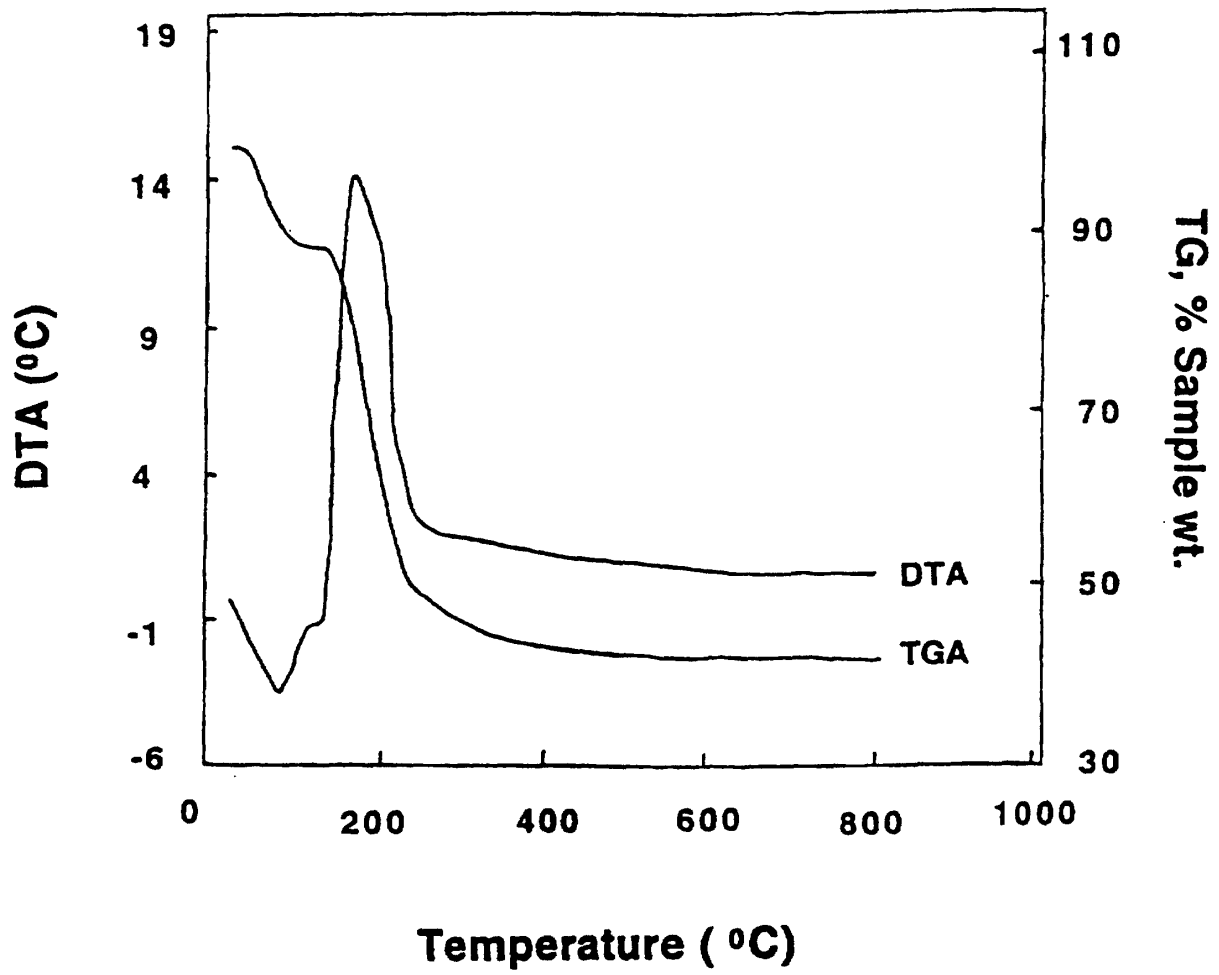
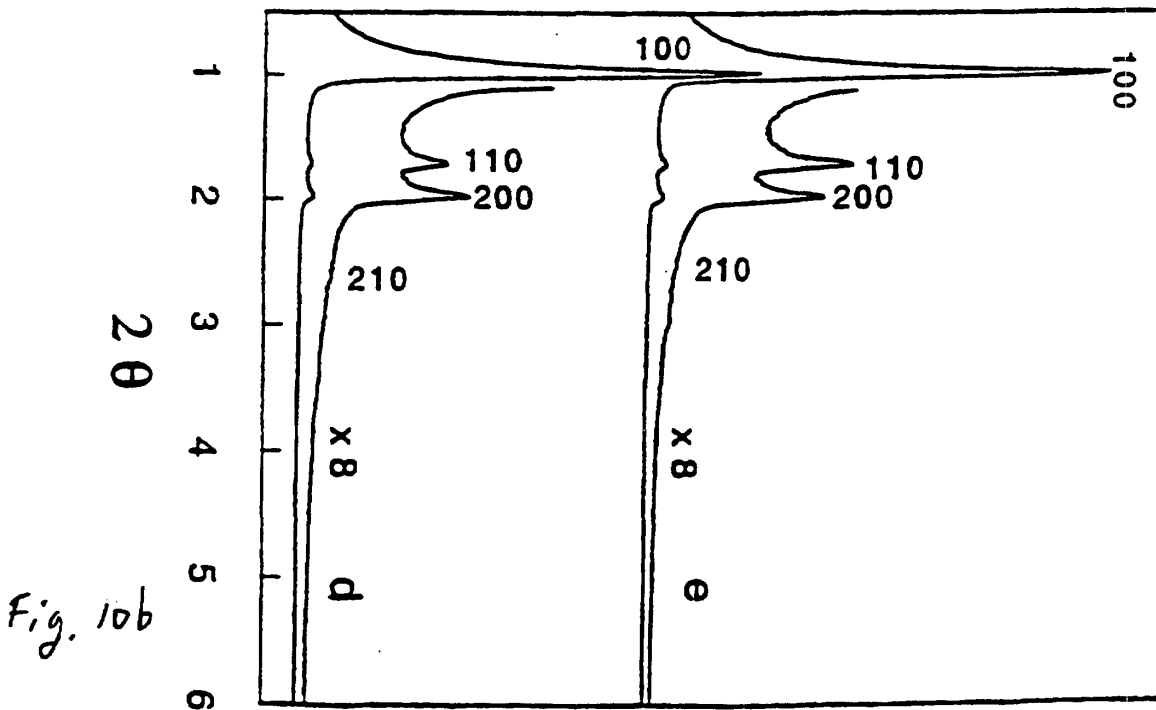
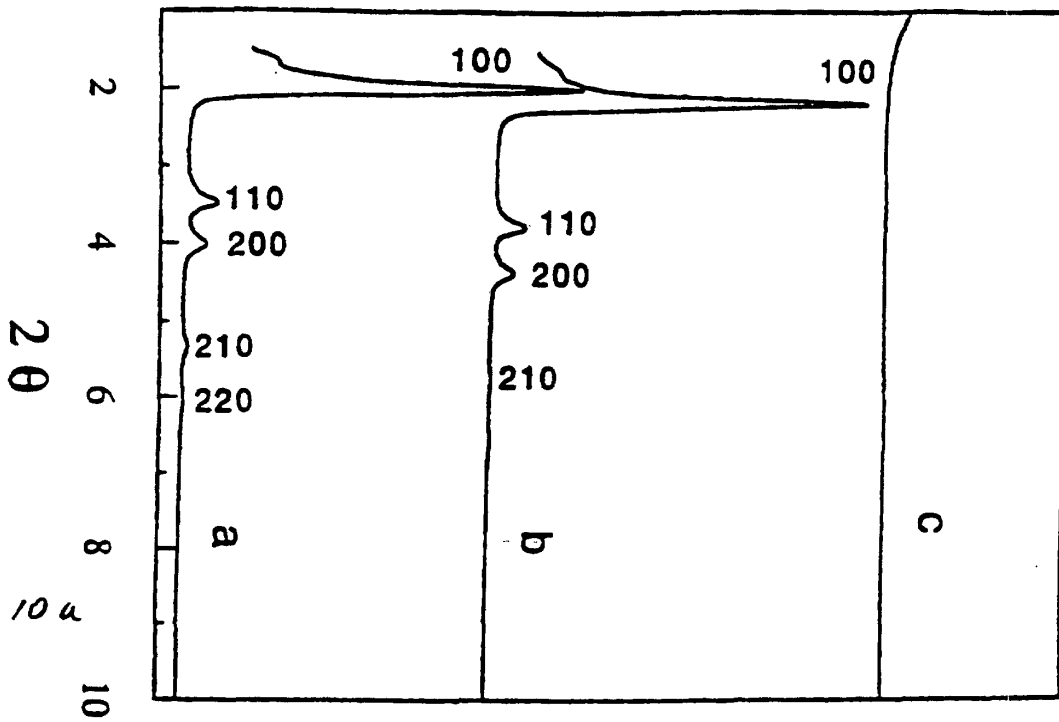


Fig. 9

Intensity



...and...
e. With a mean
glass transition
temperatures can be
temperatures, a
ever, reduction
of improved pro
ostatec with of
a lower melt vis

Fig. 11a

...a glass of
temperatures
at temperam
However, redu
ose of improve
of Hostatec wi
such a lower
... melt

Fig. 11b

TEOS/Pluronic F127 Composite

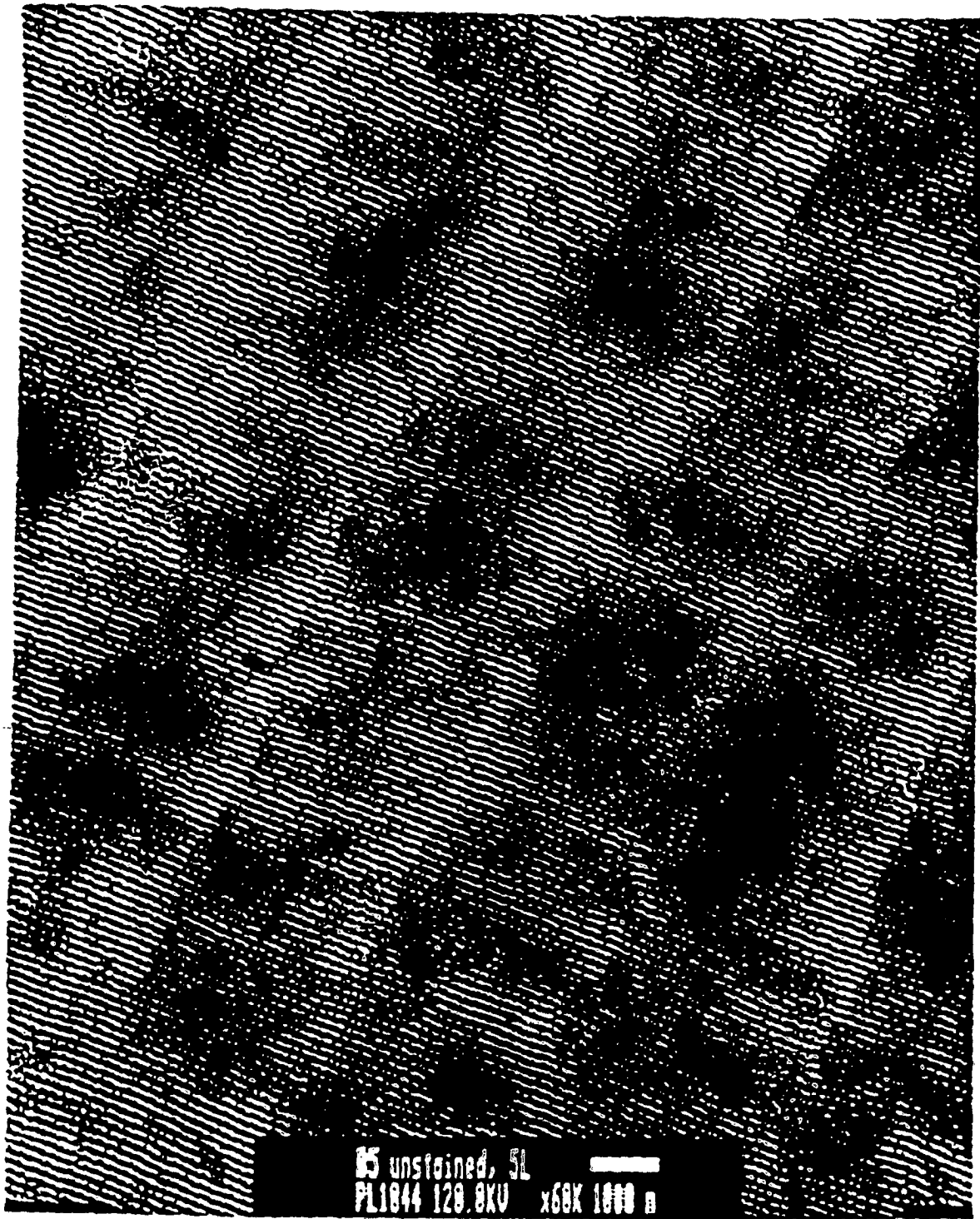
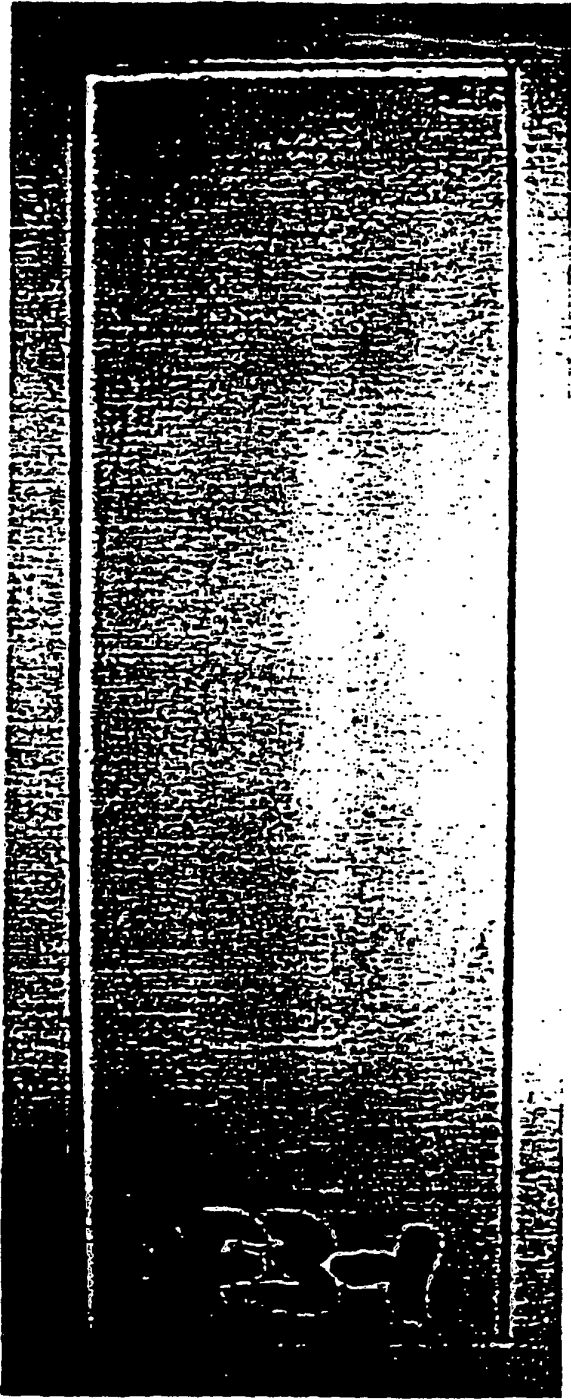


Fig. 12



Composite Thin Film

Fig. 13a

Figure 11b: XRD of Silicate/ P104 Film

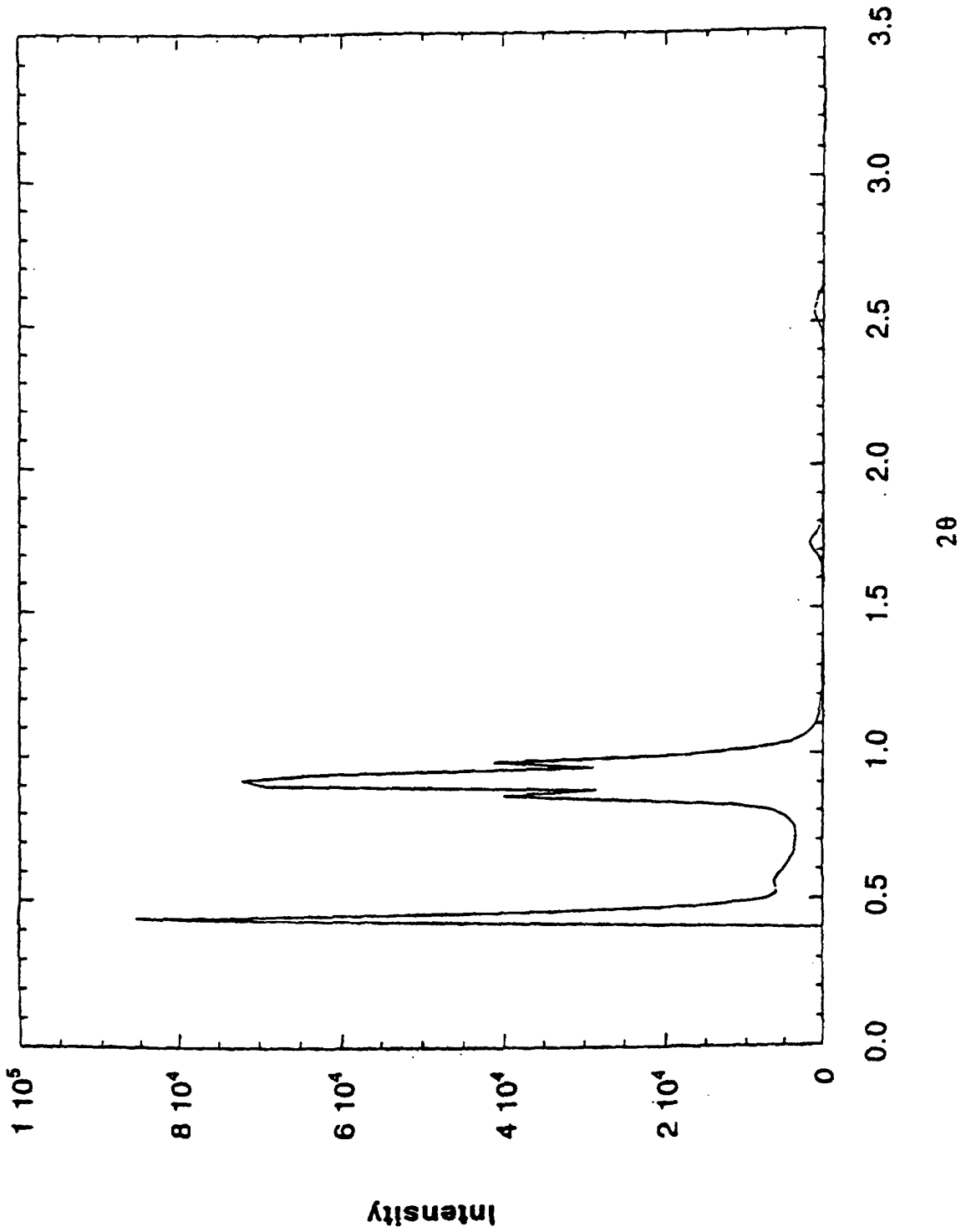


Fig. 13 b

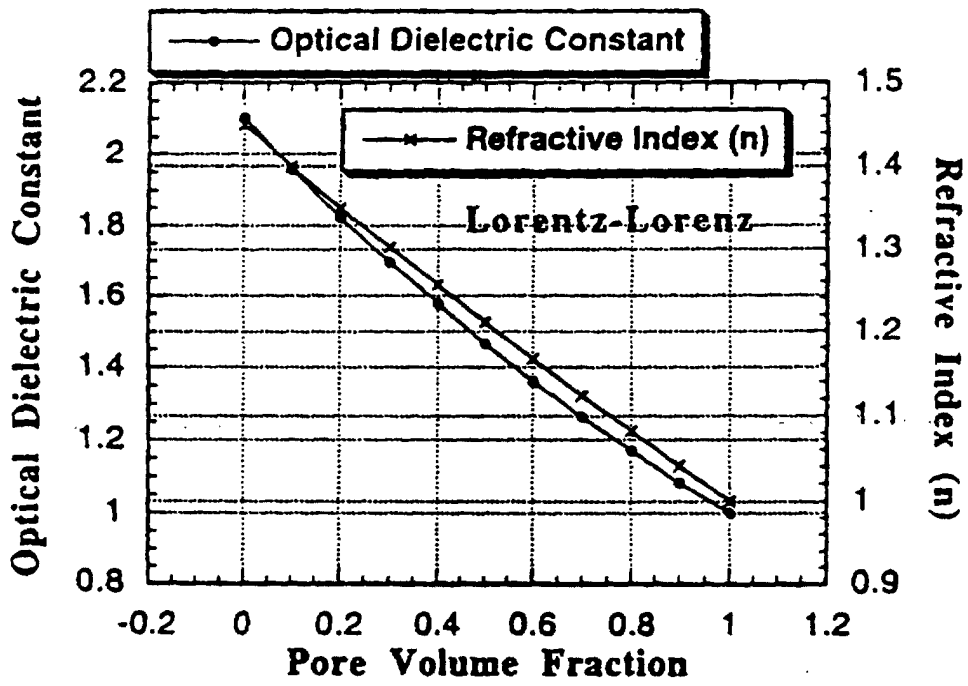


Fig. 14

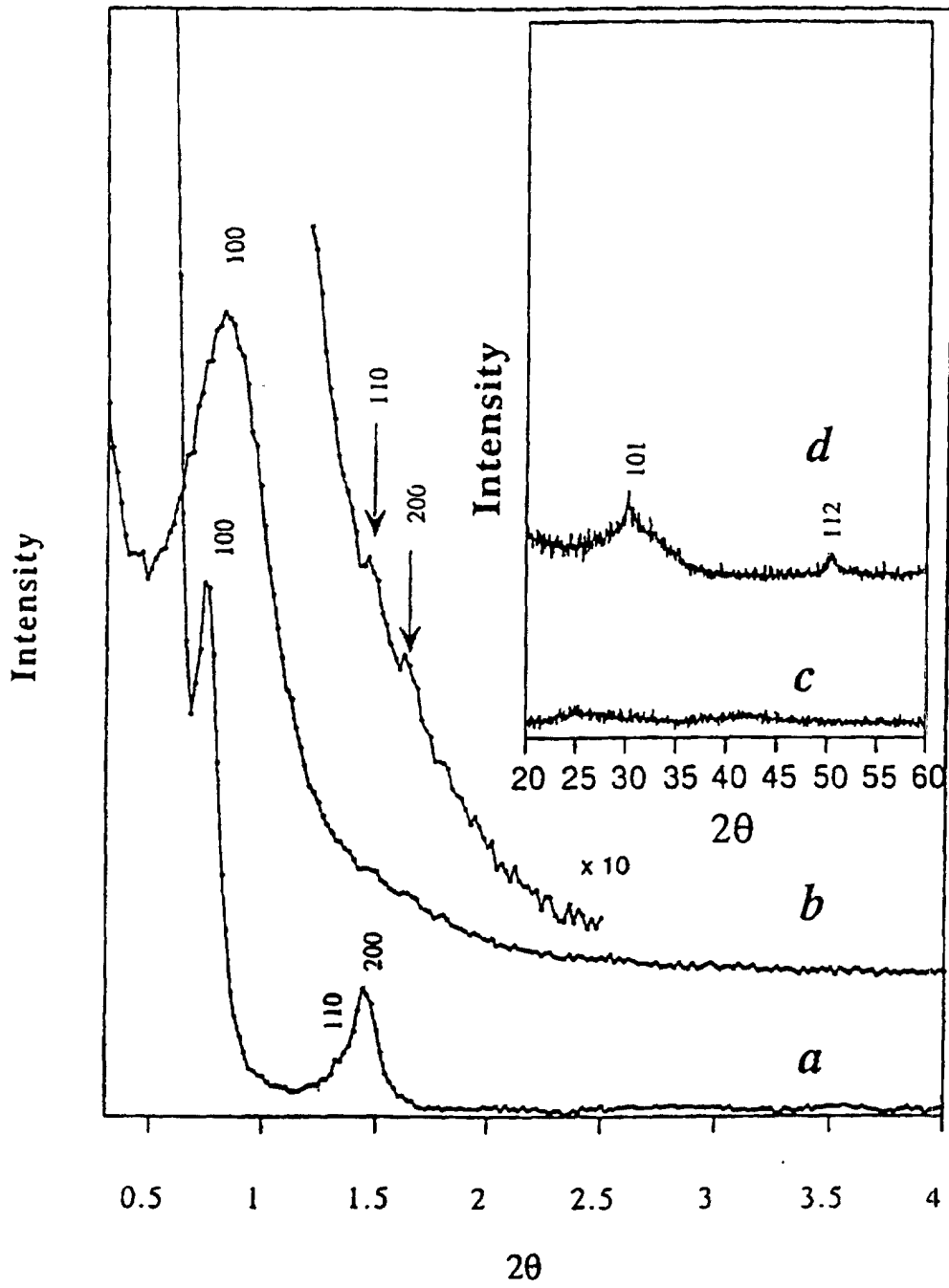


Fig. 15

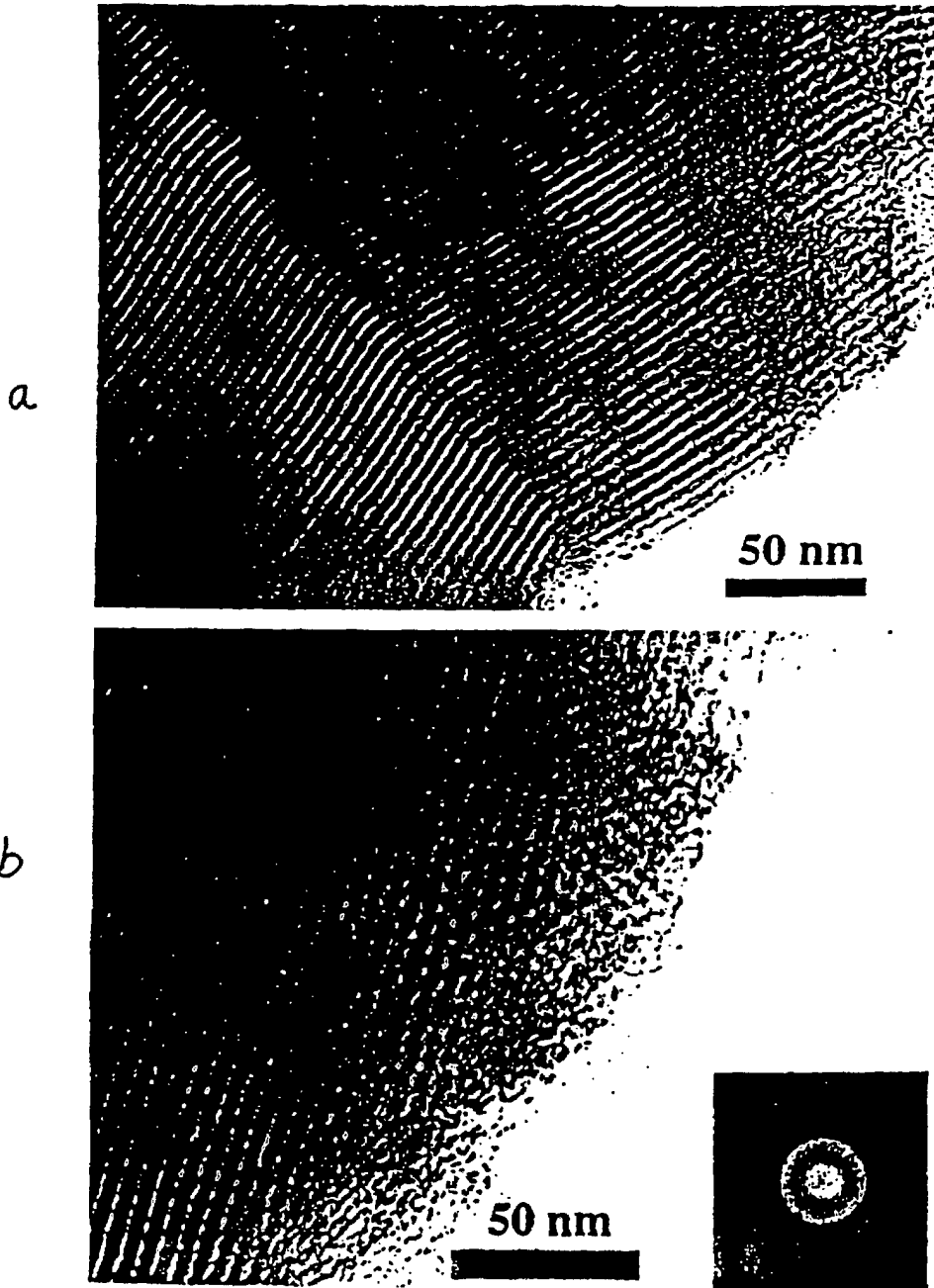


Fig. 16

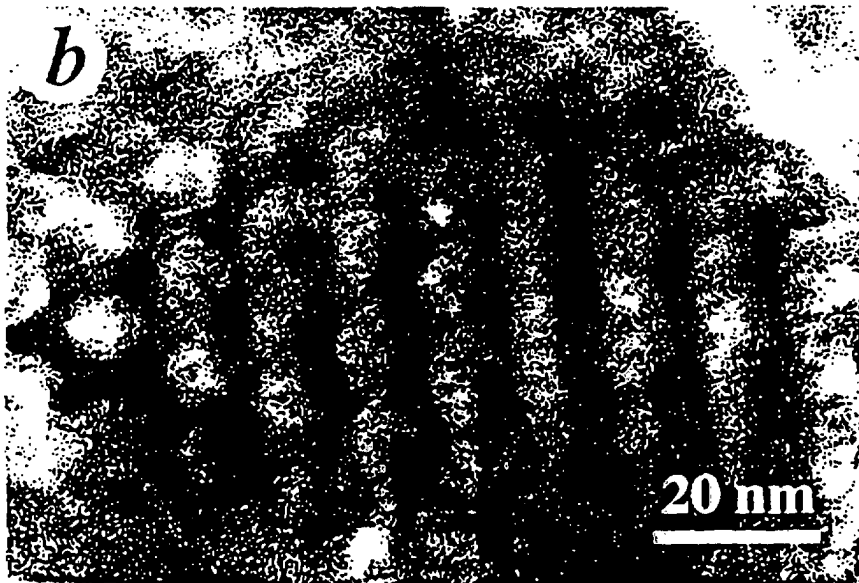
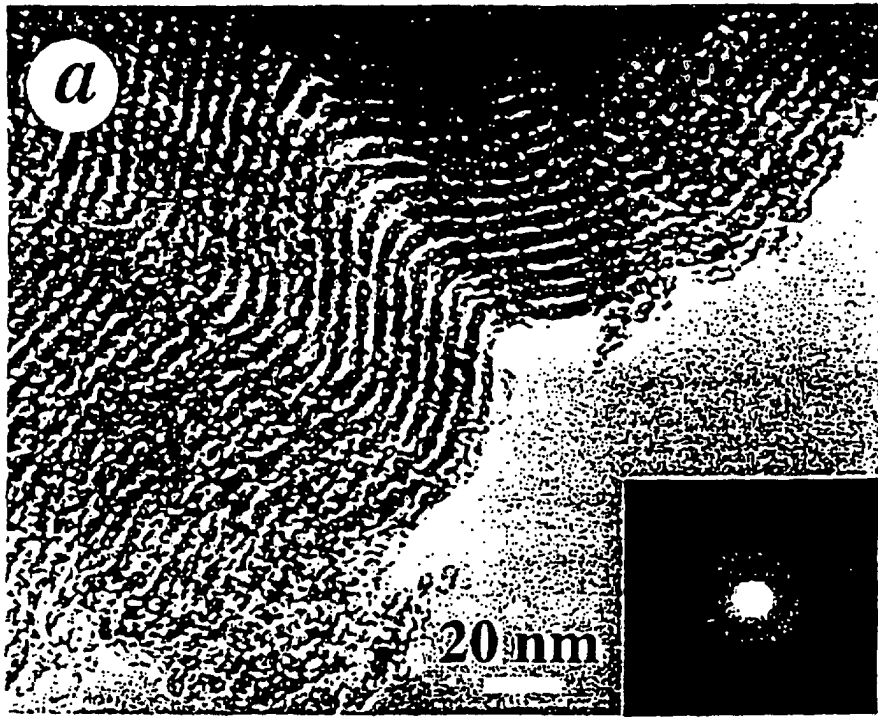


Fig. 17

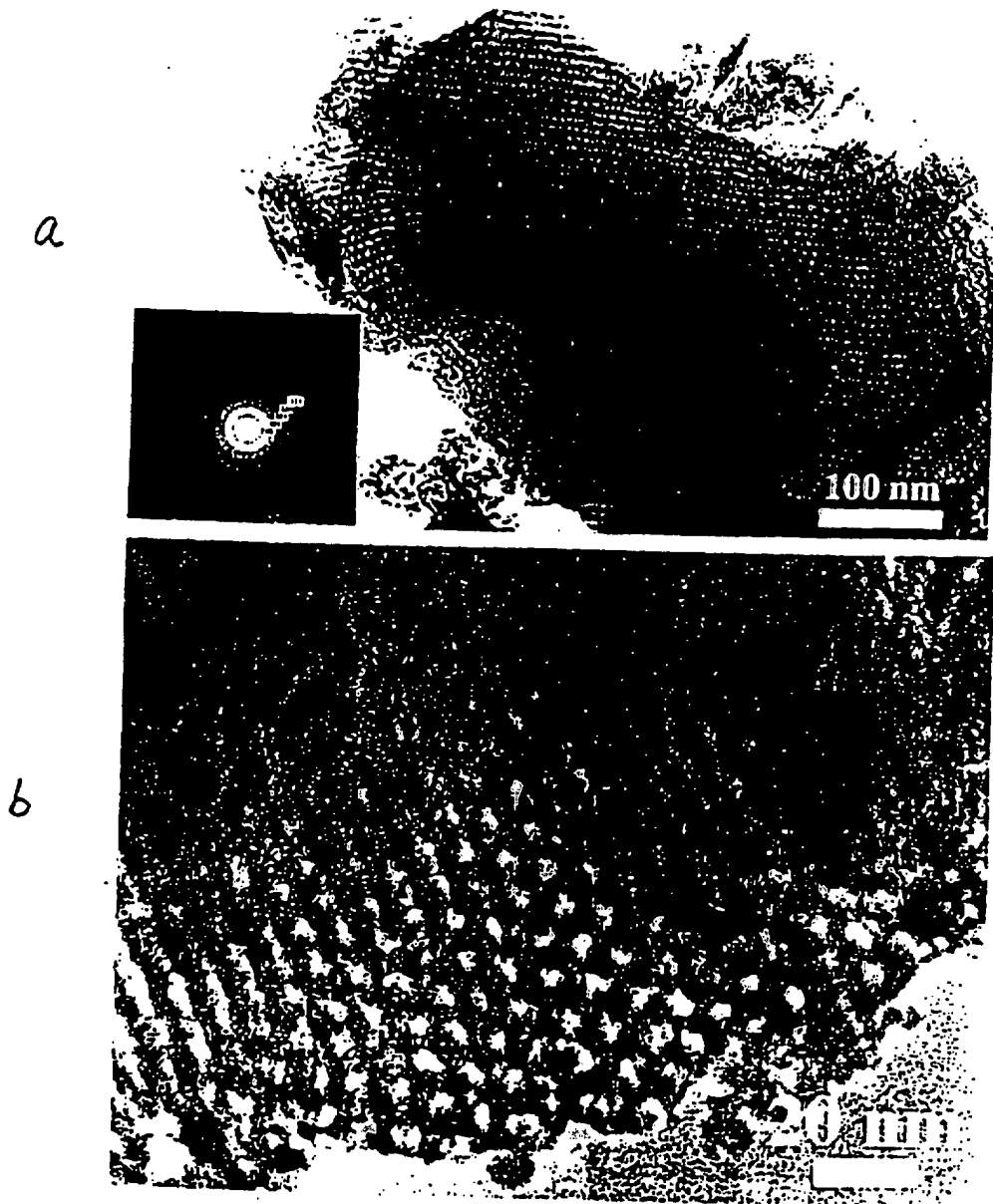
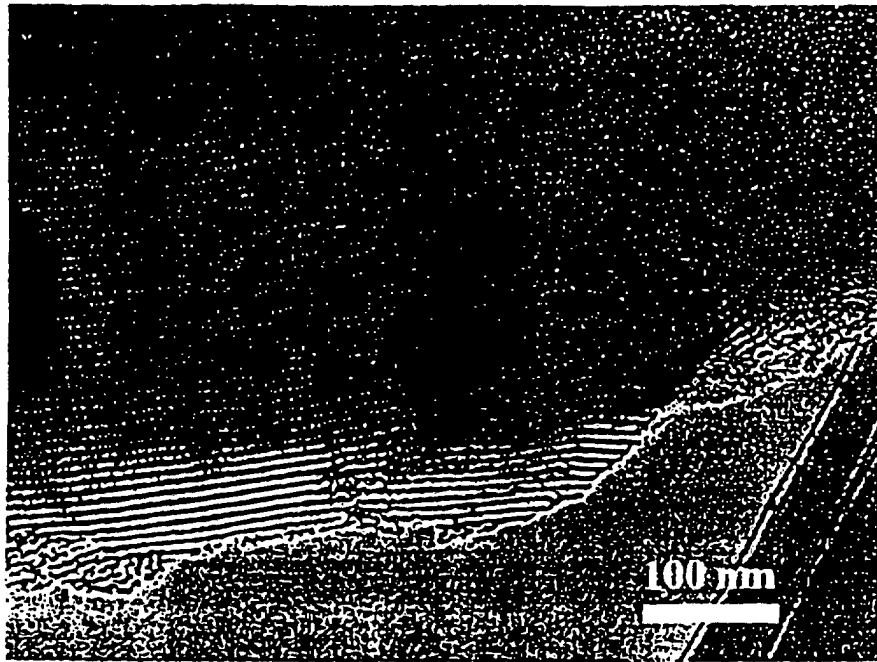


Fig. 10

a



b



Fig. 19

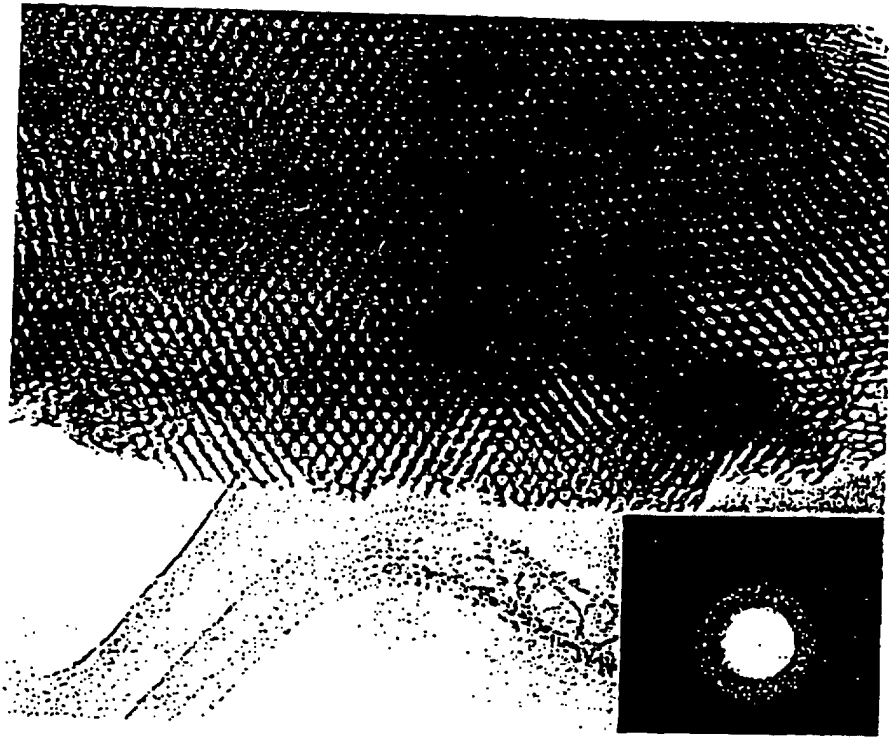


Fig. 20

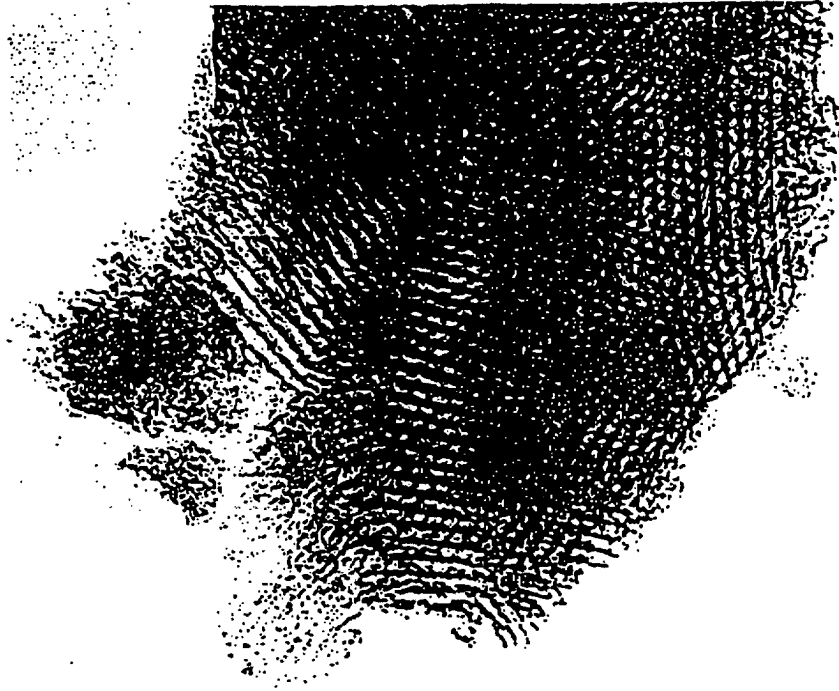


Fig. 21

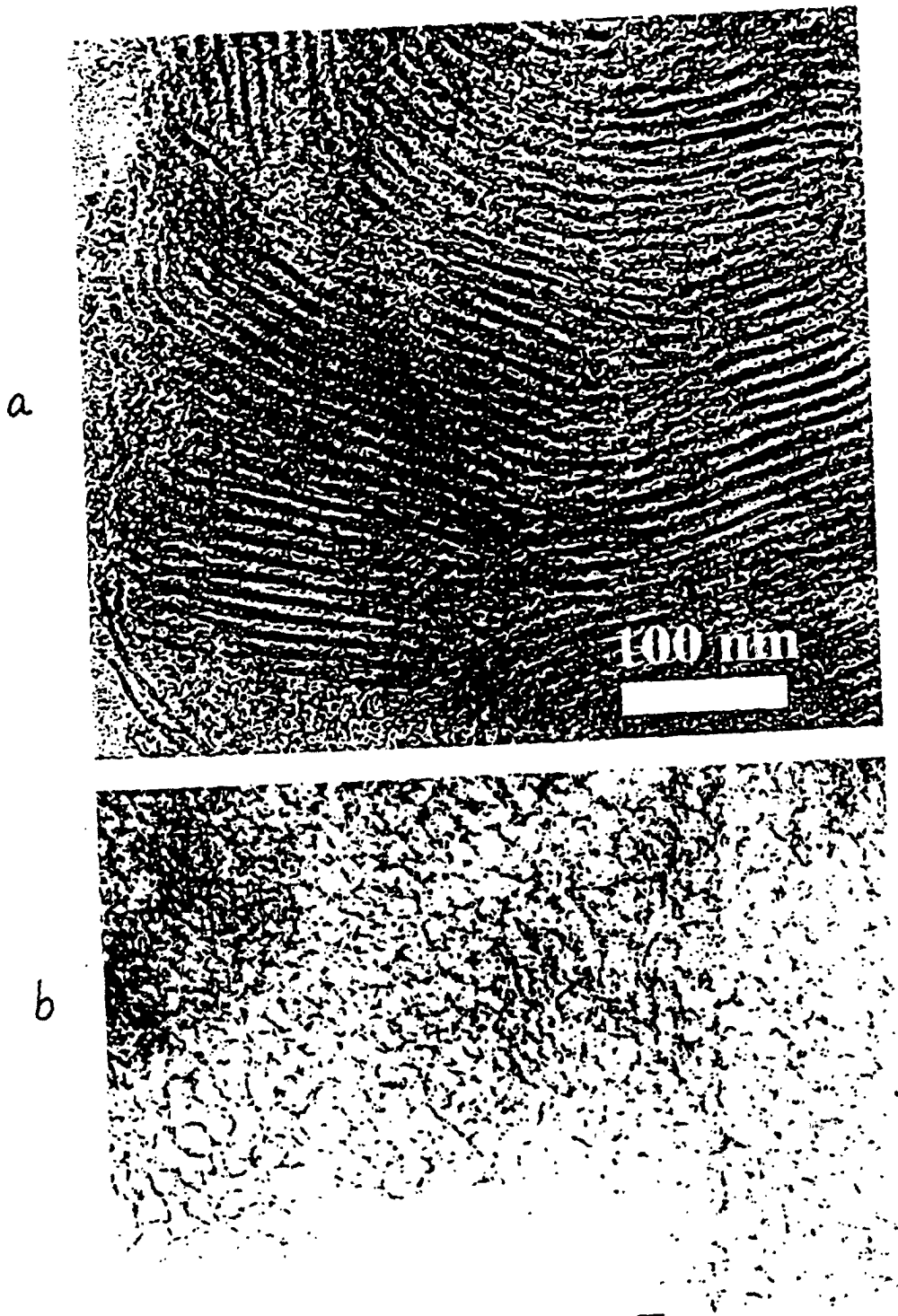
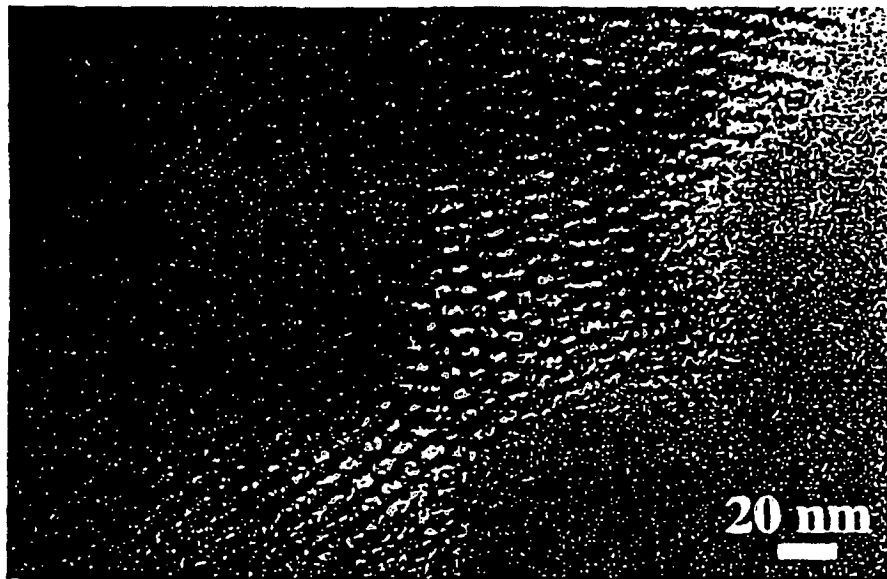


Fig. 22



Fig. 23

a



b

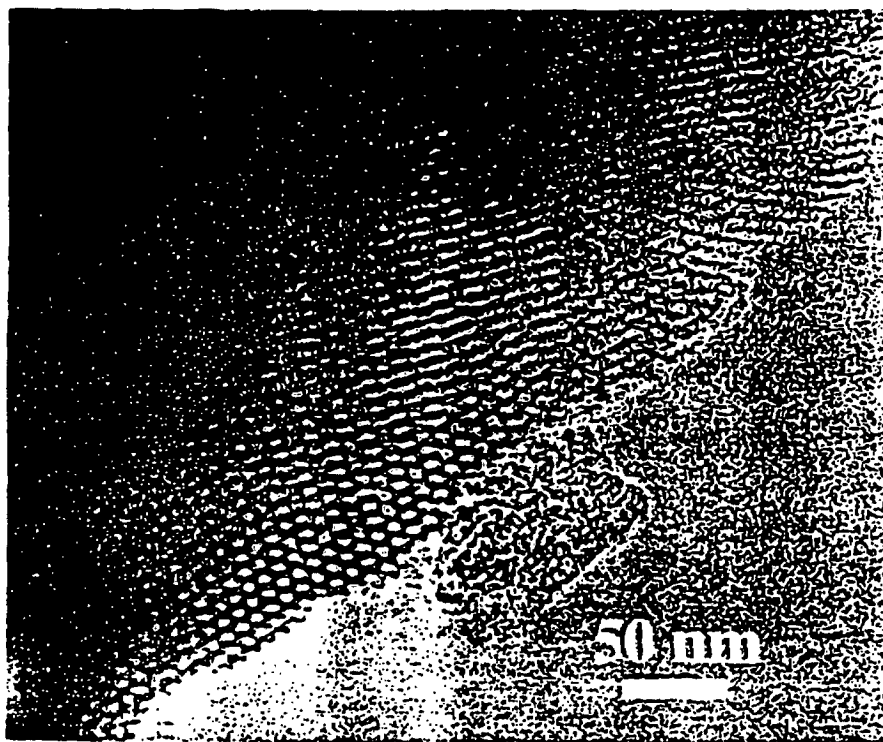
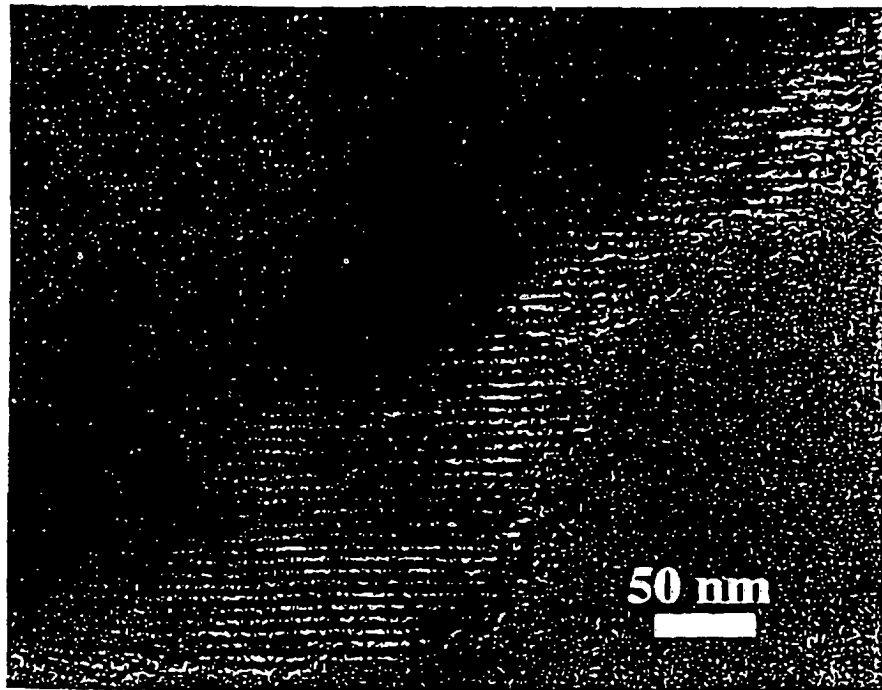


Fig. 24

a



b

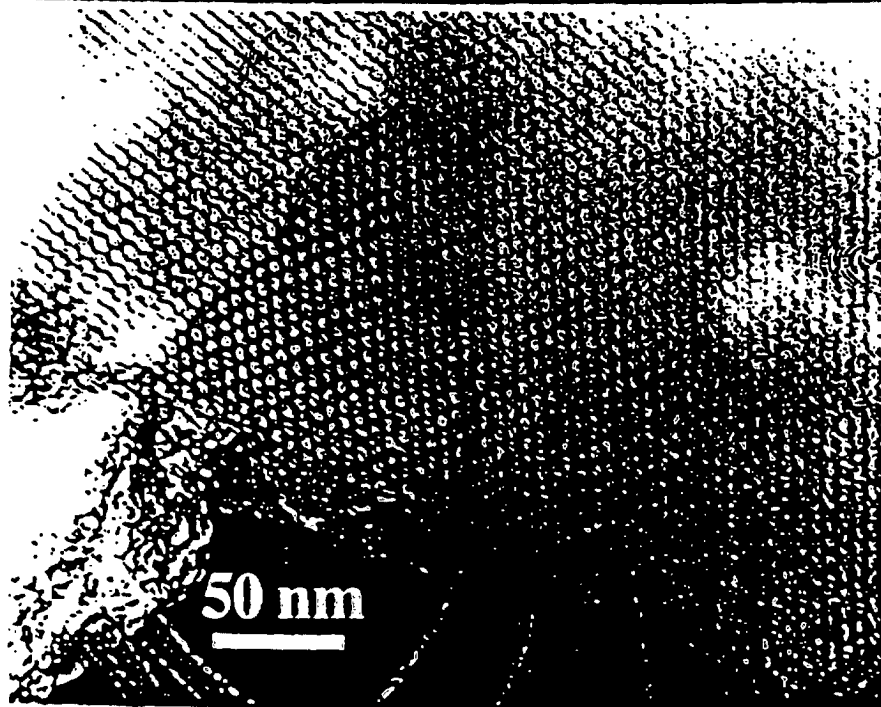


Fig. 25



Fig. 26

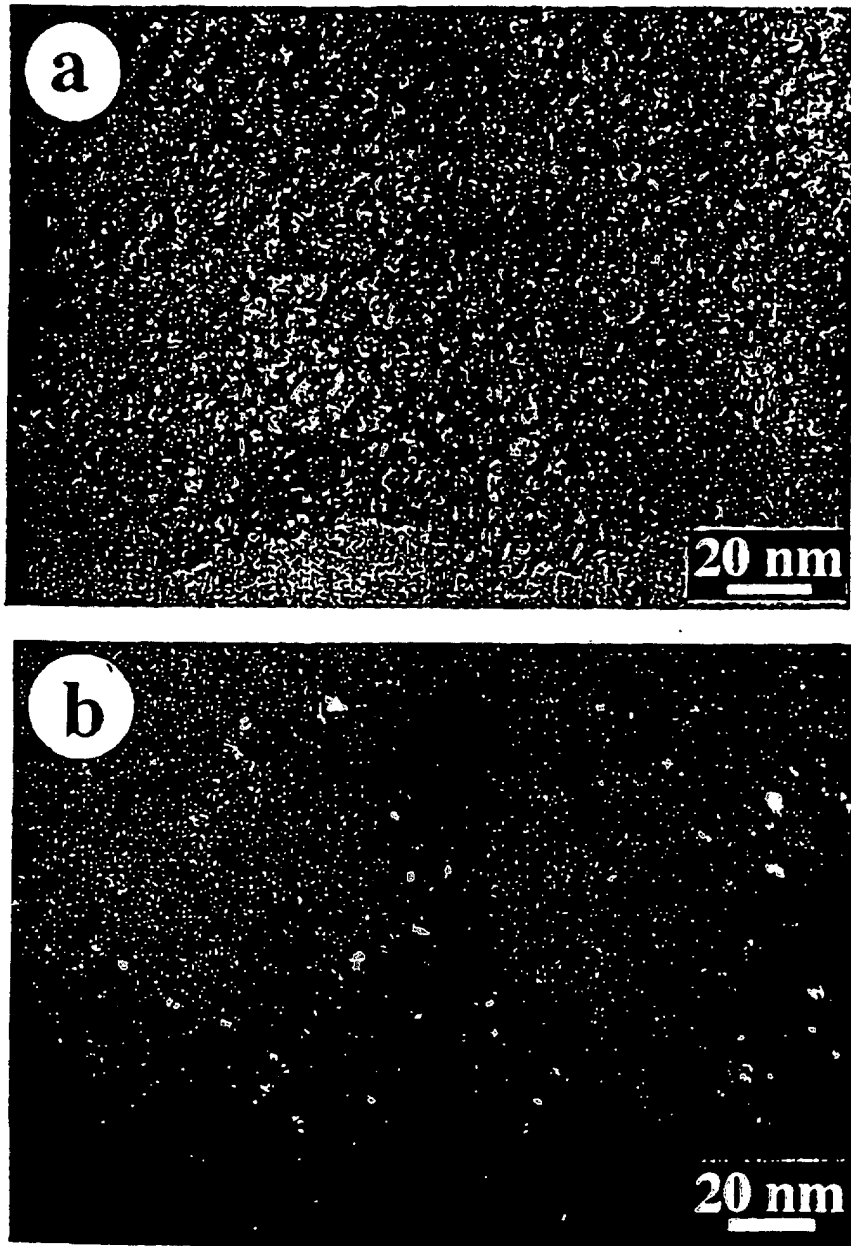
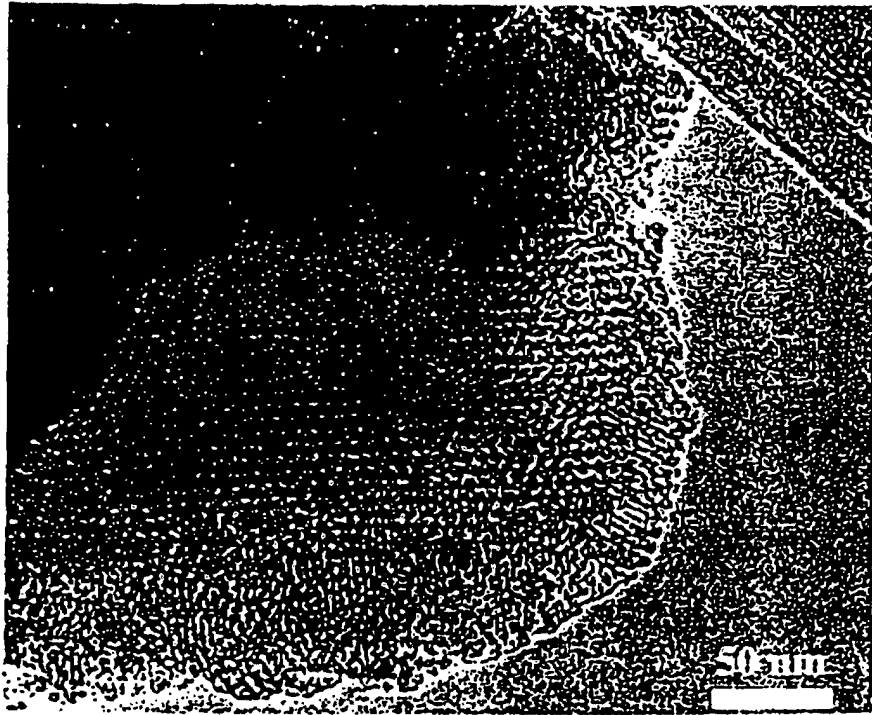


Fig. 27

a



b

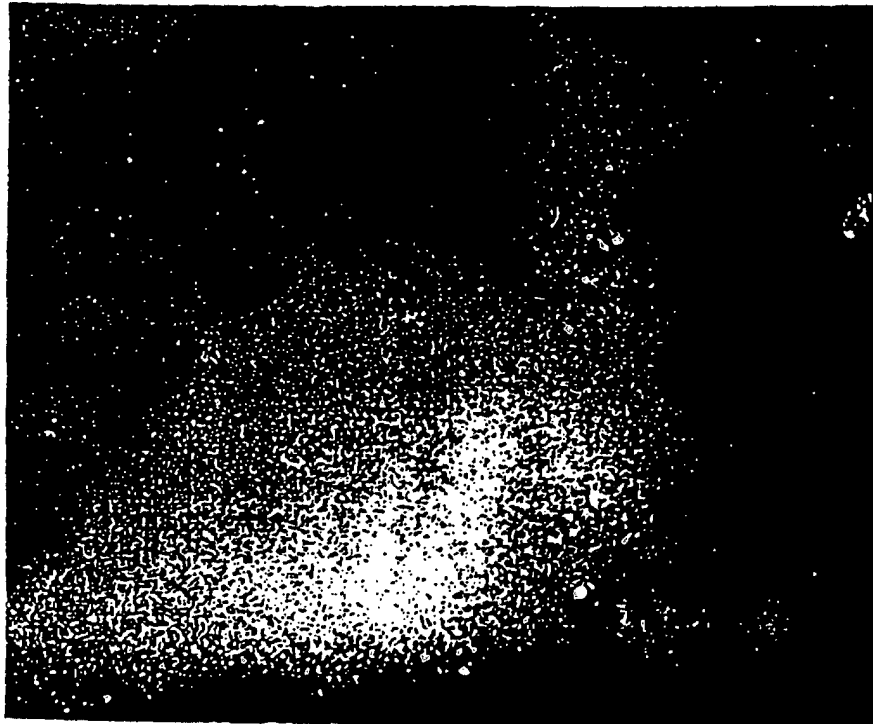


Fig. 28

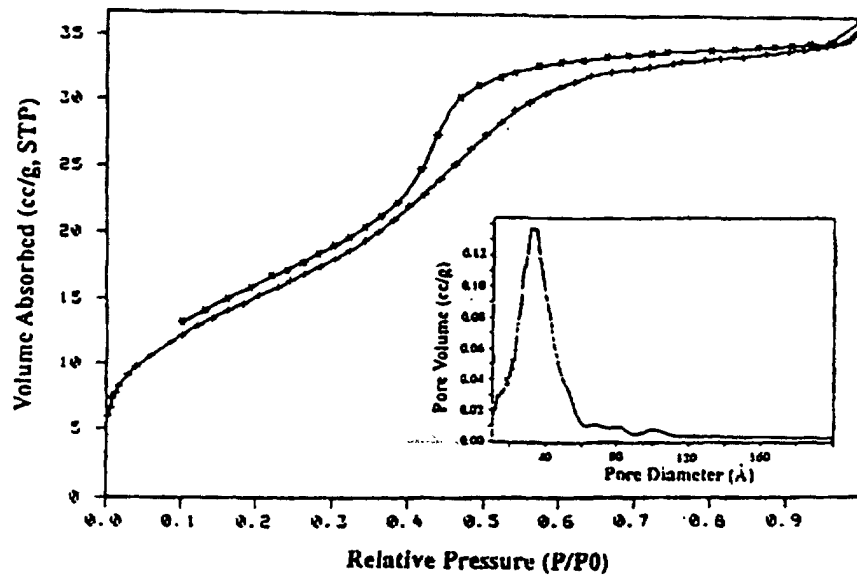


Fig. 29

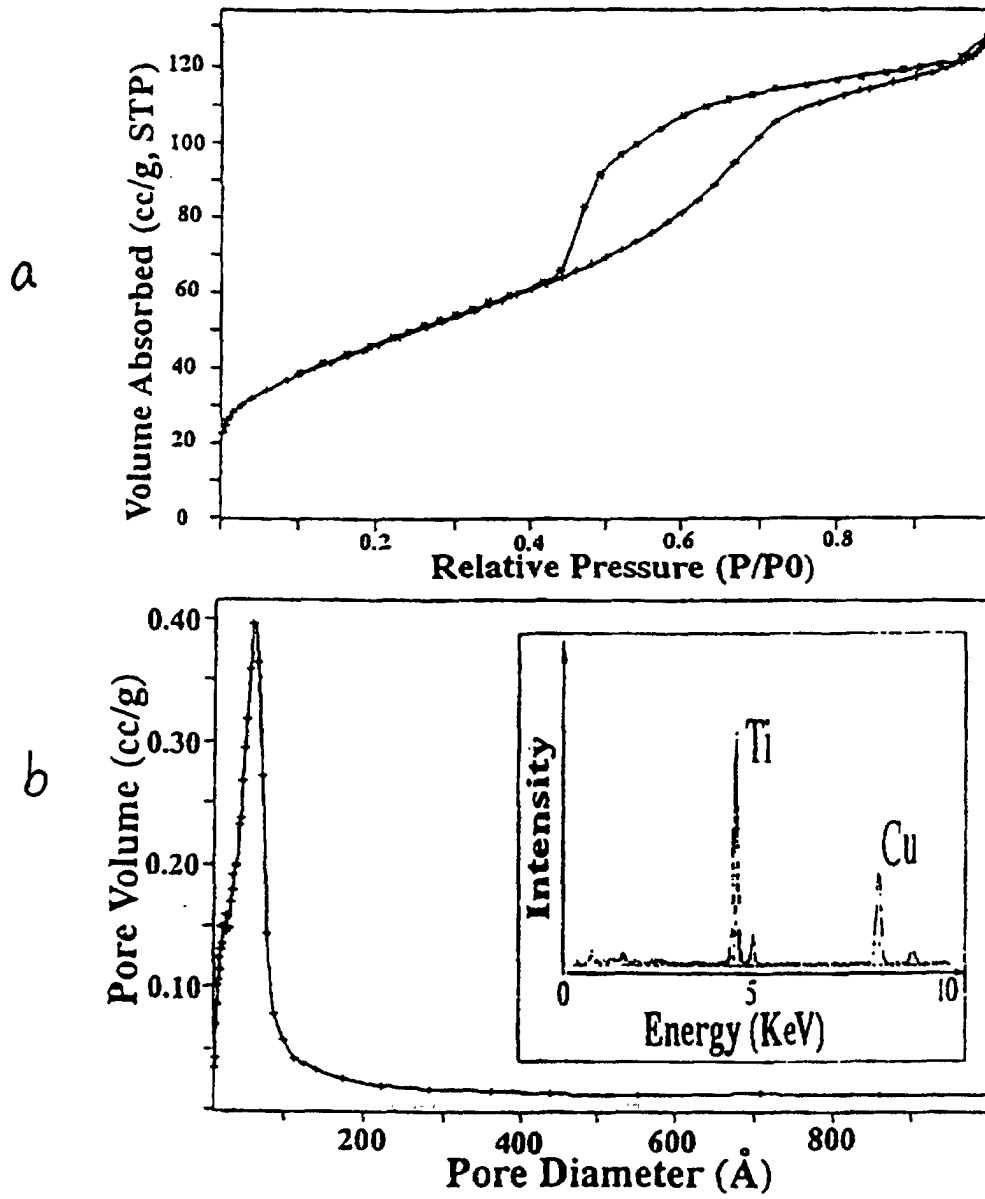


Fig. 30

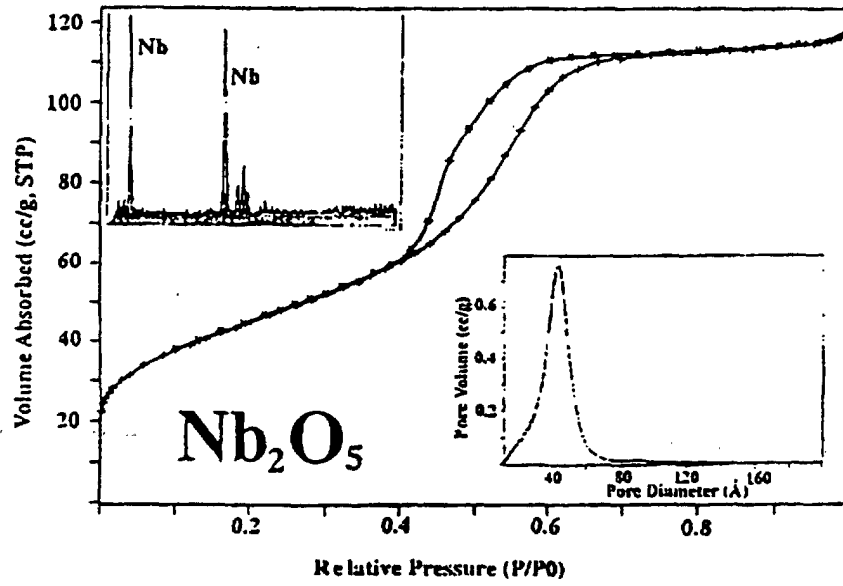


Fig. 31

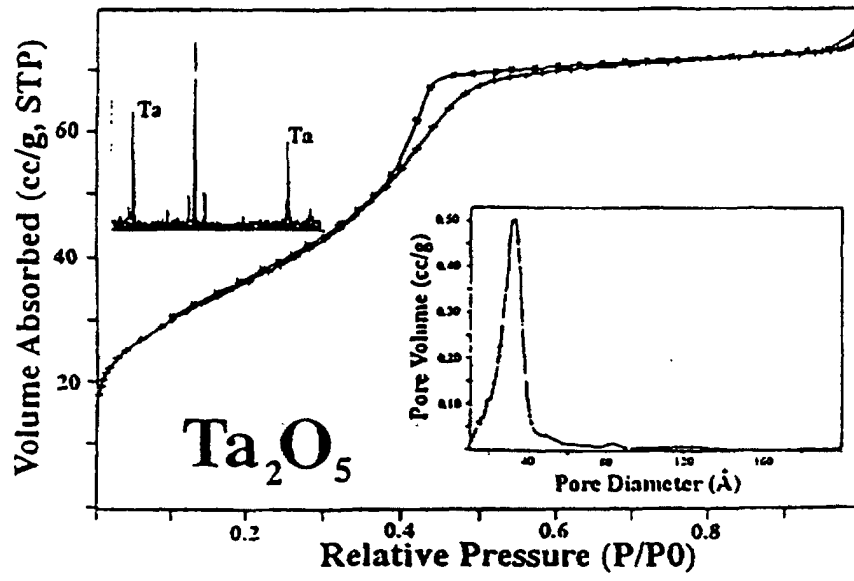


Fig. 32

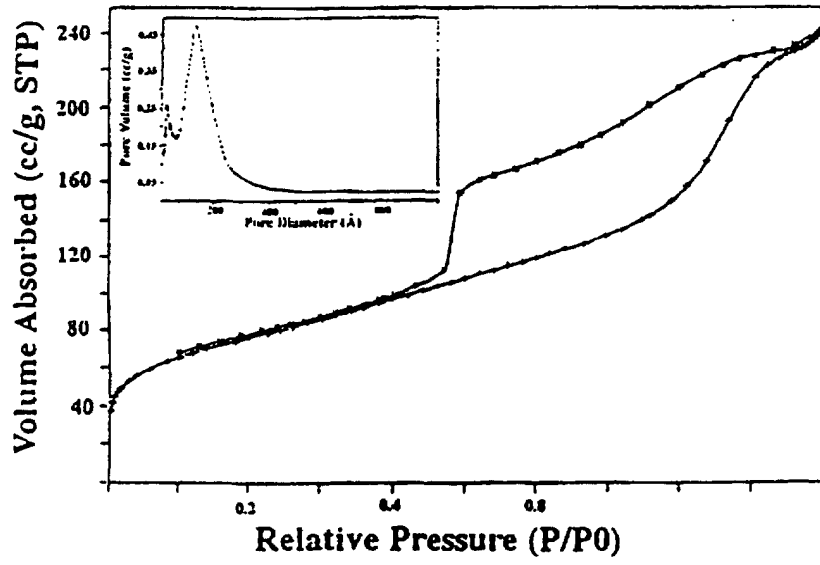


Fig. 33

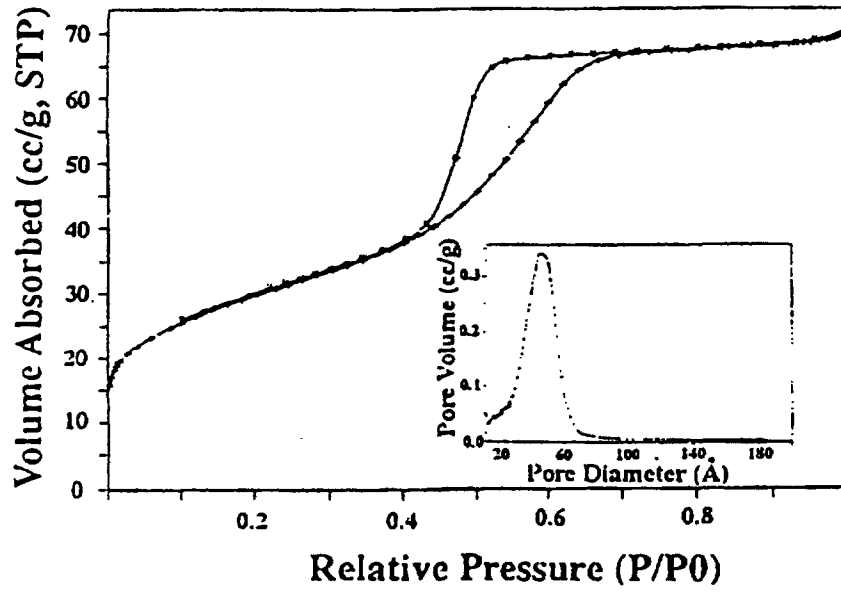


Fig. 34

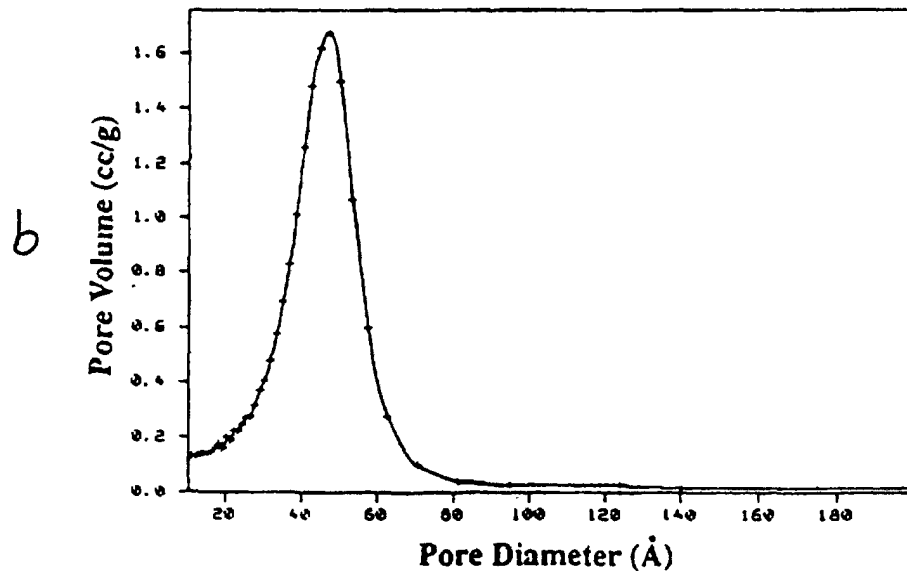
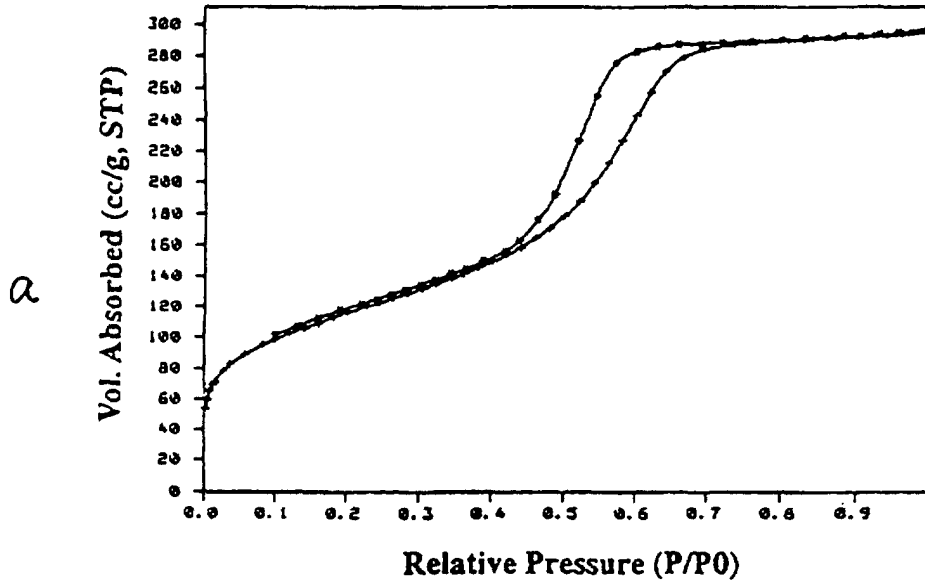
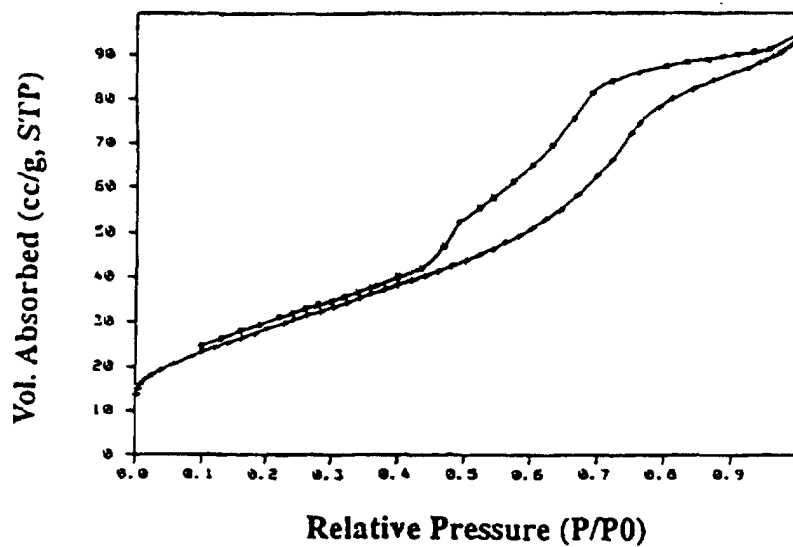


Fig. 35

a



b

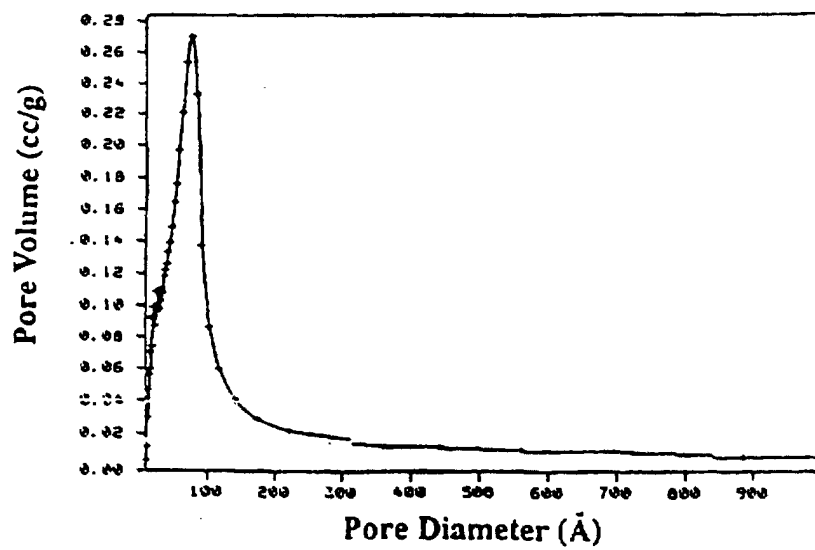


Fig. 36

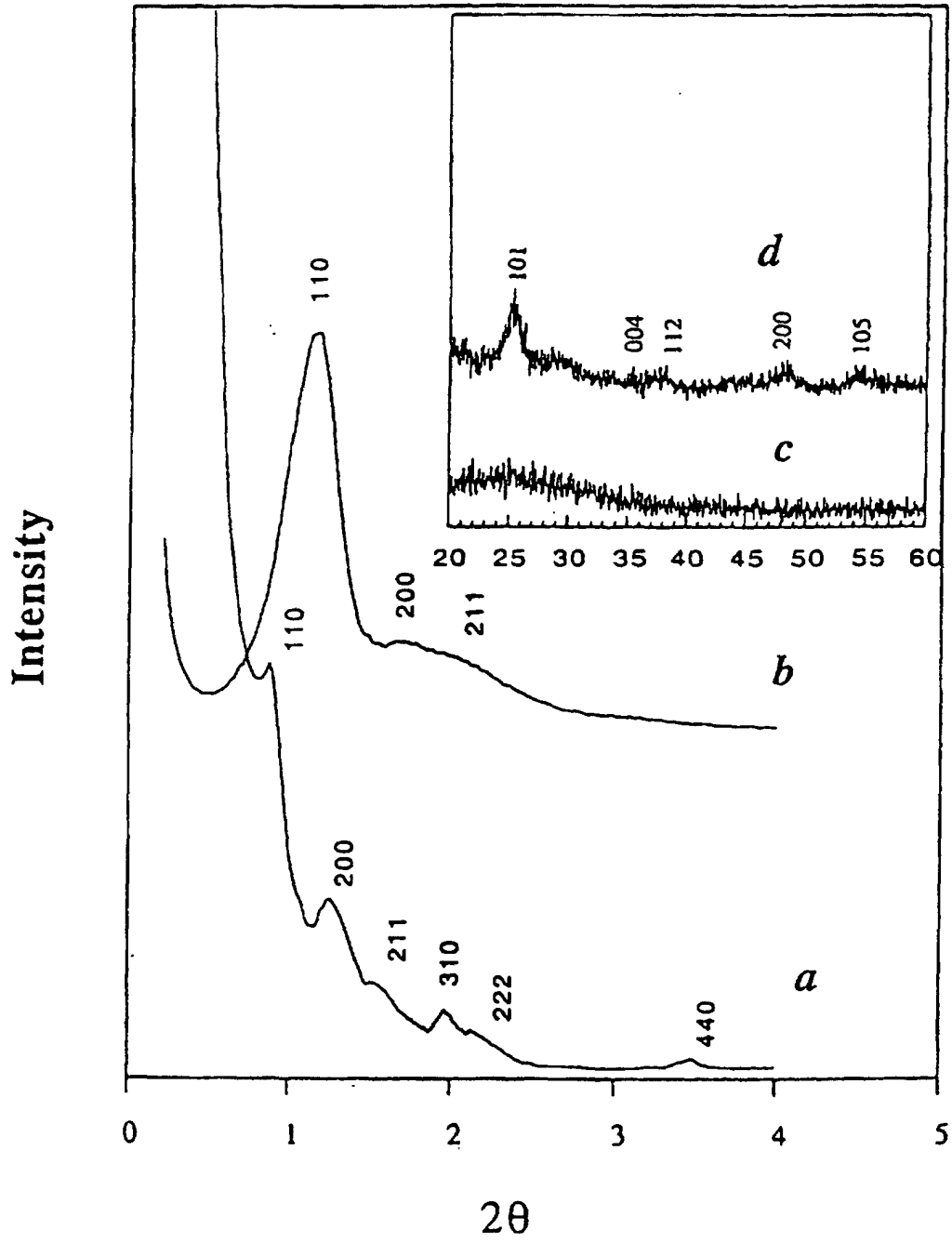


Fig. 37

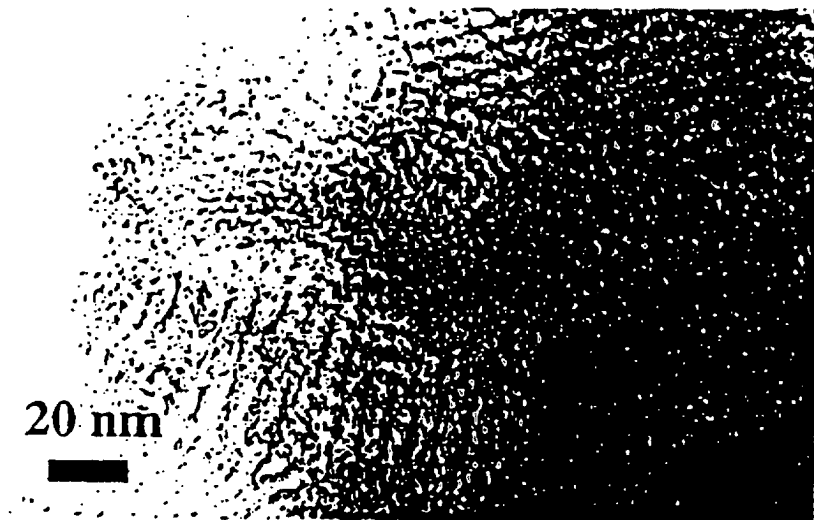


Fig. 30

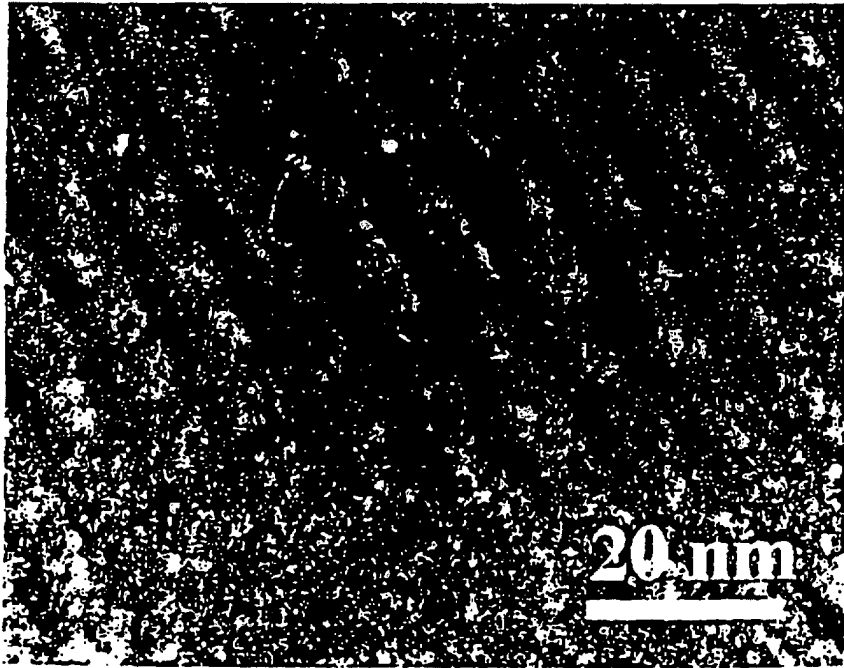


Fig. 39

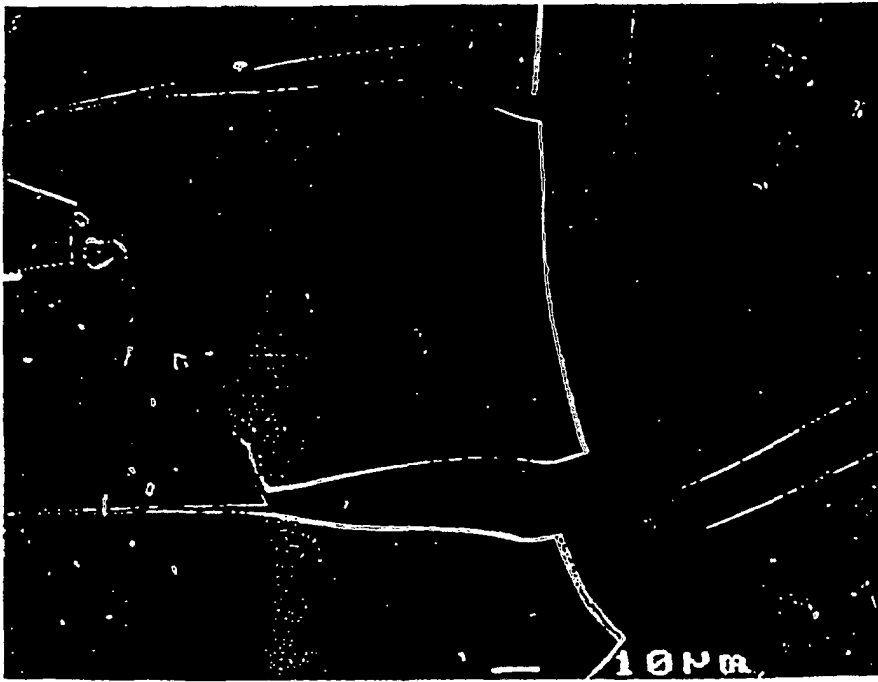


Fig. 40

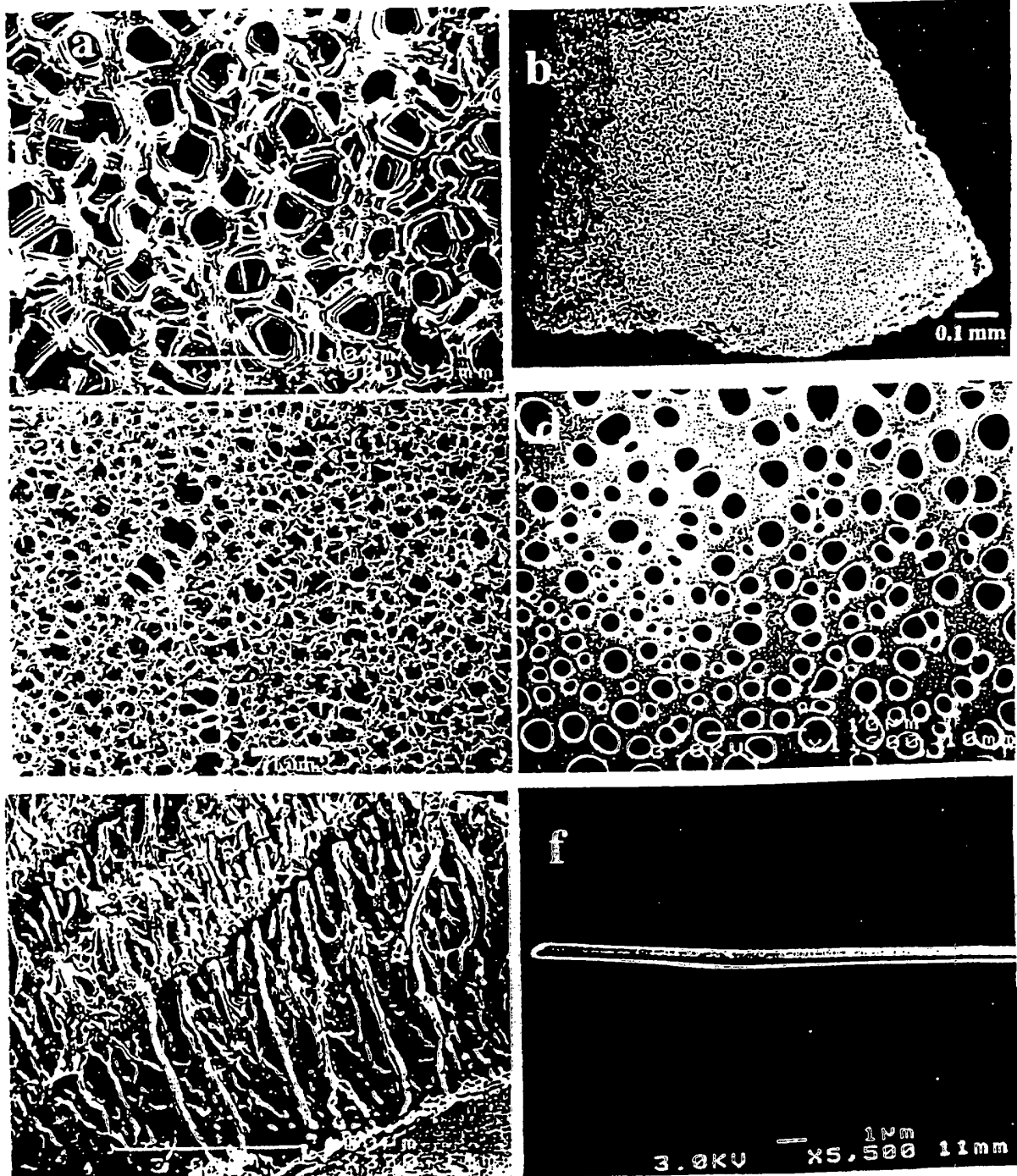


Fig. 41

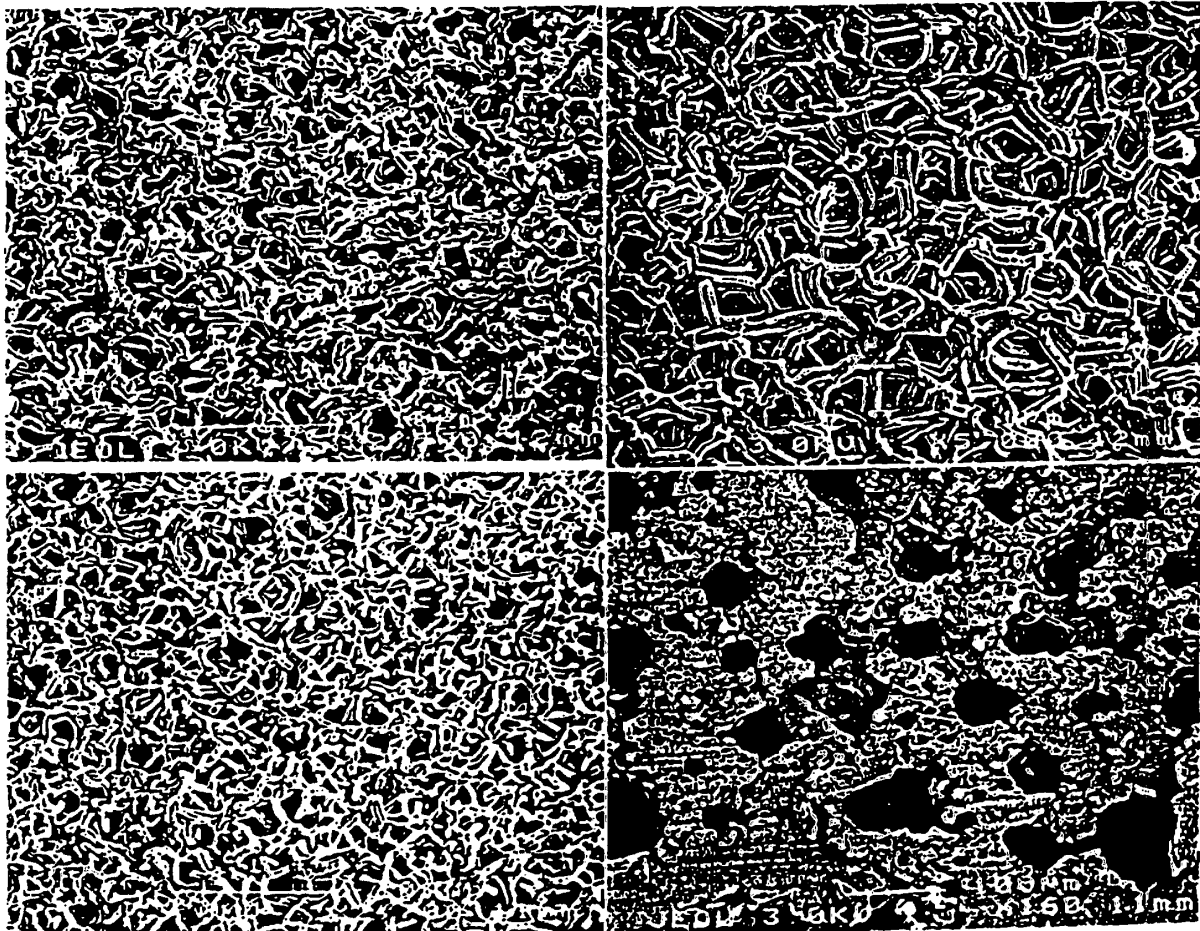


Fig. 42

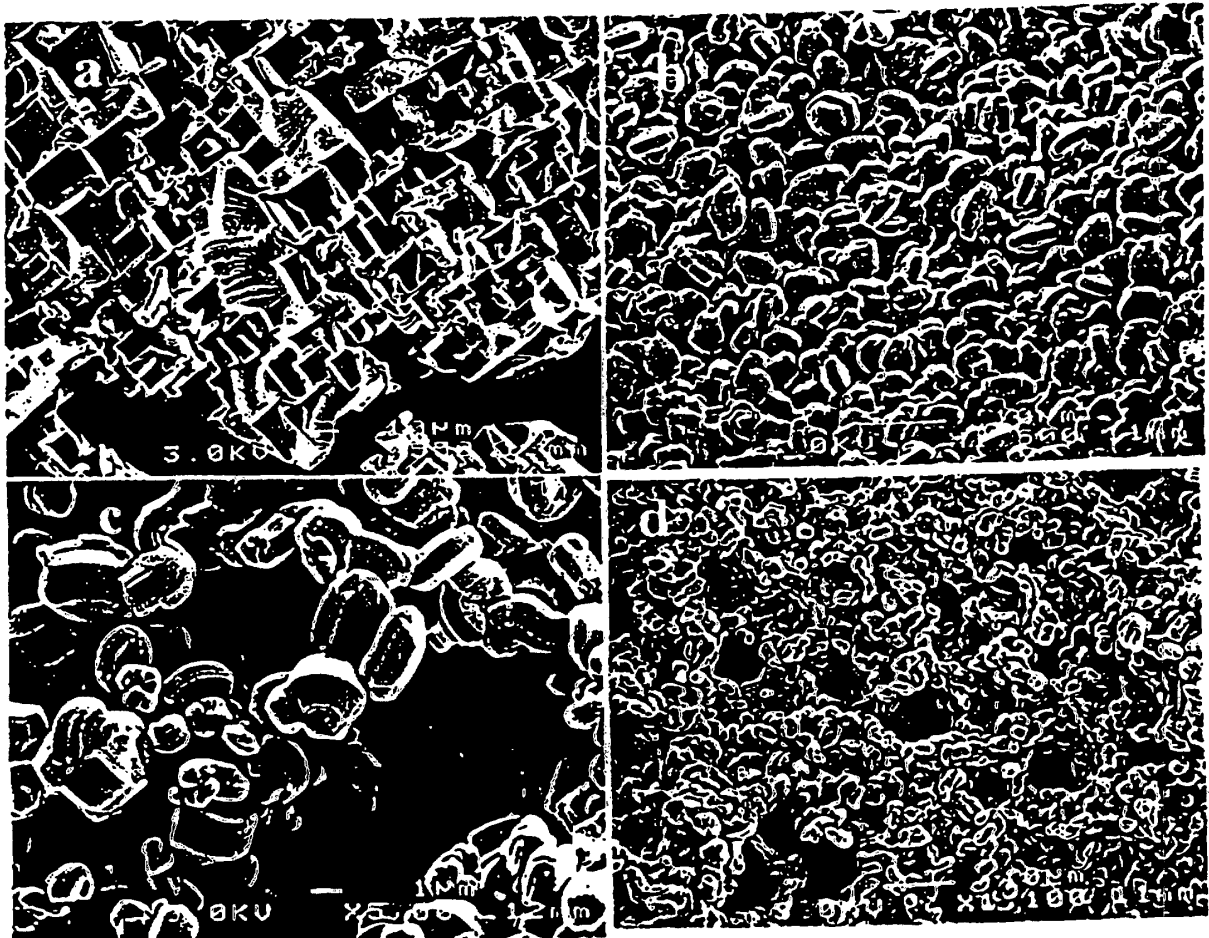


Fig. 43

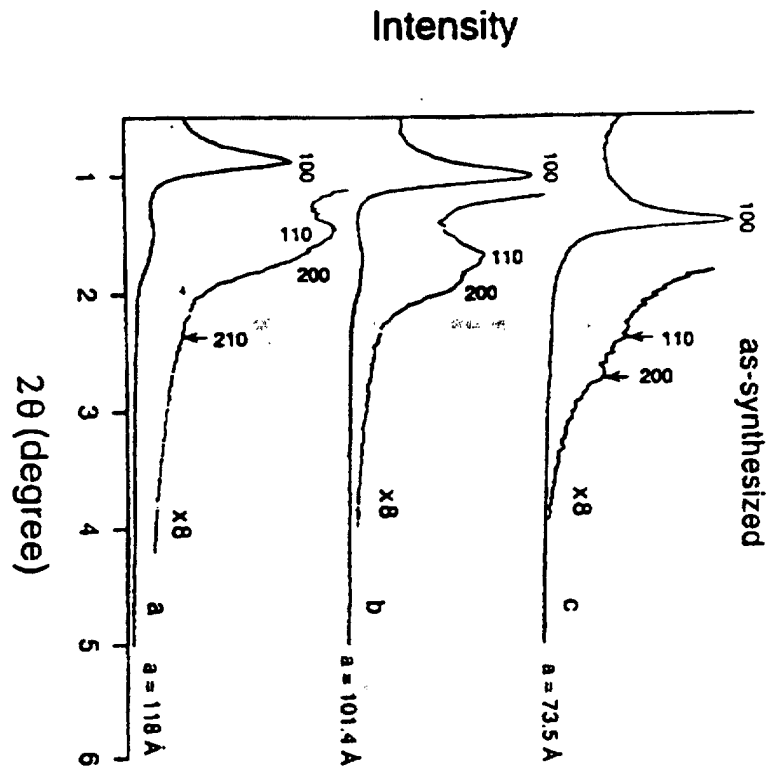


Fig. 44a

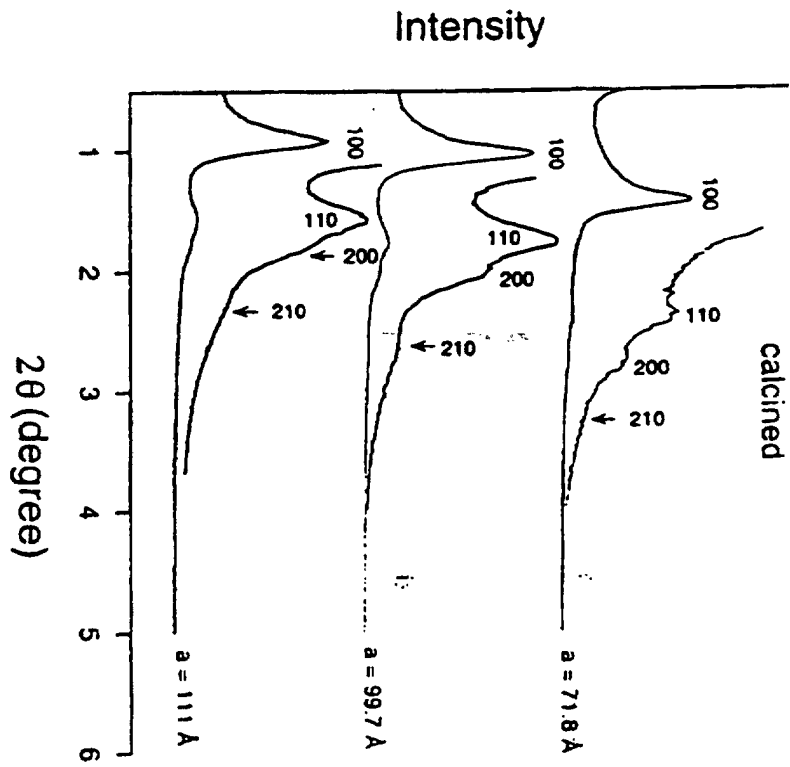


Fig. 44b

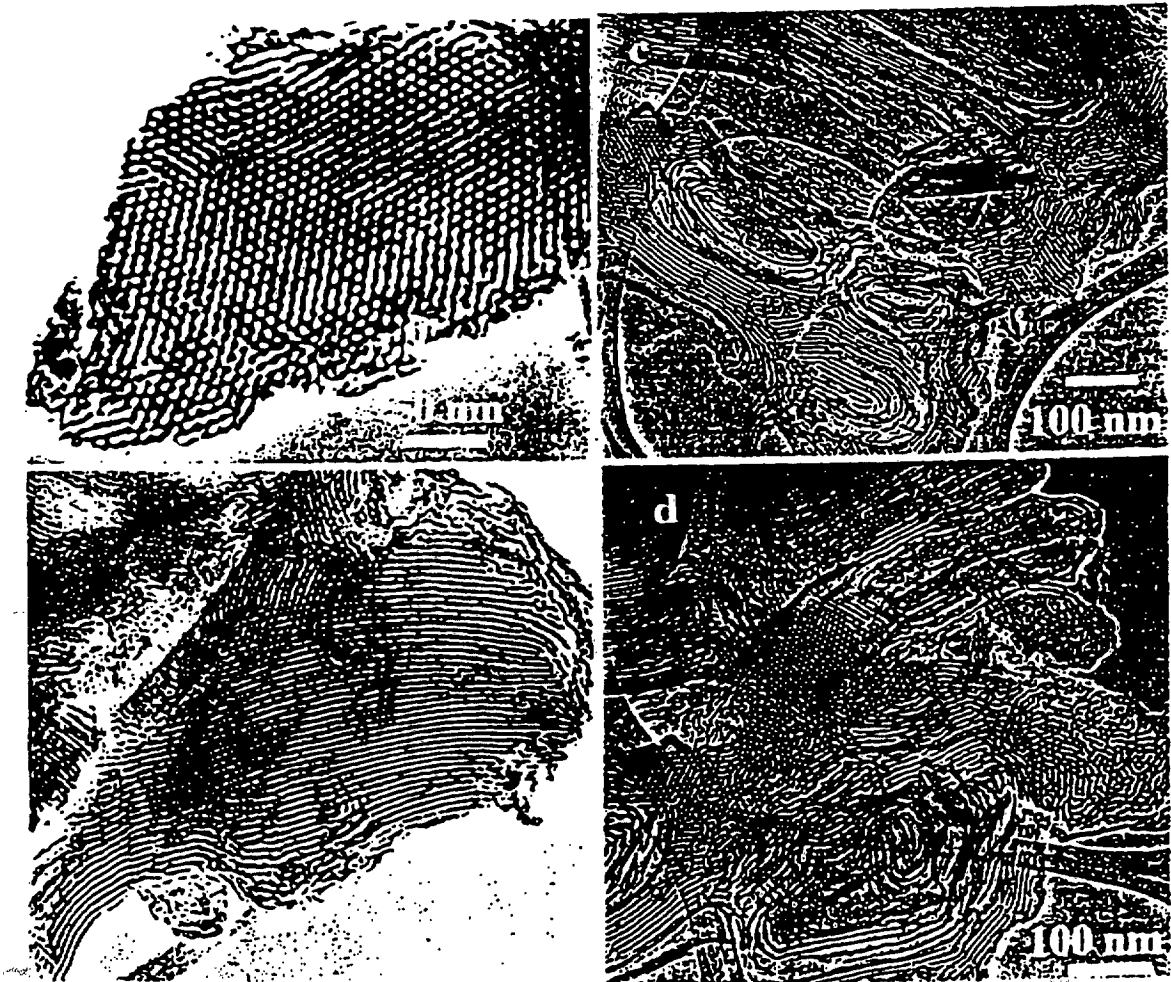
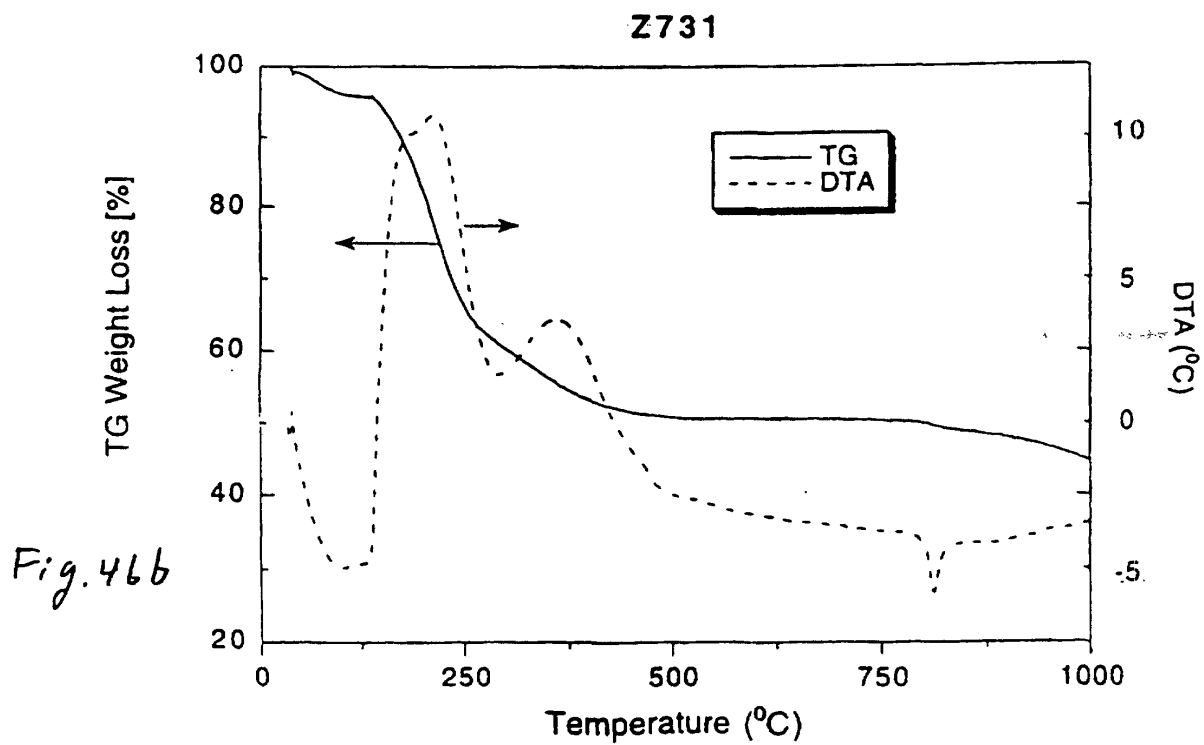
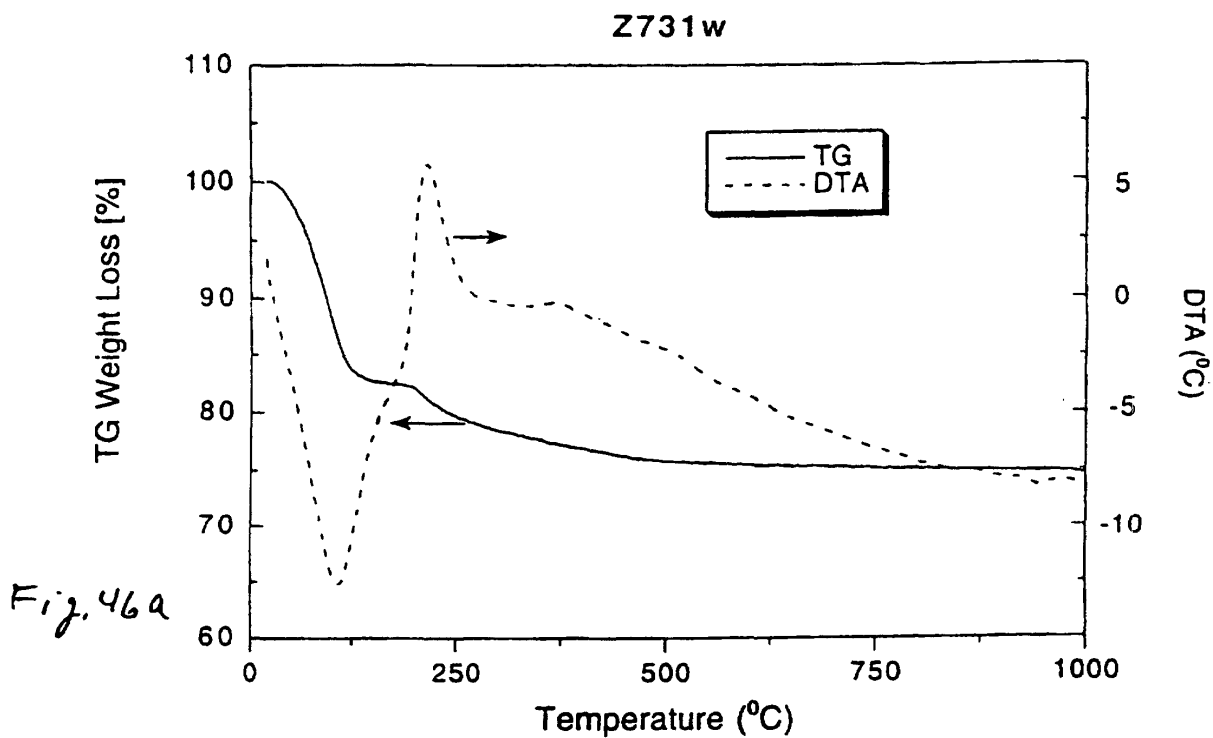


Fig. 45



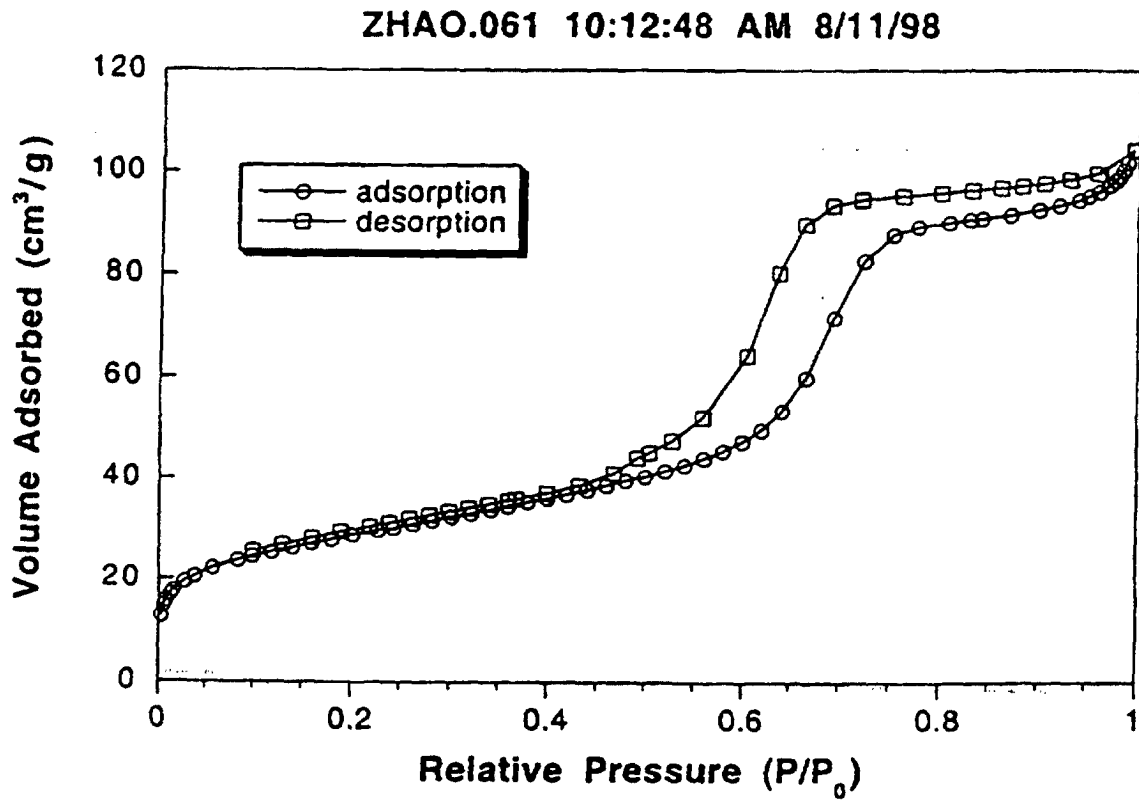


Fig. 47 a

Plot for Adsorption in Cylinders

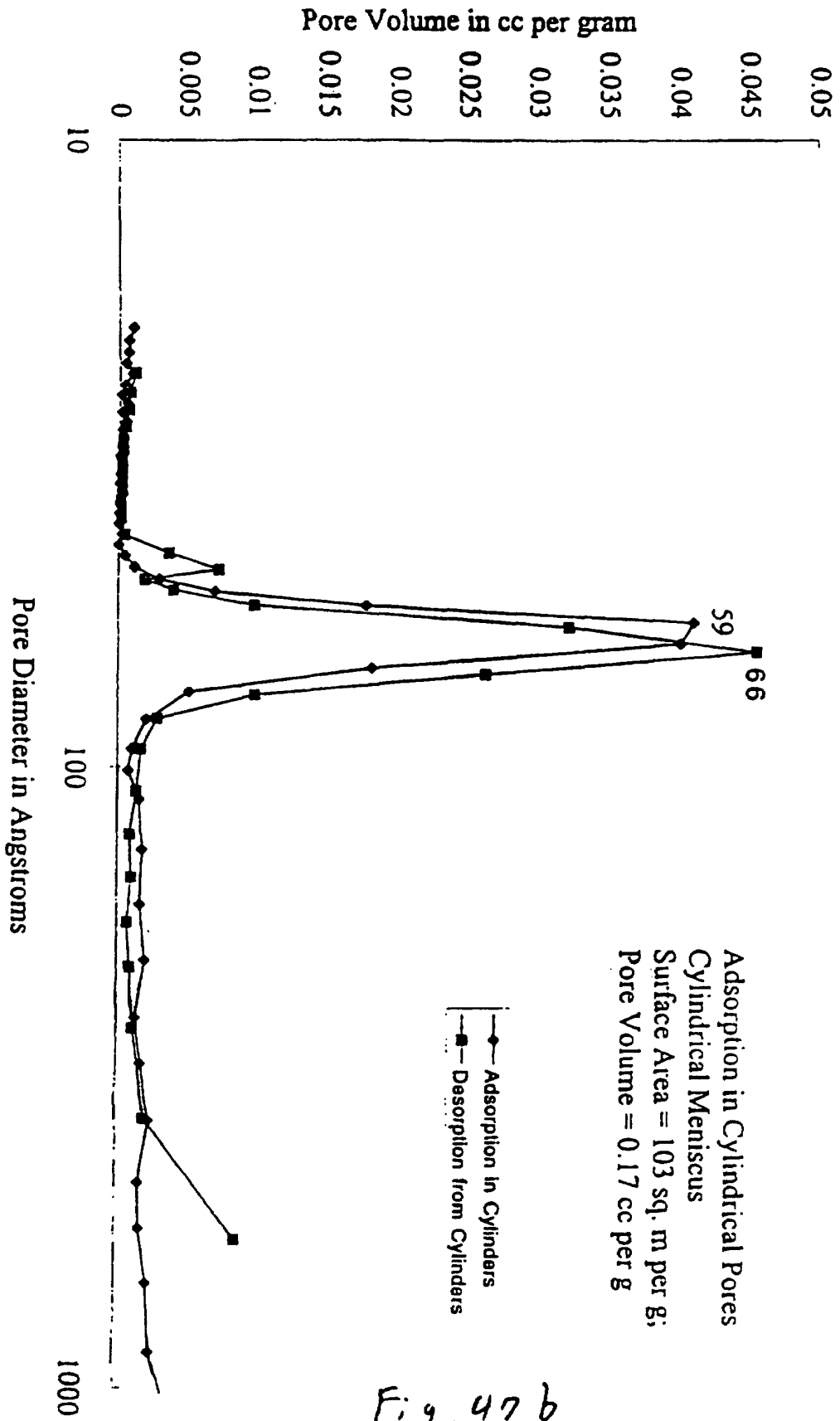
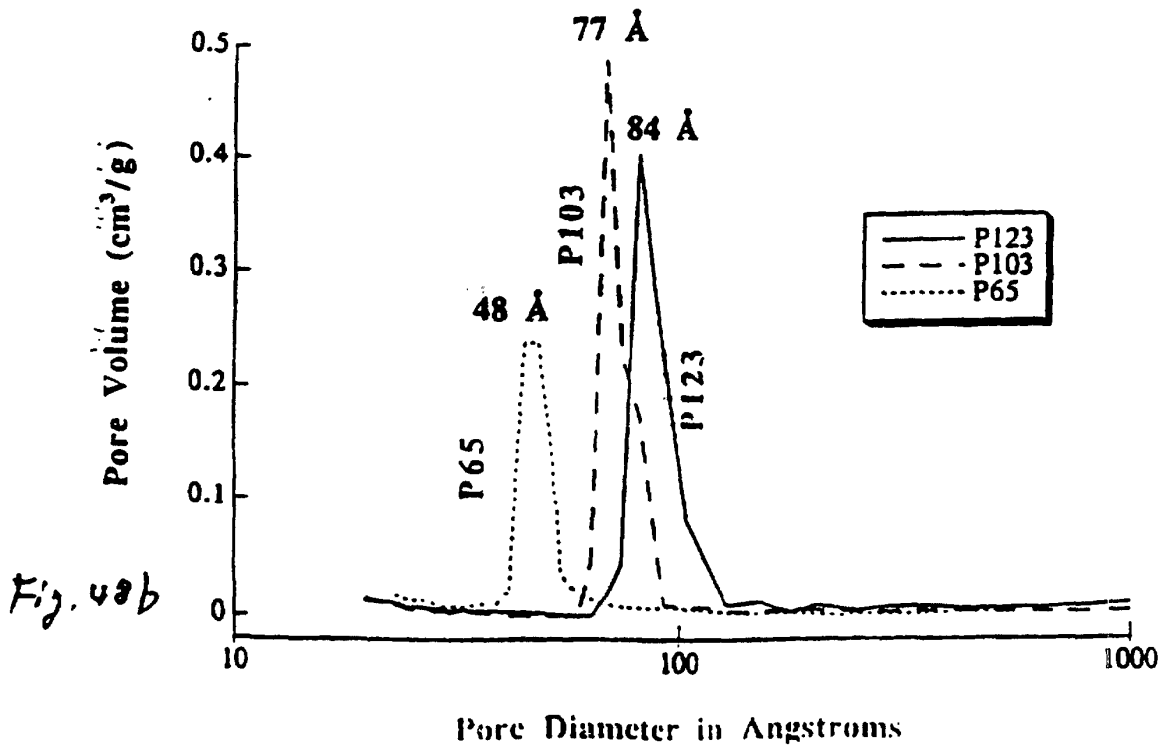
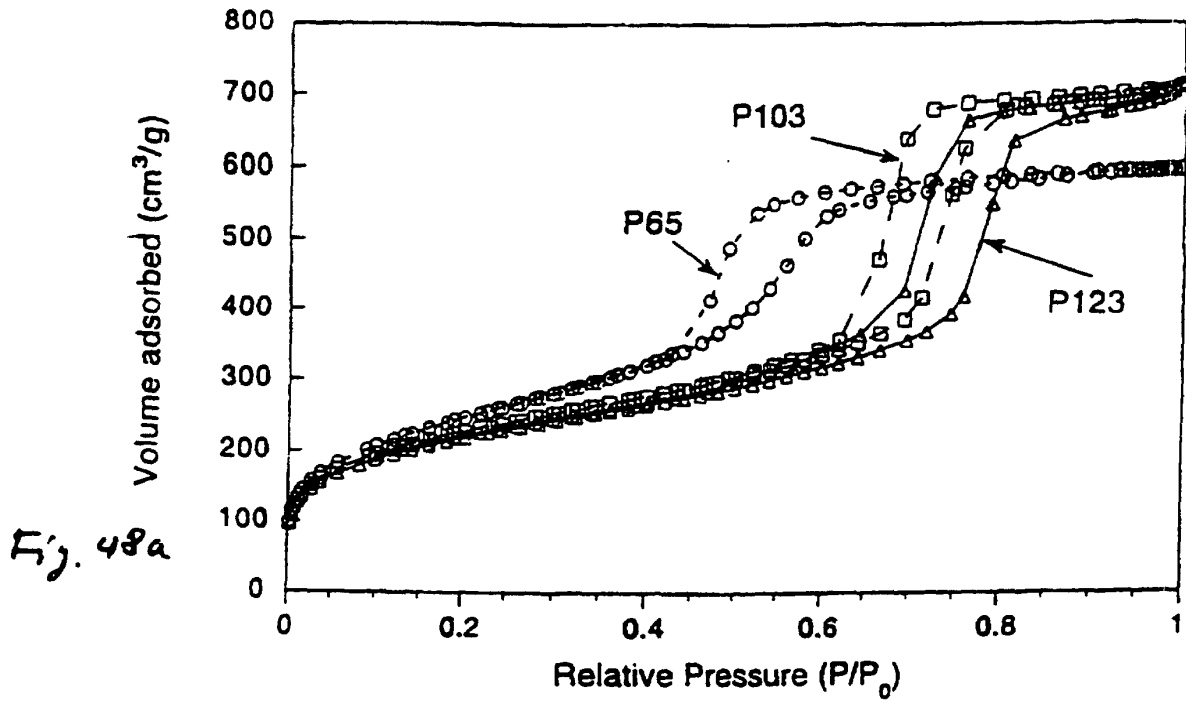


Fig. 47b



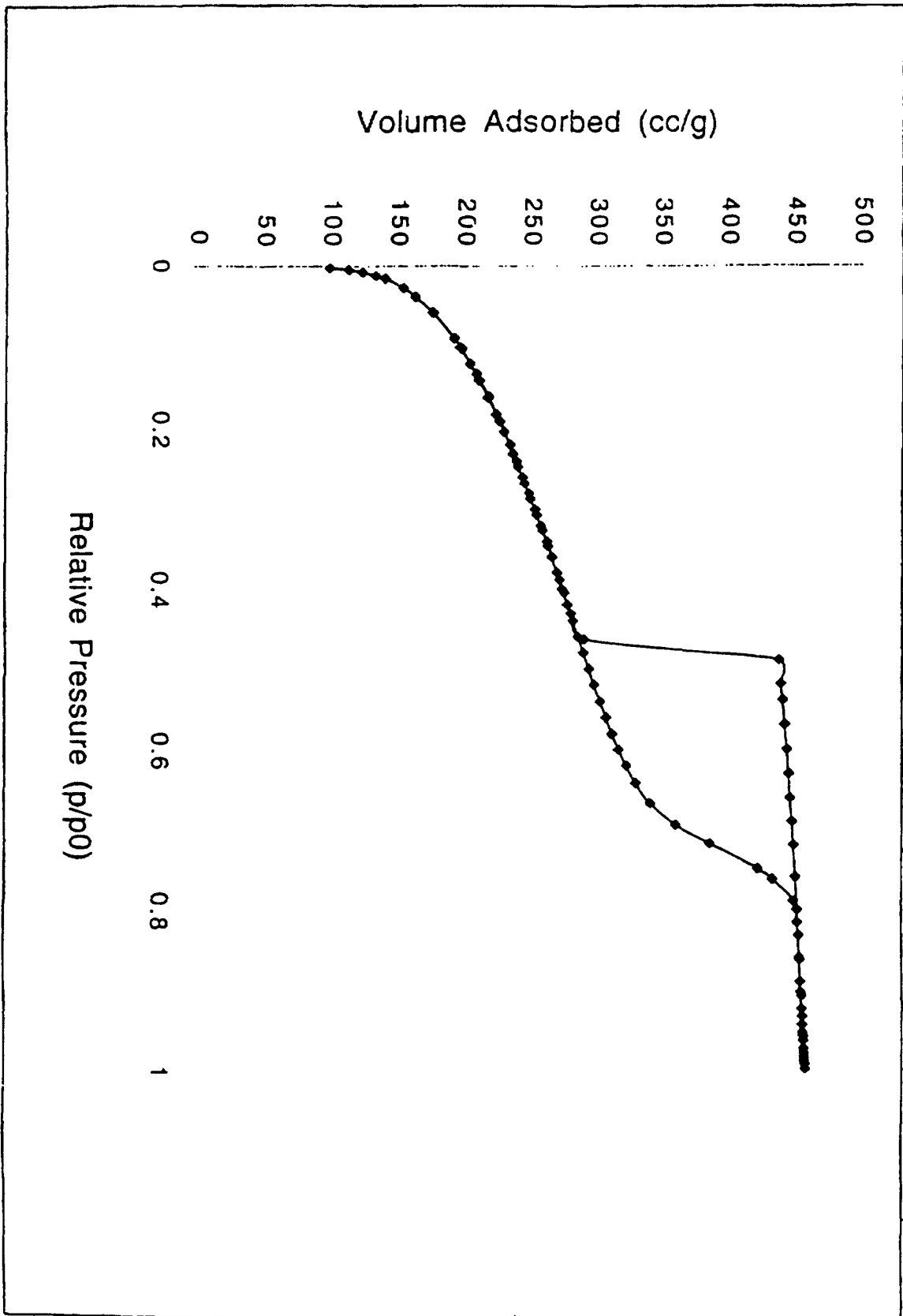


Fig. 49c

Plot for Adsorption in Spheres

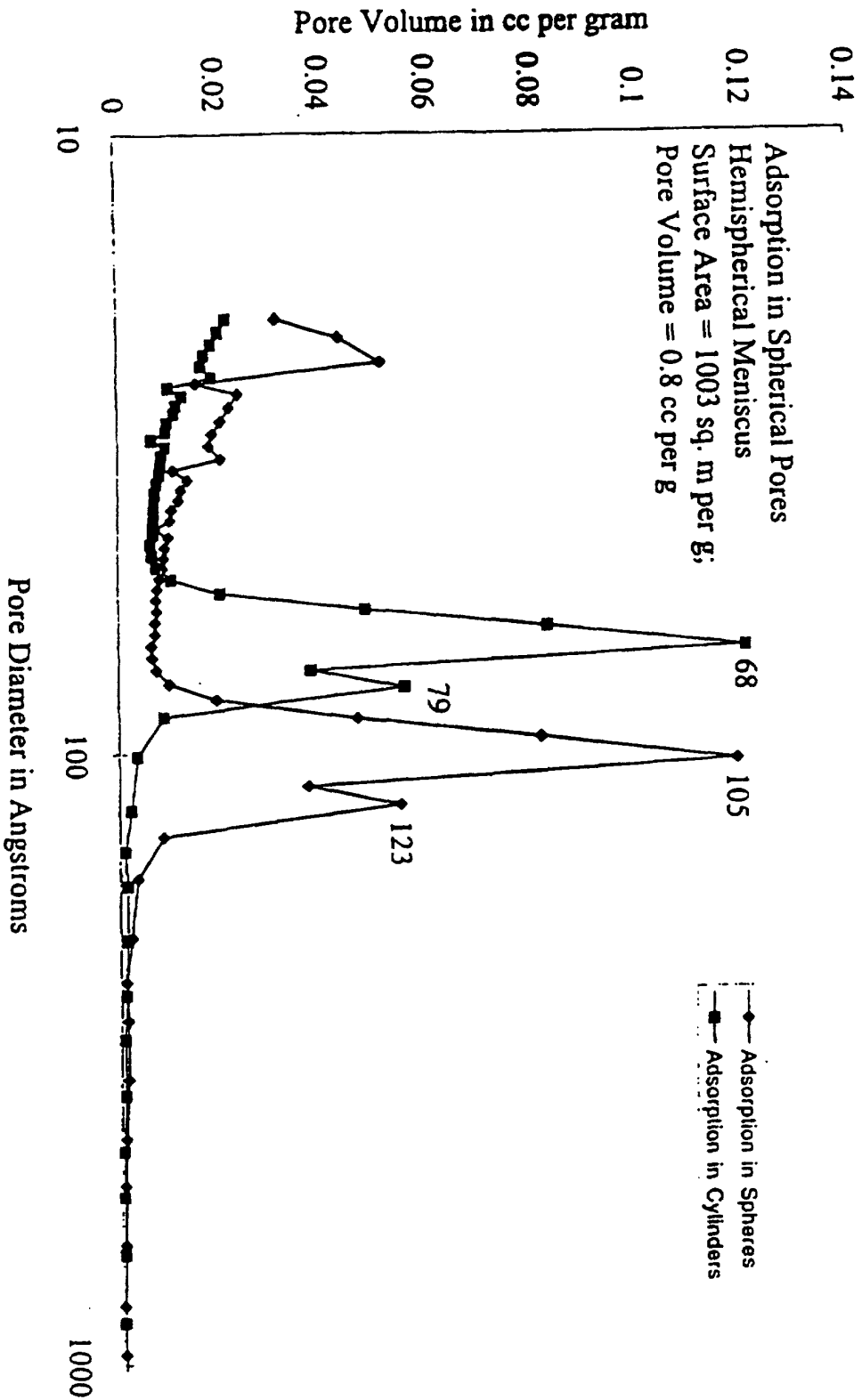


Fig. 49b

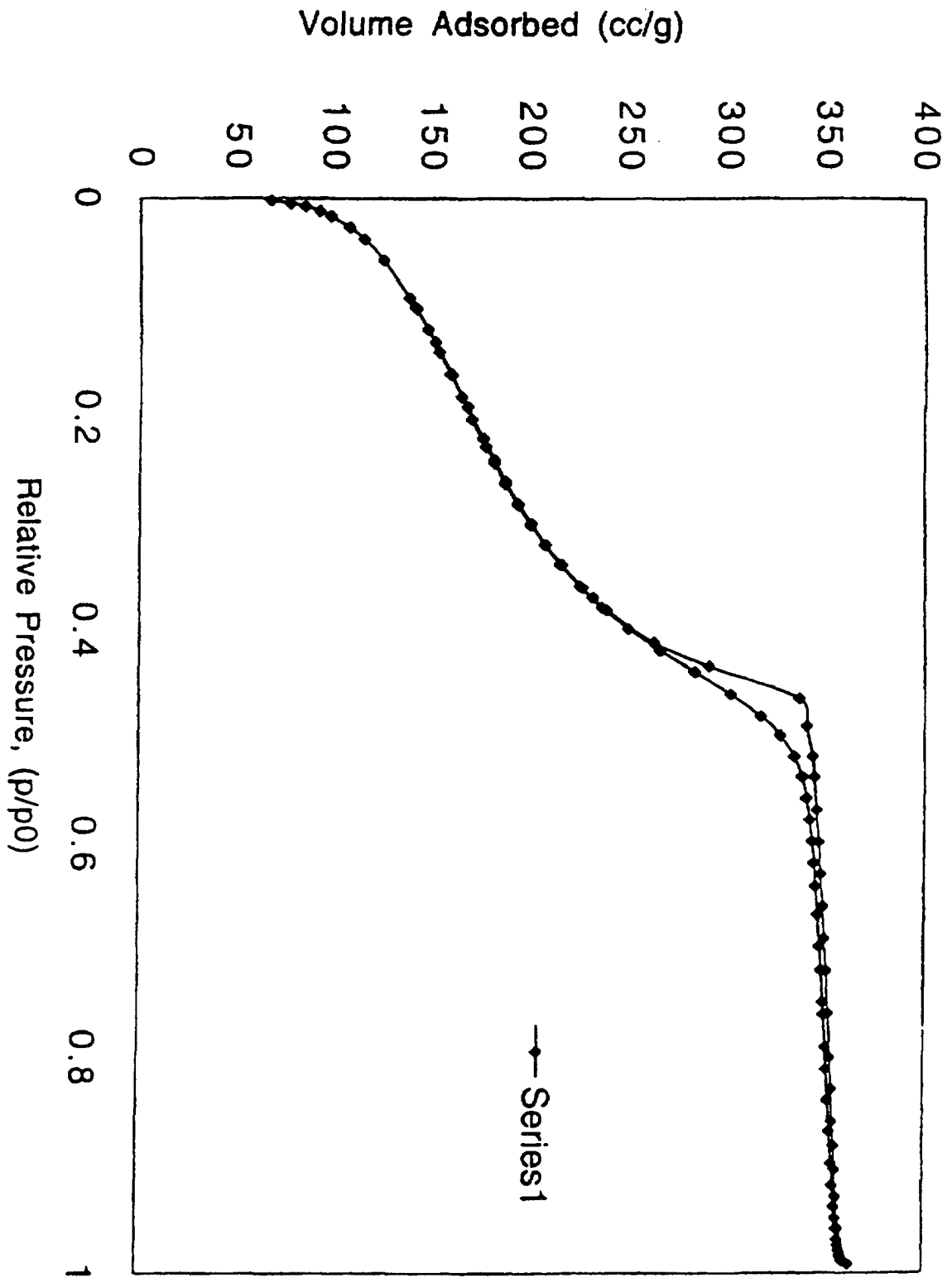


Fig. 50a

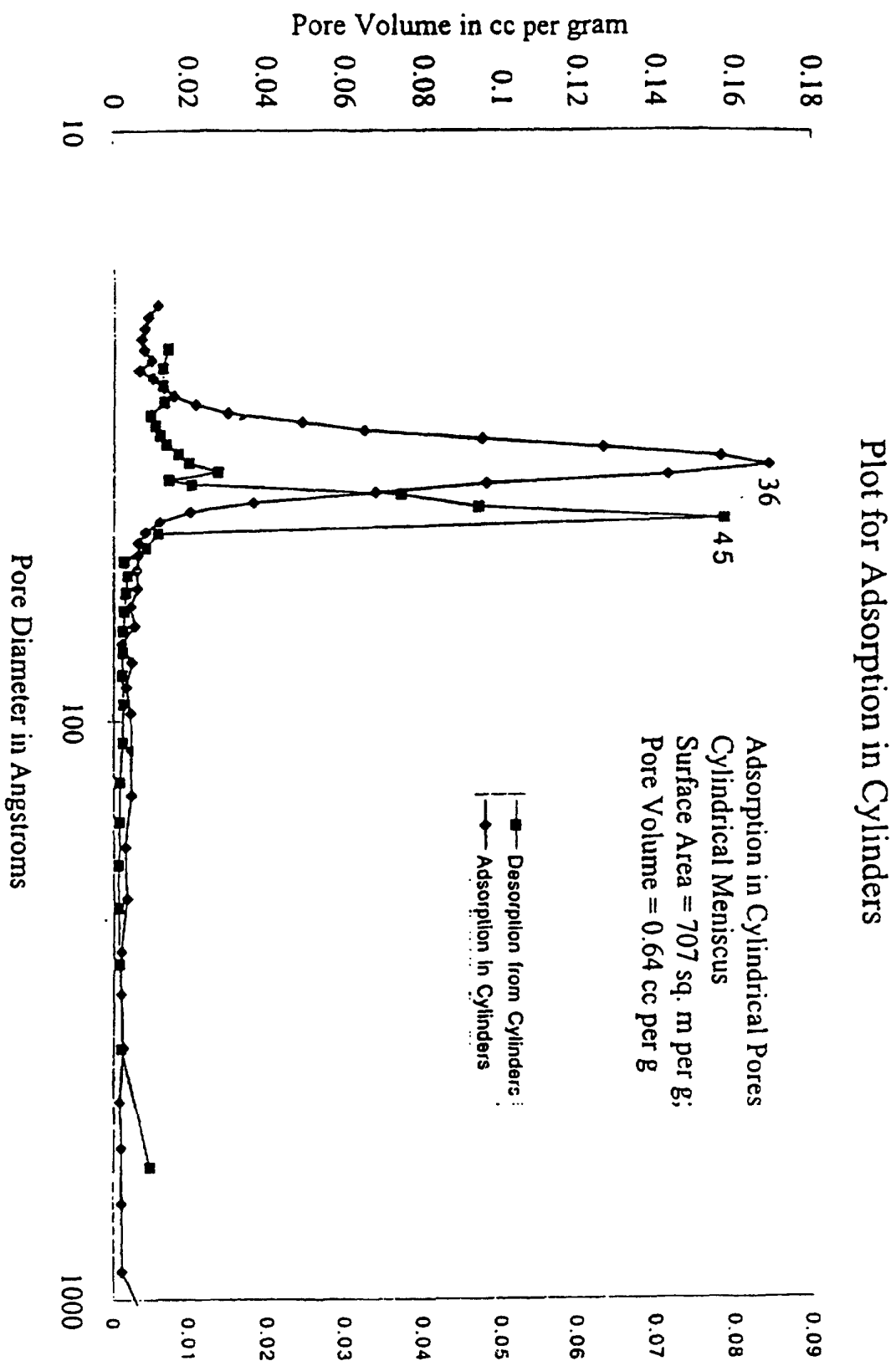
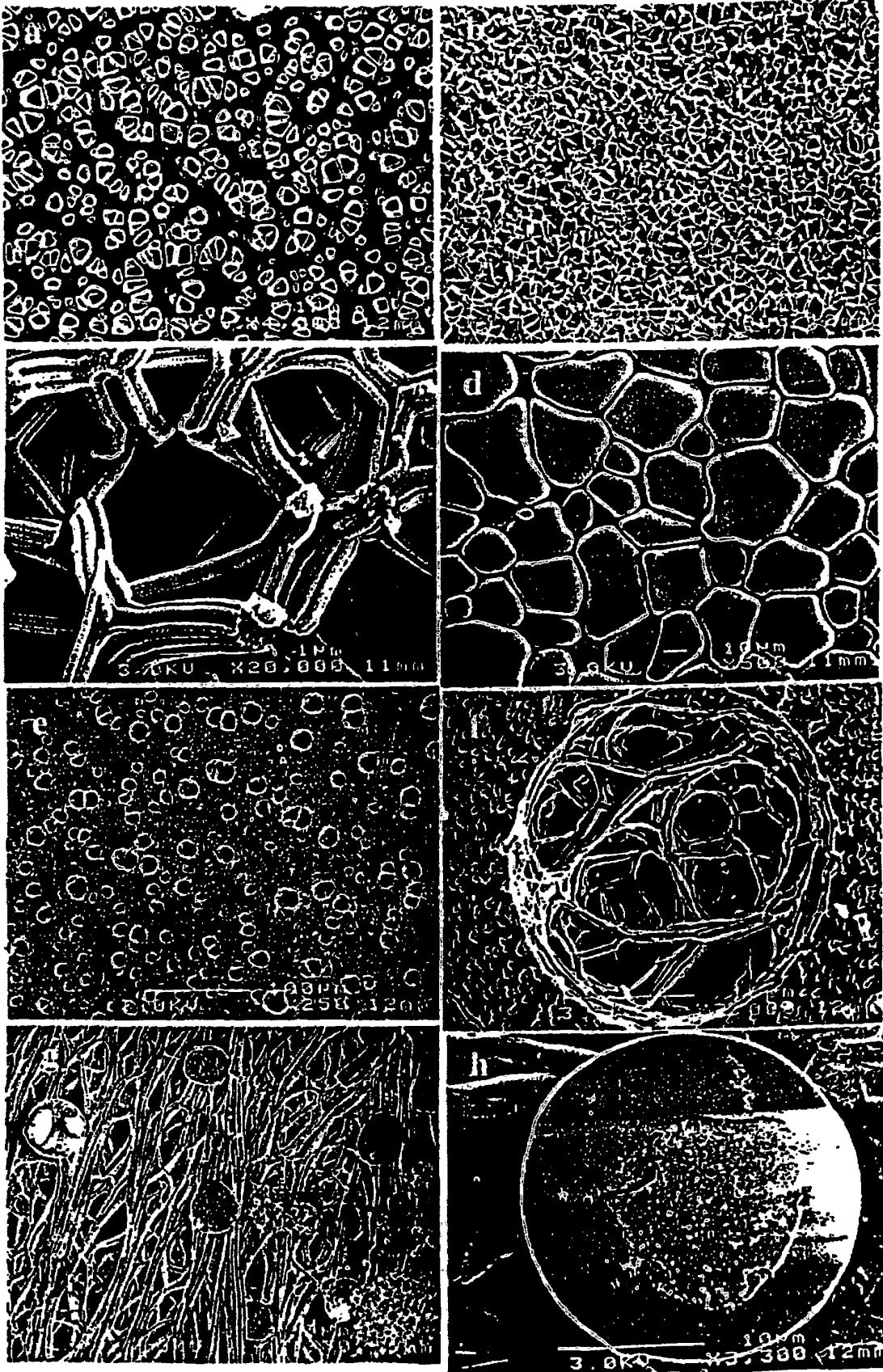


Fig. 50b



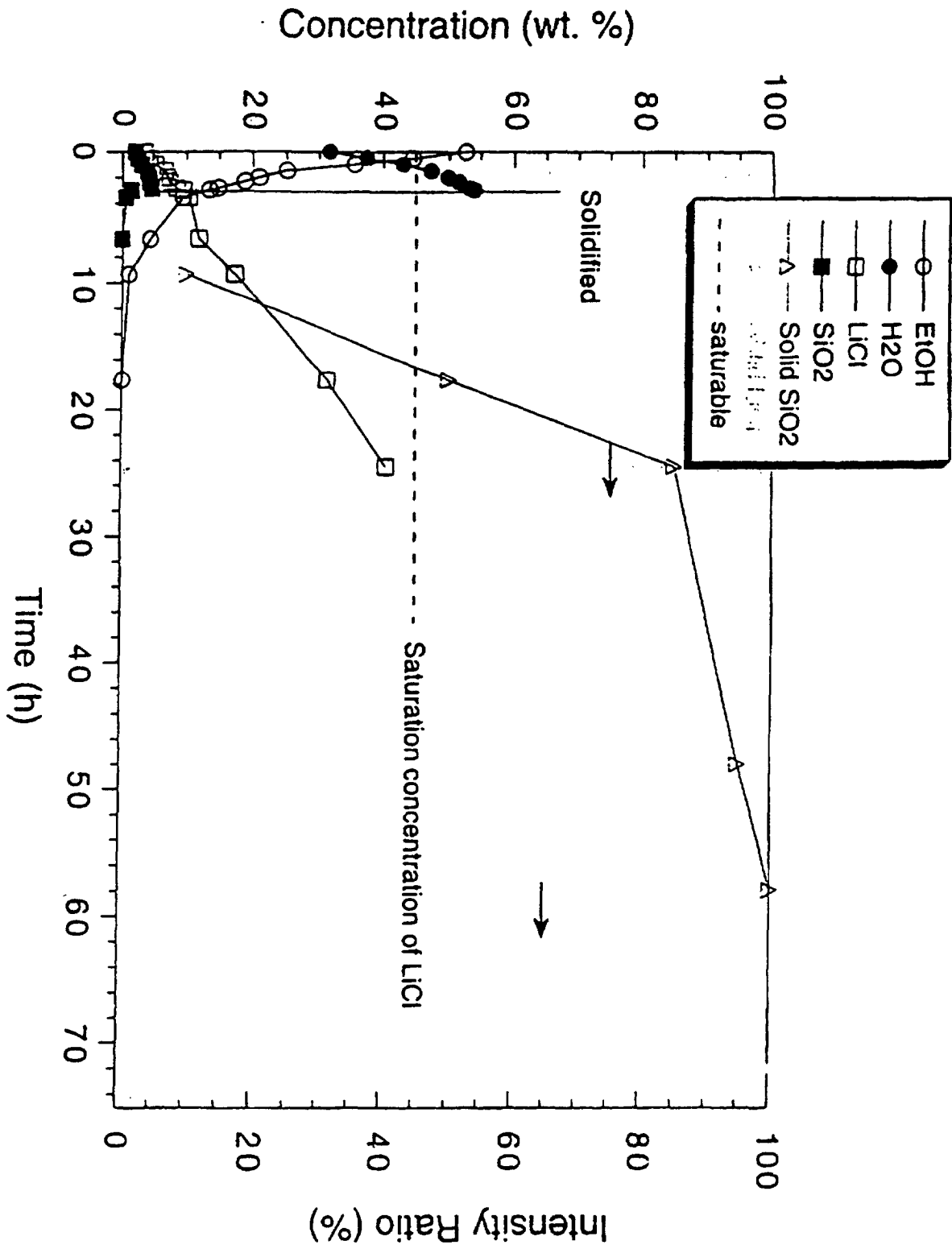


Fig. 52

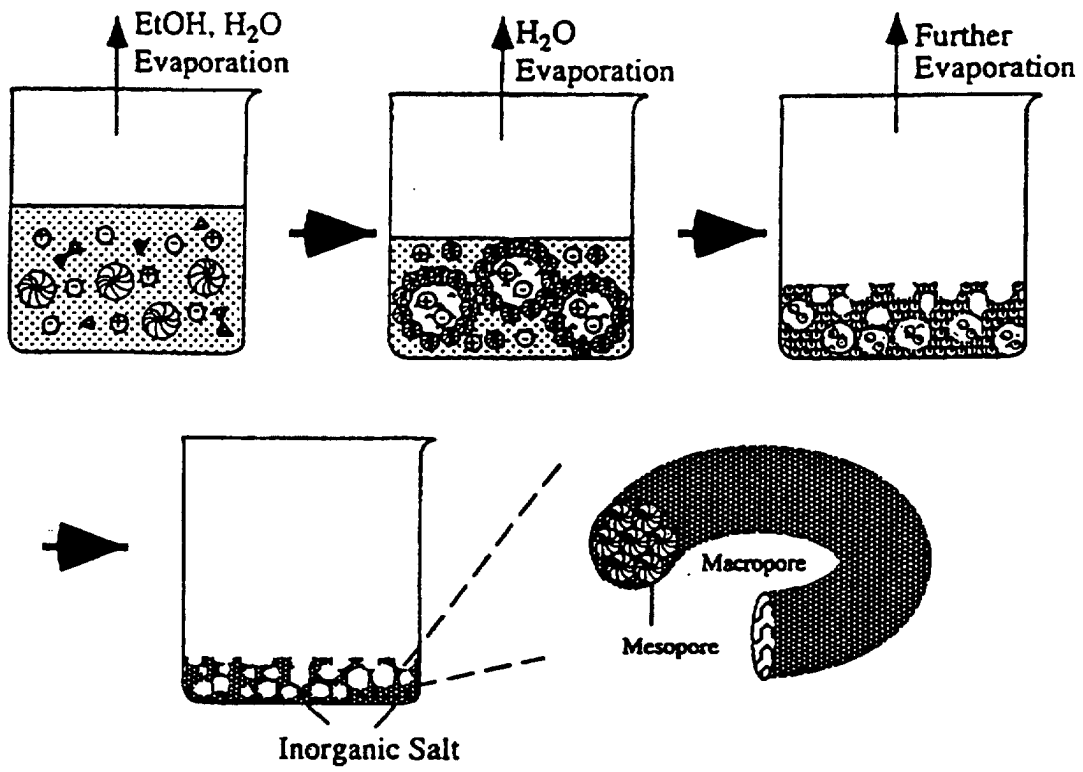


Fig. 53

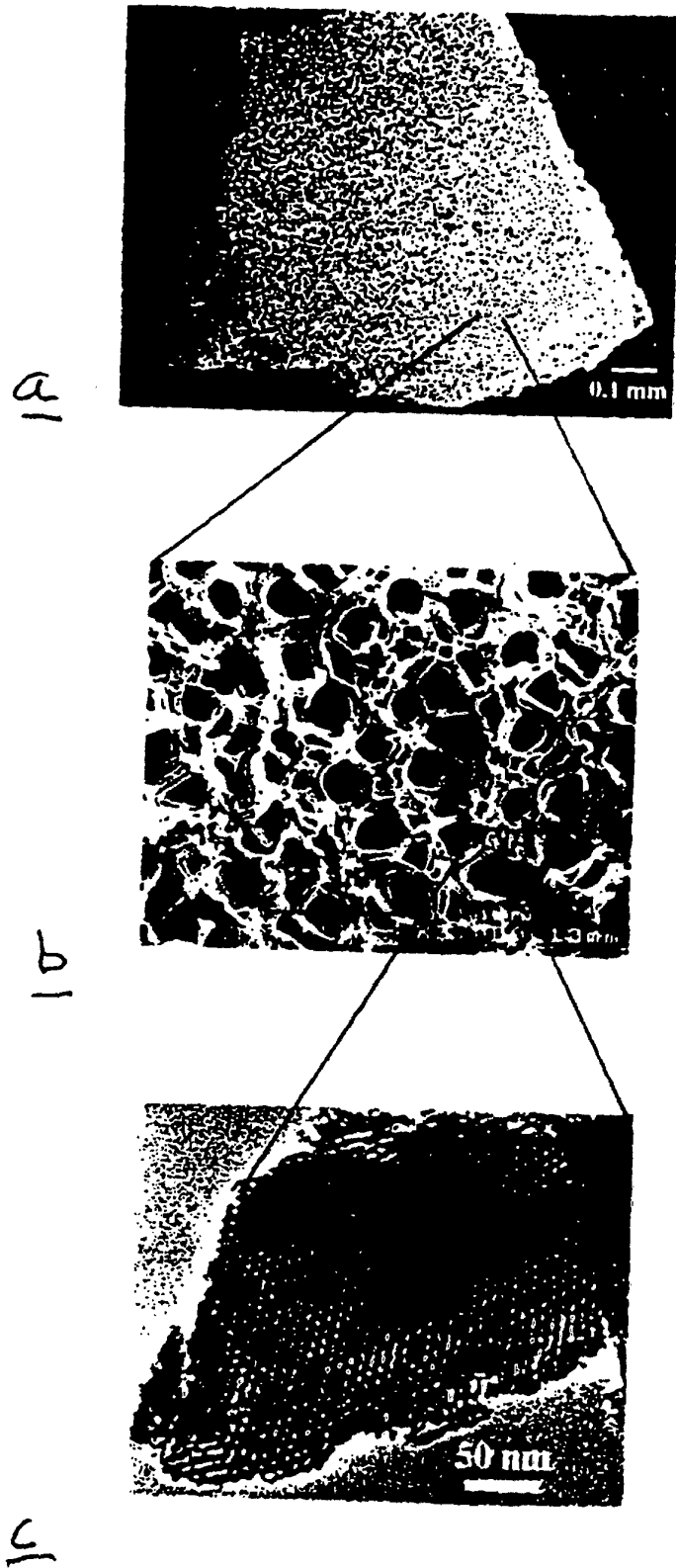


Fig. 54